Effect of coral reefs on wave attenuation and erosion: Mnemba Island, Zanzibar

Curtis Russell Swanepoel
Civil Engineering
University of KwaZulu Natal

A thesis submitted in fulfillment of the requirements for the degree of
Master of Science
2017

Supervisor: Professor D. Stretch
Co-supervisor: Dr Stefano Corbella

Abstract

Global warming and sea level rise are some of the greatest threats humanity faces today with low-lying coral reef islands most vulnerable to these threats and their repercussions.

This study focuses on the mechanisms that have resulted in the severe erosion of low-lying coral reef islands. Mnemba Island, a small island off the north-east coast of Zanzibar is used as a case study. It is a premium high value resort that is currently experiencing severe erosion. The erosion has resulted in the collapse of various structures and utilities littering the eastern beach with debris and fallen Casuarina trees which dominate the Island's eastern border.

Mnemba Island is a typical low-lying island surrounded by a coral reef platform. This study identified the key role these reefs play in wave attenuation and protecting the island from the large swell that surrounds the reef. The reef crest was found to attenuate wave heights by up to 70%. Overfishing and changes in the climate have resulted in the destruction of the coral reef communities that protect the island because of their increase hydraulic roughness and shallowness. Modelling shows that the impact of reduced bed roughness from coral degradation and just 10 cm sea level rise can result in up to 40% increase in wave height at the Island's eastern beach. Coupled with the large tidal range and increased wave heights propagating over the reef platform, wave driven forces and currents are enhanced thus disturbing the quasi-equilibrium wave climate resulting in major erosion. The fine sediments are lifted into the water column and transported into deeper sections of the reef platform. The low wave energy in the following seasons is insufficient to overcome the critical shear stresses that lift the transported sediments back into the water column and hence, a net loss of sediment off the reef platform is experienced.

Declaration

I, Curtis Russell Swanepoel, declare that this thesis in its entirety is my own and has not been submitted in part or in whole to any other University. Work taken from others has been acknowledged and adequately referenced in the text. The field work was carried out in Zanzibar and the succeeding research and results compilation was completed in the Civil engineering department of the University of KwaZulu Natal. The research was done under the supervision of Professor D. Stretch and Doctor S. Corbella.

Curtis Russell Swanepoel Date

....

As the candidates supervisor, I approve this Dissertation for submission.

Prof. D. Stretch Date

....

Dr. S. Corbella Date

....

Acknowledgments

My deepest gratitude to Professor D. Stretch and Doctor S. Corbella for choosing me as the candidate for this research. Allowing me the opportunity to travel to Mnemba Island to conduct the relevant experiments and research for two months. Your guidance, motivation and push for excellence was invaluable.

To Dr. K. Tirok for the programming guidance without which I would have surely lost hope.

To the directors of &Beyond for funding and allowing me to stay on Mnemba Island and to the staff who went above and beyond to ensure my stay was more than comfortable. Your constant support and unfaltering kindness made the field work both a success and a joy.

To my family, girlfriend and friends for their undying support and motivation throughout.

To each and all of you, I am truly grateful.

Contents

List of Figures

List of Tables

Nomenclature

δ	Boundary layer thickness
η	Surface elevation
γ	Breaker index
λ/L	Wavelength
ω	Angular velocity
ρ	Salt Water density at 1025 kgm^{-3}
τ_b	Bed shear stress
τ_max	Maximum bed shear stress
θ	Wave angle at breaking line
ε	Grain size
ξ	Iribarren number
a	Amplitude
A_i	Cross-sectional area of trap
C	Wave speed
D_{50}	Median Grain size
D_{90}	Ninetieth percentile Grain size
E	Wave energy
E_f	Wave energy flux
f	Frequency
f_c	Wave energy dissipation factor
F_D	Drag force
F_G	Gravitational force
F_i	Sediment flux through trap
F_L	Lift force
f_w	Wave friction factor
g	Gravitational acceleration at 9.8 ms^{-2}

H	Wave height
h	Water depth
H_0	Wave Height in Deep water
H_b	Wave Height at breaking point
h_b	Water depth at breaking point
$H_{s,b}$	Signigicant Wave Height at breaking point
k	Wave number
L_0	Wave length in Deep water
N	Number of streamer traps
n	Ratio of group velocity and phase velocity
r	Hydraulic roughness
T	Period
t	time
T_p	Peak period
U	Amplitude of bed velocity variations
u	Instantaneous bed velocity
x	Distance

Acronyms

SLR	Sea Level Rise
NASA	National Aeronautics and Space Administration
MSL	Mean Sea Level
LST	Long-shore Sand Transport
UV	Ultra-violet
GSC	Geosynthetic Container
ERA	European Reanalysis
EACC	East African Coastal Current
GPS	Global Positioning System
GLM	Generalized Lagrangian Mean
GEBCO	General Bathymetric Chart of the Oceans
PVC	Polyvinyl Chloride

Chapter 1

Introduction

1.1 Motivation

Sea level rise is one of the greatest challenges humanity faces today. Densely populated coastal regions, constantly expanding infrastructure and economic stability are all vulnerable to the dynamic coastlines. Melting of the polar ice-caps and the thermal expansion of water are the drivers of global sea level change and its growing threat. Satellite sea level observations from National Aeronautics and Space Administration(NASA) show a global rise of $\approx 3.4 mm year^{-1}$ with most projections showing just under one metre of sea level rise by the end of the twenty-first century. New research pubished by DeConto, and David (2016) paint a more gloomy image, with higher end predictions of greater than one metre and up to 15m by 2500. The evident threat of sea level rise is already being realized and low lying coral reef islands are most vulnerable to this.

Low lying islands (less than four metres above sea level) that litter tropical regions are typically accompanied by diverse coral reef ecosystems which are home to up to 25% of marine life on the planet. Besides the obvious need for protection of such ecosystems, the Islands themselves can be home to families like the 25 families that live on Nuatambu which is one of Solomon Islands. Nuatambu Island was measured at approximately 30,000 square metres in 1962, in 2014 it had an area less than 14,000 square metres. Tropical coral islands are also often home to luxurious resorts on which local economies are heavily dependent. Mnemba Island off the north-east coast of Zanzibar is one of such islands and is the focus of this thesis. Mnemba Island has experienced severe erosion over the last 20 years threatening the future of Island.

The threat to low-lying coral islands is not so much from sea level rise itself but from the changing hydrodynamics that accompany sea level rise. The changing wave climate disturbs the coastal equilibrium and reduces the Island's ability to recover. By understanding the wave hydrodynamics and sediment processes, coupled with in-situ measurements, it is possible to model and predict the survivability of these low-lying coral islands and identify possible coastal protection schemes.

1.2 Research Questions

Research Questions can be broken into two main components.

- What are the mechanisms of severe erosion of low-lying coral reef islands in a changing climate regime?
- What possible protection schemes can be implemented?

1.3 Aims

This study used a case study comprising of a combination of field work and numerical modelling to address the research questions.

- The aim of the field work was to obtain sufficient data on the sediment transport, local bathymetry and wave characteristics surrounding the island in an attempt to understand the cause of the erosion on site.
- To enable the setup and calibration of a model.
- To use a numerical model to supplement the field work and thereby help interpret and extrapolate the field data to further underpin the answer to the research questions.

1.4 Objectives

The objectives of this thesis can be broken into field work and overall objectives.

Field work objectives included:

- To measure the profiles along the eastern Side of the Island and measure their changes over a certain time period.
- To measure sediment transport rates and directions using a sand-trap point collection method along with a timber groyne impoundment method.
- To measure local wave data including currents by means of pressure sensors placed at different places in the reef.
- To determine the attenuation effect of the reef as waves pass over it.
- To measure bathymetry surrounding the entire Island.

The overall objectives included:

- Use the field work transects to build the full reef bathymetry surrounding Mnemba Island.
- Use the measured beach profiles to match the model beach profiles and the real profiles. This and the preceding objective are important tasks in creating a model that accurately simulates real world conditions that the wave and sediment transport are dependent on.

- Create a model that simulates the wave-breaking at the reef crest and and wave propagation over the reef flats to mimic the wave climate over coral platforms.
- Use the model forcing conditions to simulate sediment transport to identify net transport volumes and direction.
- Determine the effect of sea level rise and coral degradation on wave attenuation and sediment transport to assess the future of low-lying coral reef islands.
- Provide recommendations on coastal protection schemes that could increase the survivability of these islands.

1.5 Dissertation Outline

Chapter 2 describes the coastal dynamics and processes responsible for the shaping the coastal zone and previous research into the erosion and wave attenuation on Islands with fringing coral reefs. A thorough understanding of the processes involved are required to accurately model the conditions and analyze the results.

Chapter 3 explains why field work and modelling were used to address the research questions followed by the location and climate of the case study, the field work methodology and the model selection and setup.

Chapter 4 describes the field work results.

Chapter 5 presents the model results which are critically analysed and compared to the field work results and existing literature. The effect of the coral reef roughness on wave attenuation and sediment transport is identified along with the impact of SLR.

Chapter 6 presents the conclusions drawn from the results and recommendations on coastal protection schemes. Recommendations for further research is also included.

Chapter 2

Literature review

Chapter 2 begins with the wave generation, propagation and transformation theory followed by the near-shore hydrodynamics and the responding sediment transport. Coral reef properties are then discussed followed by the review of literature relating to wave attenuation over fringing reefs and the affect of sea level rise on these low-lying coral islands.

2.1 Ocean Waves

All surface oscillations generated in the ocean can be described as ocean waves. Mean sea level (MSL) is the sea level when you average out all these sea surface variations. Short wind generated waves and long tidal waves play the most significant part in shaping the coastal zone and are hence the focus in this thesis.

In 1774 Benjamin Franklin said:'Air in motion, which is wind, in passing over the smooth surface of the water, may rub, as it were upon that surface, and raise it into wrinkles, which, if the wind continues, are the elements of future waves.' In other words, the frictional stress that is created when wind interacts with the ocean surface results in a transfer of momentum and energy which disturb the water particles. This disturbance, along with gravity as the restoring force, creates the orbital path of the particles which translates to an oscillating water surface.
Linear wave theory describes the surface elevation (η) according to

$$\eta(x,t) = a(\omega t - kx) \tag{2.1}$$

where (a) is the amplitude, (ω) is the angular velocity and (k) is the wave number according to

$$\omega = 2\pi f \quad k = \frac{2\pi}{\lambda}$$

.

The simplest way of representing the surface elevation is the sine function shown in Figure 2.1. Here certain parameters are defined which describe the wave. Wave Height H is the vertical distance between the wave crest and trough. Water depth h is the distance from the sea bed to the still water level. Wavelength λ is the distance between two successive peaks or troughs and the ratio between the wave height and wavelength defines the wave steepness $\frac{H}{\lambda}$. The wave speed or celerity C is the speed which the wave propagates in the direction of motion. The period T is the time it takes for a wave to pass a point and the reciprocal of which is frequency f.

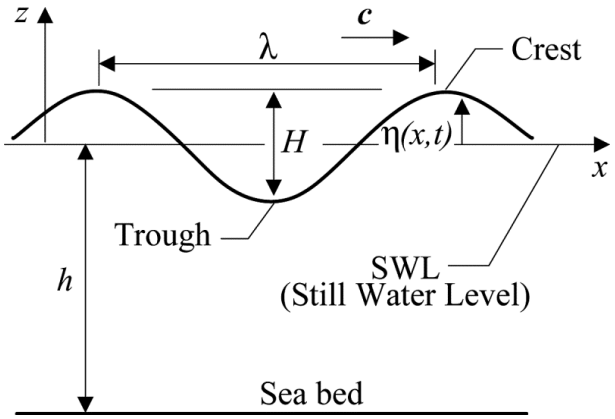

Figure 2.1: Simple representation of ocean surface. Source: (Brown et al., 2008)

Harold Jeffreys (1925) suggested that waves obtain energy from pressure differences created by the sheltering effect shown in Figure 2.2. The rear face, where the wind blows against, experiences a higher pressure than the front face which is sheltered by the waves crest. Air eddies formed in front of the wave lead to excesses and deficiencies of pressure which are then responsible for pushing the wave along (Brown et al., 2008). This theory failed to explain the formation of very small waves but holds true when:

- wind speed is greater than 1 ms^{-1},
- wind speed exceeds wave speed, and
- waves are steep enough to have a sheltering effect (Brown et al., 2008).

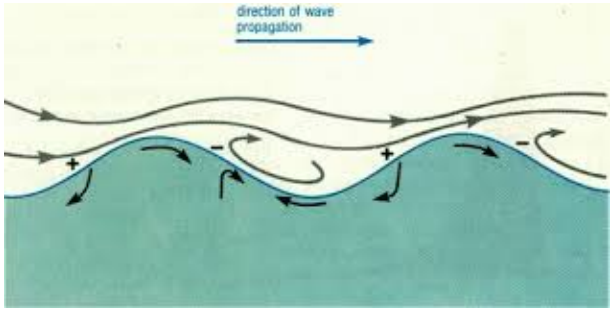

Figure 2.2: Jeffrey's sheltering hypothesis on wave generation (Positive sign indicates excess pressure). Source: (Brown et al., 2008)

2.2 Wave transformation

A fully developed sea is an idealized situation where size and characteristics of waves are constant. In reality wind variations produce wave variations creating a wave field which then propagates away from the point of generation. The deep-water waves that have the greatest wave length and longest periods are those which travel fastest and the separation of waves based on different travel rates is known as dispersion. As waves propagate from deep water into shallow water they begin to interact with the seabed. This interaction slows and transforms the wave, i.e wave height, length and direction change through a number of processes until the wave eventually breaks and loses all of its energy.

2.2.1 Shoaling

When waves propagate into shallow water with depths less than half the wavelength, the interaction with the bottom yields a decreased wave speed and wavelength according to the dispersion relationship

$$C = \sqrt{\frac{g\lambda}{2\pi}} \tag{2.2}$$

where g is the acceleration due to gravity at (9.8 ms^{-2}) and C is the wave speed in (ms^{-1}). This decrease leads to an increase in energy per unit area of the wave and so the wave height increases. Wave energy is possessed in two forms, kinetic and potential. Kinetic energy is present in the orbital motion of the water particles and potential energy is the result of the particles being displaced from their equilibrium position. The total energy(E) per unit area of the wave is given by

$$E = \frac{1}{8}(\rho g H^2) \tag{2.3}$$

where ρ is the water density (kgm^{-3}) and energy(E) is measured in Joules per square metre (Jm^{-2}). The asymmetrical nature of the waves create asymmetrical forces which play a great role in near shore sediment transport.

2.2.2 Wave Refraction

When an obliquely incident wave approaches the shore at an angle, the sections of the wave in the deeper water travel faster than those in the shallow causing the wave crest to turn toward the depth contours. This is shown in Figure 2.3. Wave angle is a major factor in sediment transport formulas and can thus enhance or diminish longshore transport rates.

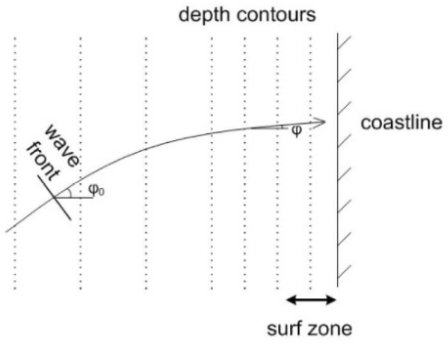

Figure 2.3: Obliquely incident wave turning towards depth contours. Source: (Bosboom and Stive, 2012)

The same phenomenon is observed when waves pass over coral reefs. Elliptical shaped coral reefs promote refraction and convergence of waves which have significant implications on sediment transport. Mandlier (2013) showed that reef configurations that promote wave convergence are more likely to retain sediments on the reef surface whereas reef platforms that promote less refraction have a higher risk of sediment loss over the leeward reef sections.

2.2.3 Wave Diffraction

Diffraction occurs when the wave interacts with a obstruction like an Island, breakwater or an abrupt change of depth (Dean and Dalrymple, 2004). Figure 2.4 shows the wave interaction with an impermeable breakwater. A part of the wave is reflected by the structure whilst the remainder of the wave bends around the obstacle into the shadow zone. The wave crests decrease in size as they extend in the shadow zone of the structure.

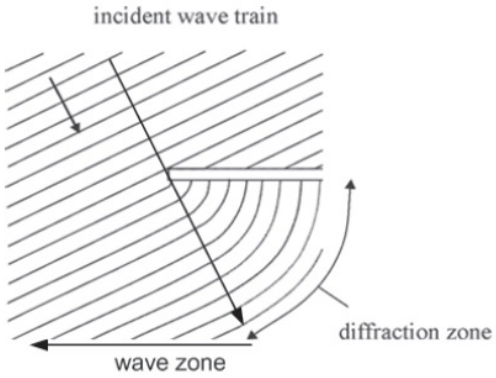

Figure 2.4: Diffraction of incident wave train. Source: (Bosboom and Stive, 2012)

2.2.4 Wave Breaking

Miche (1944) described wave breaking in terms of a limiting wave steepness. A point where particle velocity exceeds the wave crest velocity and the wave becomes unstable and breaks. In deep water this limiting steepness known as white-capping is given by

$$\left[\frac{H_0}{L_0}\right]_{max} = 0.142 \approx \frac{1}{7} \tag{2.4}$$

where the subscript '0' denotes deep water conditions. The shallow water limiting wave steepness is given by

$$\left[\frac{H}{L}\right]_{max} = 0.142\frac{2\pi h}{L} \approx 0.88\frac{h}{L} \tag{2.5}$$

which is equivalent to the breaker index (γ) given by

$$\gamma = \left[\frac{H}{h}\right]_{max} = \frac{H_b}{h_b} \approx 0.88 \tag{2.6}$$

where the subscript 'b' denotes breaker condition. The breaker index shows that in the near-shore zone when the wave height reaches a certain fraction of the water depth, a depth induced breaking ensues.

Battjies (2011) showed that the iribarren number (ξ) guides the breaking process. Shown in Equation 2.7 ,the iribarren number (otherwise known as surf similarity parameter) is a dimensionless number that represents the ratio between the bed slope steepness and the wave steepness.

$$\xi = \frac{tan\alpha}{\sqrt{\frac{H_0}{L_0}}} \tag{2.7}$$

Typical values and their respective breaker type are shown in Figure 2.5. Surging breakers occur on steep sloped shores with minimum energy dissipation as majority of the wave energy reflected back into deeper water. The curling crest that breaks over the shallow trough on a moderately sloped beach is indicative of a plunging wave. Large-scale energy dissipation occurs in the turbulent zone often creating a new wave as it moves toward the shore. The collapsing wave lies between the surging and plunging wave. The crest does not break but the lower half of the wave steepens and becomes unstable. The spilling breaker occurs on flat beaches where during breaking, a thin turbulent water line develops at the crest spilling down the face of the wave. This generally lasts for a long time as a result of the slow energy dissipation rate.

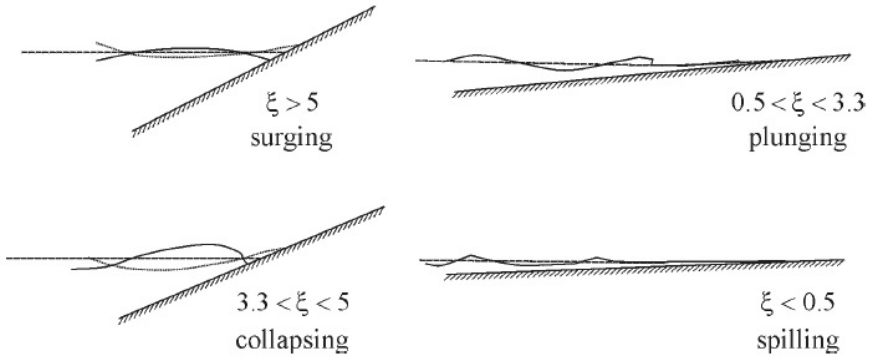

Figure 2.5: Different breaker types. Source: (Bosboom and Stive, 2012)

2.3 Wave-induced Hydrodynamics

Beneath the surface the water particles' orbital path becomes more elliptical and flattens at the bed. The oscillatory flow at the bed for wave conditions of any significance is always fully developed rough turbulent flow (Nelson, 1996). Rough turbulent flow occurs when the roughness is larger than the 'laminar' sub-layer. The flow over the bed experiences a shear stress which can set sediment grains into motion as the wave energy is dissipated.

In this area the friction factor is only a function of the relative roughness ($\frac{r}{a}$), where r is the hydraulic roughness and a is the amplitude of the oscillatory wave motion at the bed (Nelson, 1996).

2.3.1 Bed Shear stress

Wave friction factor

Jonsson (2011) developed the wave friction factor (f_w) to determine the bed shear stress. It is a dimensionless parameter used to determine the maximum bed shear stress (τ_{max}) due to horizontal oscillatory water particle velocities. In comparison to the current friction factor which relates the bed shear stress to the depth-averaged velocity, the wave friction factor relates the bed shear stress to the free-stream velocity. The maximum bed shear stress for linear waves is given by

$$\tau_{max} = 0.5\rho f_w U^2 \tag{2.8}$$

where U is the amplitude of the bed velocity variations. Determination of the friction factor for rough bed and turbulent flow is less straight forward as aspects like bed material and structure need to be considered.

Wave energy dissipation factor

The wave energy dissipation factor (f_e) is defined in terms of the time averaged rate of wave energy dissipation due to bed friction. (f_e) can be evaluated by considering the total wave energy and its characteristics spectral parameters or based on individual frequency components. Whence

$$\frac{dE_f}{dx} = (\tau u)_{mean} = \frac{2}{3\pi}\rho f_w U^3 \tag{2.9}$$

where E_f is the Wave energy flux, τ is the instantaneous bed shear stress, u is the Instantaneous bed velocity, U is the amplitude of bed velocity variations and x is the distance in direction of wave propagation.

It has been shown by various authors that for fully developed rough turbulent flow ($f_w \approx f_e$) making the two interchangeable (Jonsson, 1963),(Swart, 1974),(Nielsen, 1992). This is important in the determination of coral reef hydraulic roughness.

2.3.2 Radiation stresses

The momentum carried by propagating waves can be thought of as mass in motion or flux. There is only a contribution to momentum between the crest and trough because below the trough the velocity varies harmonically. Radiation stress is the depth-integrated flux of momentum. Wave momentum fluxes are proportional to wave energy and thus wave breaking creates imbalances. To restore the balance, wave breaking forces in surf zone act in the direction of propagation. This can result in lowering or raising of the mean water level along with driving a long-shore current when waves approach the shore obliquely (Bosboom and Stive, 2012).

When considering a vertical plane perpendicular to wave propagation, there are two radiation stress components from the wave induced horizontal flux of momentum. These are the transfer of momentum ($\rho\vec{u}$) through the plane where the particle velocity is normal to the plane and the wave induced pressure force that acts on the plane, both of which are shown in Figure 2.6.

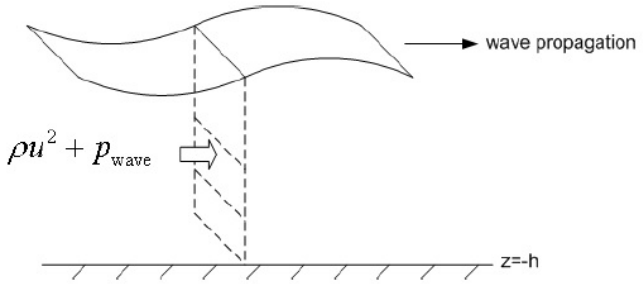

Figure 2.6: Wave-induced horizontal flux of momentum through a vertical plane perpendicular to wave propagation. Source: (Bosboom and Stive, 2012)

The general expressions for the radiation stress for waves traveling in a direction θ relative to the positive x-direction (parallel to wave propagation) are

$$S_{xx} = Normal\ \ stress\ \ in\ \ x-direction = (n - \tfrac{1}{2} + ncos^2\theta)E \tag{2.10}$$

$$S_{yy} = Normal\ \ stress\ \ in\ \ y-direction = (n - \tfrac{1}{2} + nsin^2\theta)E \tag{2.11}$$

$$S_{xy} = S_{yx} = Shear\ \ stress = ncos\theta sin\theta E \tag{2.12}$$

where n is the ratio of the group velocity and the phase velocity ranging from 0.5 in deepwater to 1 in shallow water.

2.3.3 Cross-shore balance

The magnitude of the radiation stress S_{xx} depends on wave height, wavelength and water depth. Referring to Equation (2.10), an increase in n as depth decreases results in an increased S_{xx} in the shoaling region. The increased S_{xx} in the landward direction requires a seaward directed resultant force to achieve equilibrium in the water column. Equilibrium is reached by a slight difference in water level with the landward side being the lower of the two, this is wave set-down and it occurs outside the breaker zone.
Radiation stress S_{xx} decreases rapidly in the surf zone during wave breaking, this results in a landward directed force. To achieve equilibrium once again, the landward side of the water column must be higher to create a seaward directed pressure, this phenomenon is called wave set-up. Both set-up and set-down are illustrated in Figure 2.7.

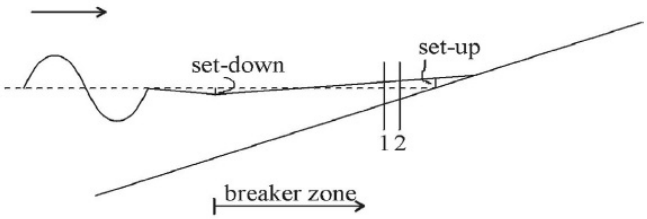

Figure 2.7: Wave set-down and set-up. Source: (Bosboom and Stive, 2012)

The coastline acts as a closed boundary and hence there must be a return current below the trough level to compensate for the flux above the trough level. This return current is called undertow and is important for seaward sediment transport because of its relatively high seaward directed velocity in the lower water column (Bosboom and Stive, 2012).

2.3.4 Alongshore Balance

The transfer of momentum from the obliquely approaching wave motion to the mean water flow creates a long-shore current. However, unlike in the cross-shore direction, there is no hydraulic pressure gradient that can occur in the uninterrupted alongshore direction to restore equilibrium (Bosboom and Stive, 2012). The restoring force is thus supplied by bed shear stress $\vec{\tau_b}$ as shown in Figure 2.8. The long-shore current, broken into segments based on position in the cross-shore direction, is an important factor in long-shore sediment transport calculations.

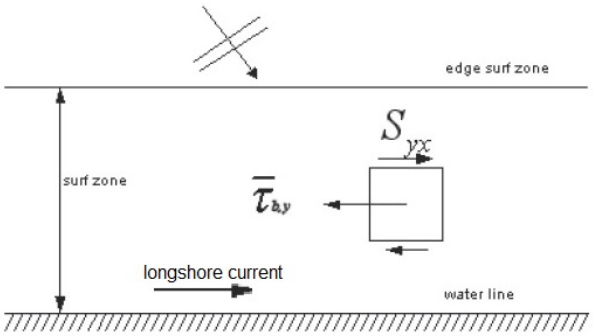

Figure 2.8: Forces on the water column. Source: (Bosboom and Stive, 2012)

2.4 Tides

Tides are long-period waves generated by the gravitational force of the moon, and to a lesser extent the sun, on the oceans. It varies periodically based on the position on Earth relative to the moon and sun resulting in tidal cycles of low and high water levels.
Primary control of the tide is the lunar cycle of 24 hours and 50 minutes creating either a Diurnal or semi-diurnal tide based on the location of the earth. A Diurnal tide consists of a single low and high tide per day with semi-diurnal consisting of two of each per day. There is a distinct variation of the tidal range every fortnight coinciding with the alignment of the earth-moon-sun system. This particular alignment results in a Spring tide where the tidal range is higher than average. Neap tide occurs when the earth-moon-sun system are at right angles to each other resulting in a lower than average tidal range. Tidal range can vary from a few centimetres up to 15 metres and can be broken into:

- Microtidal Range<2m
- Mesotidal 2m<Range<4m
- Macrotidal Range>4m

The effect of macro tides on coastal erosion and beach dynamics has been the topic of many studies. Spring tides and the rising tide are generally linked to erosion events whilst neap and falling tides are linked to accretion (Chee et al., 2014). Tidal induced currents can be the major contributor to sediment transport in areas like reef flats, sheltered bays and estuaries where wave action is minimal. High tides can also allow waves to propagate over reef flats that are exposed during low tides. Figure 2.9 shows the global tidal ranges.

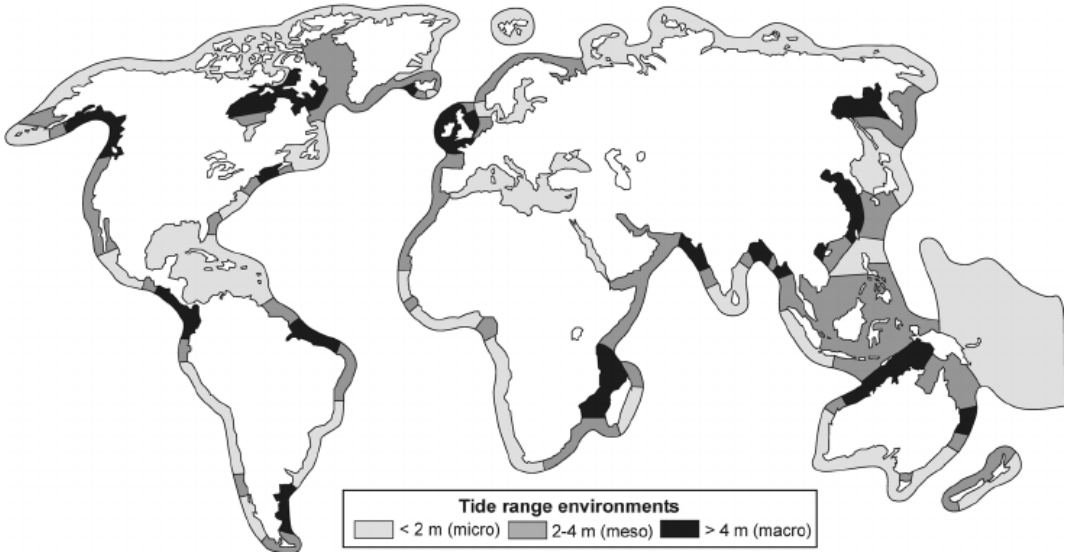

Figure 2.9: Tidal range Global Map. Source: (Brown et al., 2008)

2.5 Sediment Transport

2.5.1 Sediment Properties

In the coastal zone the sediments found are a result of physical and chemical weathering or of biological origin (coral remains, molluscs and other shell organisms). The most common products of weathering are Quartz and clay which make up a large portion of ocean sediments (Brown et al., 2008). Where terrigenous sediments are scarce, shallow-water carbonates accumulate, creating the fine, white sandy beaches that are typical of tropical coastal regions. Carbonates and quartz sediments are non-cohesive whereas clay is cohesive due to it's chemically active surface area. Clay sediments can increase the overall cohesiveness of the bed even when they constitute only a small part of the total sediment which in turn makes it more difficult for sediments to be eroded. Figure 2.10 shows how sediments are classified according to their diameter.

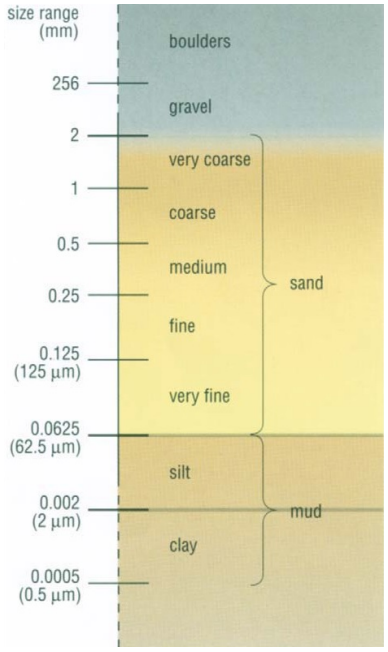

Figure 2.10: Sediment size distribution. Source: (Brown et al., 2008)

Important sediment properties with regard to sediment transport include:

- **Grain size** = the median particle diameter (d_{50}) is an important input factor in transport rate calculations.
- **Grading** = The distribution of grain sizes.
- **Shape** = Particle shape affects how they lock into each other either increasing or decreasing the required erosive force to set the particle into motion.
- **Density** = Which depends on the mineral composition.
- **Fall velocity** = The velocity with which particles settle is called the fall velocity (W_s) and affects the transport rate of sediments. When there is a large concentration of suspended particles, the upward movement of the fluid as the particles settle hinders the settling of surrounding particles slowing them down.

2.5.2 Initiation of Motion

Sediments can only move if the water exerts a large enough shear stress on the grains, the critical shear stress ($\tau_{b,cr}$) describes the point where motion is initiated. The forces acting on the grain can be broken into a lift, drag and gravity force as shown in Figure 2.11.

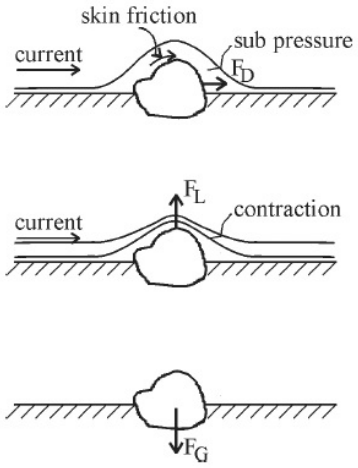

Figure 2.11: Forces acting on an individual grain. Source: (Bosboom and Stive, 2012)

The lift force is created by the separation and contraction of flow over the grains. The higher velocity according to Bernoulli creates a lower pressure resulting in lift due to the differential pressure. The drag force is a combination of skin friction and differential pressures upstream and downstream of the grain and like the lift force is proportional to the particles surface area and the shear velocity squared.

Once motion is initiated, transport can occur in 4 different modes namely sliding, rolling, saltation and suspension. Sliding and rolling grains are continuously in contact with the bed as they move as named whereas saltating grains skip along the bed. These three make up the bed load and the suspended load is made of particles kept in suspension by turbulence which move irregularly in the water column until deposition.

2.5.3 Long-shore Transport

The induced alongshore currents discussed in Section 2.3.4 are the drivers of long-shore sand transport (LST). Typically a dynamic equilibrium occurs, where sediments transported down the coast are naturally replaced with those from up the coast. Although sediments in the long-shore can move both up and down the coast based on seasonal wind and wave directions, the prevailing conditions result in a net littoral drift. The cross-shore distribution of LST has three separate zones, namely the incipient breaker zone, inner surf zone and the swash zone. Transport in the breaker zone as expected was influenced by the breaker type. Transport in the inner surf zone indicated that wave height was the main factor. Transport in the swash zone which accounts for significant part of total transport was found to show dependence on wave height, period and beach slope Smith et al. (2009).

On steep beaches the long-shore transport by swash and backwash is more dominant than transport caused by long-shore currents. The swash from obliquely breaking waves drives sediment up the beach face at an angle to the shoreline. The backwash then drags the sediment back at right angles to the beach, this swash and backwash result in a zig-zag pattern which moves sediment along the beach.

Coastal structures like breakwaters and groynes interrupt the natural littoral drift and starve the beaches down-drift of the structure. Figure 2.12 shows an example of sediments being trapped by the structure and being eroded away down-drift of it. The use of coastal structures thus requires careful and thorough investigation into the effect the structure will have on the beach.

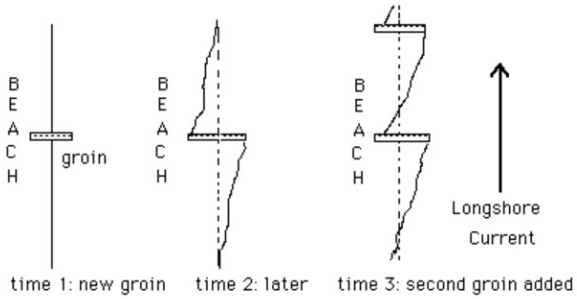

Figure 2.12: The effect of coastal structures interrupting the littoral drift. Source: (Bosboom and Stive, 2012)

2.5.4 Long-shore transport rate

CERC

The estimation of LST and understanding the cross-shore distribution is essential to ensure long term beach stability. The most widely used LST formula is the CERC equation (Shore protection manual, 1984). This method takes into account both the bed and suspended load and is based on the principle that LST is proportional to wave power per unit length of beach (Rijn, 2002). Developed by the US NAVY CORPS, the CERC formula does not take into account the particle size or beach slope and is given by

$$Q = \frac{K}{16\sqrt{\gamma_b}} \rho g^{\frac{3}{2}} H_{s,b}^{\frac{5}{2}} \sin(2\theta_b) \tag{2.13}$$

where Q is the long-shore transport rate (immersed weight),K is an empirical coefficient, $H_{s,b}$ is the significant wave height at the breaker line and θ_b is the wave angle at the breaker. The value for K has been a topic of much debate. The shore protection manual recommends a value of $K = 0.77$ however this value over predicts measured transport rates for particles sizes ranging between 0.2mm and 0.6mm and beach slopes where $\tan(\beta)$=0.01 - 0.1 (Rijn, 2002). For design applications where sufficient field data is available, K can be calibrated yielding long-shore transport rates with reasonable confidence upwards of 50 percent of measured rates (Smith, Wang, and Zhang, 2003). The CERC formula cannot be applied when tidal current velocities are significant and is thus not applicable on areas like tidal flats with high tidal ranges. Rijn (2002) found that the CERC formula also yields results too large for measured values from high energy events and far too large for low wave conditions.

Kamphuis

Measured field data is unrepeatable and has many uncertainties. Using physical models, kamphuis developed a relationship for estimating LST rates applicable to both field and model data, this equation is given by

$$Q = 2.33(T_p)^{1.5}(\tan\beta)^{0.75}(d_{50})^{-0.25}(H_{s,b})^2|\sin(2\theta)^{0.6}| \tag{2.14}$$

where Q is the LST rate of underwater mass in (kgs^{-1}), T_p is the Peak wave period seconds) and $\tan(\beta)$ is the Beach slope in degrees. By including the effects of the bed slope and grain diameter it resulted in a much refined equation but still with inaccuracies during storm events and low wave conditions.

2.5.5 Cross-shore Transport

Cross-shore transport is a result of water motion due to waves and undertow. The onshore and offshore directed forces created during wave breaking are referred to as constructive and destructive respectively. On most beaches an equilibrium occurs over a period of months to years with off-shore being dominated during high energy events and on-shore movement during non-storm conditions (Davidson-Arnott, 2010).

Referring to Figure 2.13 of the velocity profile, close to bed net flow is onshore whilst 10-20cm above the bed the net flow is offshore and above the wave troughs is generally onshore. So for sediment to get into the off-shore flow zone their needs to be sufficient energy to suspend the particles high enough in the water column.

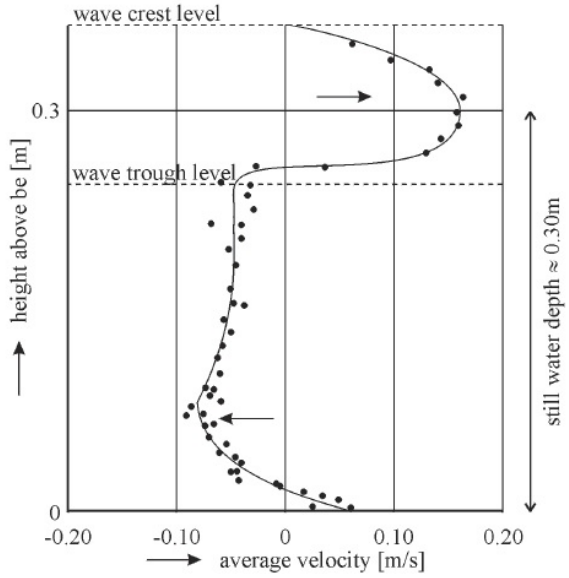

Figure 2.13: On-shore and off-shore velocity distribution. Source: (Bosboom and Stive, 2012)

2.5.6 Field Measurement of Long-shore and cross-shore transport

There are many instruments available for measuring suspended sediment transport on coastal environments. These include optical samplers, acoustic samplers and pump samplers but the focus in this thesis is on mechanical methods like the streamer trap.
Streamer sand traps are a point collection method that collect sediments at specific locations over defined time limits. The name is derived from long sieve cloth bags that stream out in the current and trap sediment whilst allowing water to flow through. The streamer developed by Krauss (1987) shown in Figure 2.15 consists of a polyester mono-filament sieve cloth attached to a streamer mouth frame. The streamer and mouth frame are then attached to a stainless steel rack.

Polyester mono-filament was chosen as it does not stretch or degrade in sea water and the end of the streamer bag is tied to trap the sediments that enter. Several streamers can be used at once in order to measure both bed and suspended load. The mouth opening is directed opposite to the current direction and the trap is held in place by the user.

Advantages of this method include:

- Traps provide absolute measurement.
- Traps provide transport rates over minutes and seconds and thus can be related directly to specific waves and currents that caused the sediment to move.
- Traps can measure sediment distribution in the water column (Bed load and suspended load).
- Traps are light & portable and many can be deployed simultaneously.
- Simple to use and easy to construct, requiring little maintenance.
- Trapped sediments can be weighed quickly and easily in the field.

Disadvantages include:

- Limited to wave conditions of $\approx 1m$. This is so users can hold them firmly in place whilst getting hit by waves as shown in Figure 2.14.
- Eddies created as currents & waves flow past the device and user can cause the streamer to wrap around the rack, blocking sediments from entering.
- Streamers measuring the bed load can cause scour and create extra suspended sediments.

Figure 2.14: KRAUSS streamer sediment trap in surfzone. Source: (Krauss, 1987)

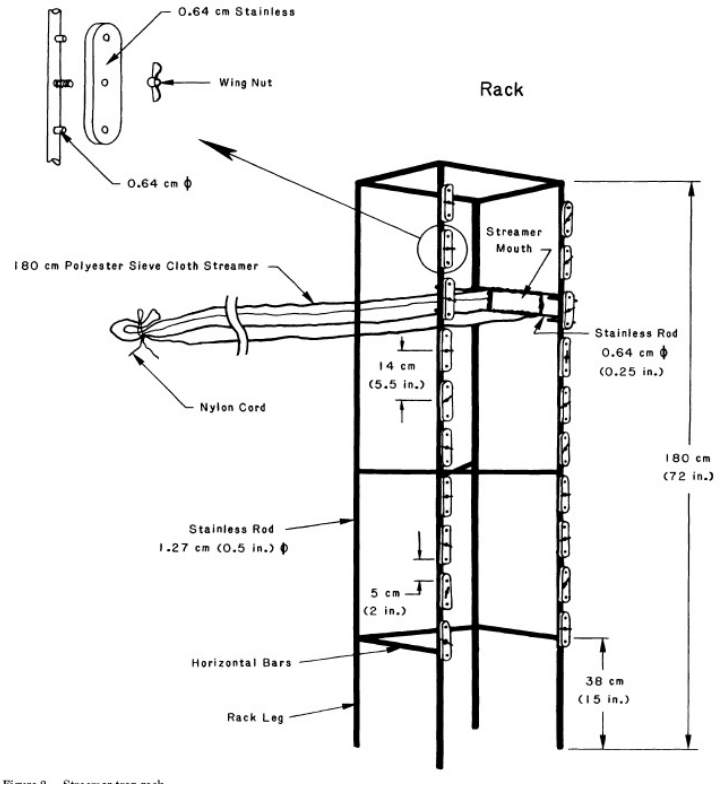

Figure 2.15: KRAUSS streamer sediment trap design. Source: (Krauss, 1987)

The calculation of LST rate from the streamer traps is done by integrating the measured sediment flux both vertically and horizontally. The sediment flux between two adjacent streamers is given by

$$\delta F_i = \frac{(\frac{F_{i+1}}{z_{i+1}} + \frac{F_{i-1}}{z_{i-1}})}{2} \delta Z_i \tag{2.15}$$

where F_{i+1} and F_{i-1} are the sediment fluxes through the upper and lower traps and z_{i+1} and z_{i-1} are the vertical width of the opening of the upper and lower traps respectively. δZ_i is the vertical distance between mounted traps (Krauss, 1987).
The sediment flux at one trap array I is then found by summing the sediment flux from each trap and the flux between adjacent streamers

$$I = \sum_{i=1}^{N} (F_i) + \sum_{i=1}^{N-1} (\delta F_i) \tag{2.16}$$

where N is the number of streamers on the trap. Finally the LST rate can be found using

$$Q = \sum \frac{I_i + I_{i-1}}{2} A_i \tag{2.17}$$

where I_i is the sediment flux measured at trap array i and A_i is the cross sectional area between traps I_i and I_{i+1}. The value can then be converted to cubic metres per year.

Measurement of the Bed load transport can be done using the temporary impoundment method. Temporary groynes can be constructed out of local sourced materials like timber and are used to obstruct the flow and either result in an accretion or erosion of sediment on a particular side of the structure, providing an indication of the direction of sediment movement. The main advantage of the impoundment method is that it can encompass high wave energy events, provided the structure is not up-rooted. Disadvantages include escaped sediments and poor surveying techniques. Figure 2.16 shows an example of a timber groyne and how sediments have been trapped indicating a transport direction from right to left of image.

Figure 2.16: Temporary timber groyne illustrating transport direction from right to left of image

Both streamer traps and the groyne impoundment method were utilised in the Case study of this thesis as further detailed in 3.5.2.

2.6 Coral reefs

Coral reefs are living organisms, their hard structure is built in layers through the continuous secretion of calcium carbonate by the coral polyps. These hard structures form the foundation for further growth and over time coral colonies group together to form a reef (Knowlton, 2016). They are typically found in shallow tropical climates, preferring warm and clean water between 2-30 metres. Reef type can be determined by its structure and are defined in Table 2.1 and illustrated in Figure 2.17.

The greatest threats to coral reefs are water temperature rise, sedimentation and ocean acidification alongside more direct coral destruction through over-fishing and over-harvesting. Higher temperatures from global warming result in coral-bleaching, a process in which coral lose the microscopic algae needed to produce food for the coral, effectively starving the coral. Sedimentation results in coral smothering as the increase in concentration of suspended particles reduce the light available for photosynthesis and coral growth. Increased acidity reduces the coral's ability to build their hard calcium carbonate structure leaving the coral weak,brittle and vulnerable. Over-fishing and over-harvesting decimate coral colonies and vessels/ methods used contribute even further through coral scaring by collisions with anchors and boats (Knowlton, 2016).

Table 2.1: Different types of reefs based on structure

Reef Type	**Definition**
Fringing	Most Common, grow around islands and continents, separated from shore by shallow and narrow lagoons.
Barrier	Similar to fringing but separated by deeper lagoons, called such because at their shallowest point they can reach the water surface forming a "barrier".
Atoll	Rings of coral with lagoons within them,located off-shore.

(a) (b) (c)

Figure 2.17: Reef types.(a)Fringing.(b)Barrier.(c)Atoll. Source: (Knowlton, 2016)

2.7 Dynamic islands

Low lying coral islands are highly dynamic and adjust their position and shape along with the changing conditions. Recent studies suggest that islands can still grow with these changes and sea level rise (Kench, Owen, and Ford, 2014). Sea level rise as expected would reduce island size through erosion but coupled with fast vegetation growth, eroded and then deposited sediments can also increase the area of the island elsewhere. Maintaining an almost quasi-equilibrium making the island more susceptible to sea level rise. Island growth can also be attributed to the introduction of alien vegetation, through anthropogenic or natural causes, it can quickly push the vegetation line seaward as sediments are trapped. Kench et al. (2015) outlines the future success of some reef islands due to sediment accretion from wave action on atoll islands in the Pacific. It was found that increased wave action during high seas would break reef structures and deposit the coral sediments on the island raising island elevation.

Other processes that follow the erosion on tropical reef islands however typically shift the bias to island size reduction rather than growth. Fallen trees that once trapped sediments create a highly energetic zone when waves collide with them picking up sediments and compounding the erosion rate. The fallen trees themselves also collide with the banks removing further sediment.

Reef islands in the pacific are a strong indication of the future (or lack thereof) that low lying reef islands face. In contrast to the possible growth of Central Pacific Islands found by Kench et al. (2015), are reports of complete island disappearance due to sea level rise. Using historic aerial and satellite imagery and local knowledge,(Albert et al., 2016) identified 11 islands of which 5 have completely disappeared and 6 have severe shore line recession between 1947 and 2014. The higher than global average 7 mm yr^{-1} sea level rise in the last two decades at the Solomon Islands has resulted in decreased wave attenuation over the reefs and increased erosion rates. Sheltered areas protected from wave energy have seen little shore line recession with the sea level rise reinforcing the synergy of wave action and sea level rise in island erosion. Figure 2.18 shows one of the Solomon island's stages of erosion based on satellite imagery.

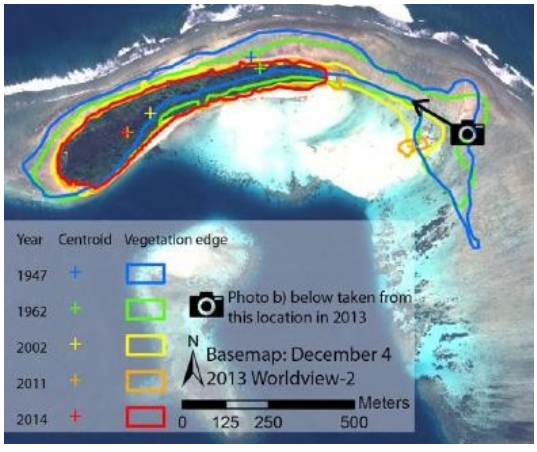

Figure 2.18: Vegetation line recession on one of the Solomon Islands. Source: (Albert et al., 2016).

2.8 Coral reef wave attenuation

With the vulnerability of coastal communities increasing, extensive investments and planning are being made in the use of natural coastal protection schemes. Natural defenses with comparable wave attenuation characteristics as artificial breakwaters.

Ferrario et al. (2014) found that coral reefs made up of a crest and flat as illustrated in Figure 2.19, can reduce wave energy by up to 97% with effectiveness inversely proportional to depth. The reef crest is the seaward edge of the reef, typically shallower than the flats and responsible for the greatest wave dissipation. The fore reef is characterized by steep slope and often almost vertical incline. The reef flat extends from the shore and is characterized by periods of tidal emersion, poor flow circulation and collection of sediments.

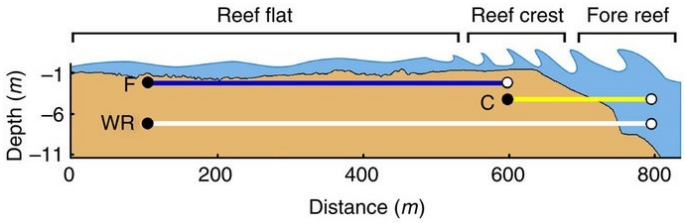

Figure 2.19: Typical reef structure. Source: (Ferrario et al., 2014).

A meta-analysis of 255 studies on coral reefs and wave attenuation was done by Ferrario et al. (2014) in order to qualitatively compare the effects of the different reef environments. It was found that the reef crest dissipated up to 86% of the wave energy due to the induced wave breaking with the flats responsible for 67% reduction of the remaining energy, shown in Figure 2.20. The study also concluded that 50% of wave energy and height reduction on the flat occurred in the first 150 m behind the reef crest.

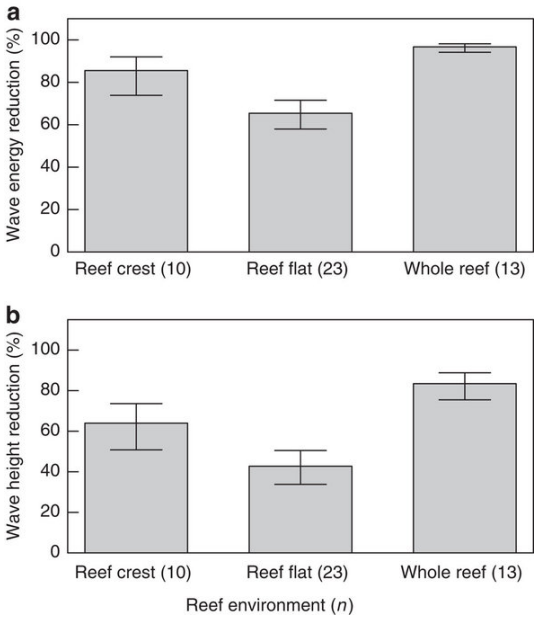

Figure 2.20: Energy and wave height reduction per region. Source: (Ferrario et al., 2014).

After bathymetry, bottom roughness is critical in wave attenuation. Coral degradation results in reduced bottom friction and effectively increased water depth. This decreased interaction with wave troughs allows waves to propagate further without breaking and reach the beach more consistently.

2.9 Hydraulic roughness of coral reefs

Nelson (1997) provided estimates for reef top hydraulic roughness derived from observed transformation of natural waves where bed friction dampening was the only transformation process. On moveable beds (sand) the hydraulic roughness (r) and amplitudes of water motion oscillations (a) at the bed vary depending on wave conditions and thus changes in r are from the variability of the bed. On fixed beds like coral reefs (a) is the only variable. Knowing the invariable roughness, the applicable relative roughness and friction factor can be determined for any water and wave condition(Nelson, 1997).
John Brewer reef in Australia was used for testing by Nelson as depth was constant which eliminated shoaling and refraction. There were no surface piercing obstructions or barriers which eliminated diffraction and the careful selection of wave datasets allowed the elimination of the effects of wave-breaking. Using the fact that wave friction factor is equal wave energy dissipation factor in fully developed rough turbulent flow as outlined in section 2.3.1, Nelson derived an equation for f_e in constant water depth

$$f_e = \frac{3g}{8\pi^2}\frac{H_1 - H_4}{H_1 H_4}\frac{C_g}{\delta x}(T_p \sinh(kh))^3 \tag{2.18}$$

where H_1 and H_4 are two measurement points that lie along the predominant wave direction, δx is the distance between H_1 and H_4 and k is the wave number. Hydraulic roughness estimate can then be found by equating Equation 2.18 with Equation 2.19 developed by Swart (1974)

$$f_e = \exp(5.213(\frac{r}{a})^{0.194} - 5.977) \tag{2.19}$$

The significance of the work by Nelson is the comparable nature of the John Brewer data obtained to other reefs. Obtained roughness values and wave measurements can be used to estimate roughness values of similar reefs (Nelson, 1997). Nelson (1997) also found through the comparison of f_e for movable sand beds and fixed coral reefs that the coral reefs may be no rougher in hydraulic terms than sandy beds under the same depth and wave conditions.

2.10 Sea level rise

Few studies have been done on the response to sea level rise of coral islands ((Grauss and Macintyre, 1998) and (Ogston and Field, 2010b)) as most studies have focused on water acidification and temperature rise effects. Buddemeier and Smith (1988) suggest that coral reef flats may benefit from the reduced air exposure brought upon by rising sea levels if protected from waves and heavy sedimentation.

Tide gauge data for Zanzibar showed large inter-decadal trends of both increasing and decreasing levels according to Partnership (2012). Partnership (2012) used data from the Tanzania Meteorological Agency which showed an increase in Mean high water level for Zanzibar for the period of 1984-2004 (Figure 2.21.

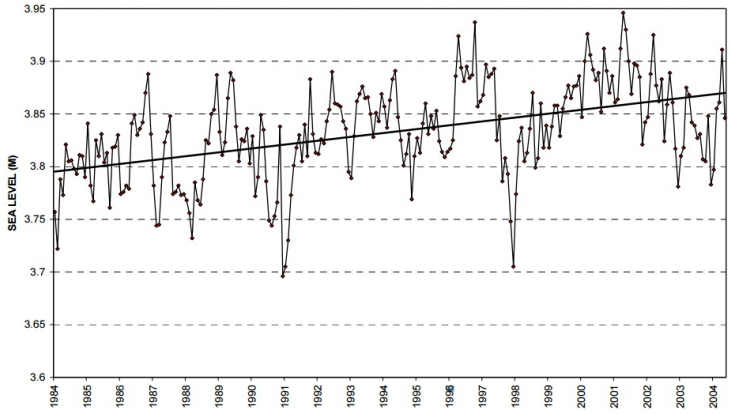

Figure 2.21: Monthly mean High Water Level for Zanzibar (1984-2004). Source: (Partnership, 2012).

In contrast to the reports of Partnership (2012), Mahongo and Francis (2012) found sea-levels are falling at around -3.6mm per year between (1985-2005) at Zanzibar. The fall was attributed to the increased strength of the north-easterly winds and a possible reduction in strength of the East African Coastal current (Mather, 2012).

Ogston and Field (2010b) showed in their one dimensional model of Molokai, Hawaii that the twenty first century sea level rise will not only increase wave heights but also suspended sediment concentrations and extended periods of elevated turbidity on reef flat's. Storlazzi et al. (2011) calibrated a two dimensional model of Molokai with in-situ measurements. The model was used to determine the effect of different forcing conditions on sediment transport and the contribution sea level rise would have on these conditions. Changes in reef roughness were not included based on the findings of Buddemeier and Smith (1988) that coral accretion rates are only 1-4 mm per year in contrast to 8-16 mm per year predicted by Grinsted, Moore, and Jevrejeva (2009). This would mean despite coral accretion the projected sea level rise for the years 2000-2100 will create a net increase in water depth. The reef structure is shown in Figure 2.22

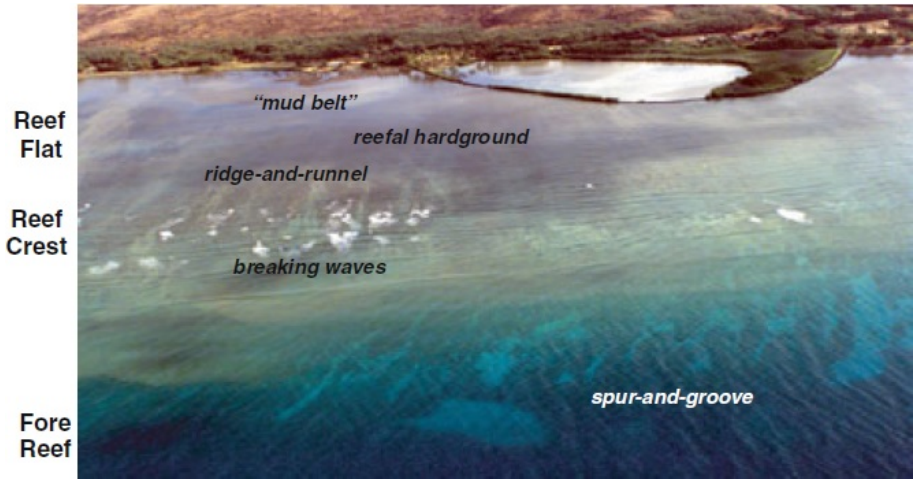

Figure 2.22: Molokai fringing reef, Hawaii. Source: (Ogston and Field, 2010b)

With confidence the model was reproducing the real in-situ conditions the model water level was increased(+0.10 m, +0.25 m, +0.50 m and +1 m). Storlazzi et al. (2011) found that as sea level increased, the breaking wave height at the reef crest decreased and the location of maximum wave breaking moved landward as more wave energy was able to propagate onto the reef flat. This in turn resulted in greater wave heights on the reef flat. The depth limited nature of the waves on Molokai fringing reef was highlighted by the landward decrease of wave height and energy dissipation from wave breaking. Peak bed shear stress also increased with SLR as larger waves propagated over the reef crest. All these phenomenon are illustrated in Figure 2.23.

The increased wave height in turn increased wave-driven currents. The model showed that the greatest current increase would be on the inner reef flat where water depth is on the order of hydraulic roughness of the coral reef. This finding was supported by Presto et al. (2006) who showed current speed was statistically greater during periods of higher sea level. Increased currents result in a lower residence time on the reef flat which can potentially alter chemical and physical properties of the water column. Continuing with the domino effect is the negative reaction of the coral to these physical and chemical changes.

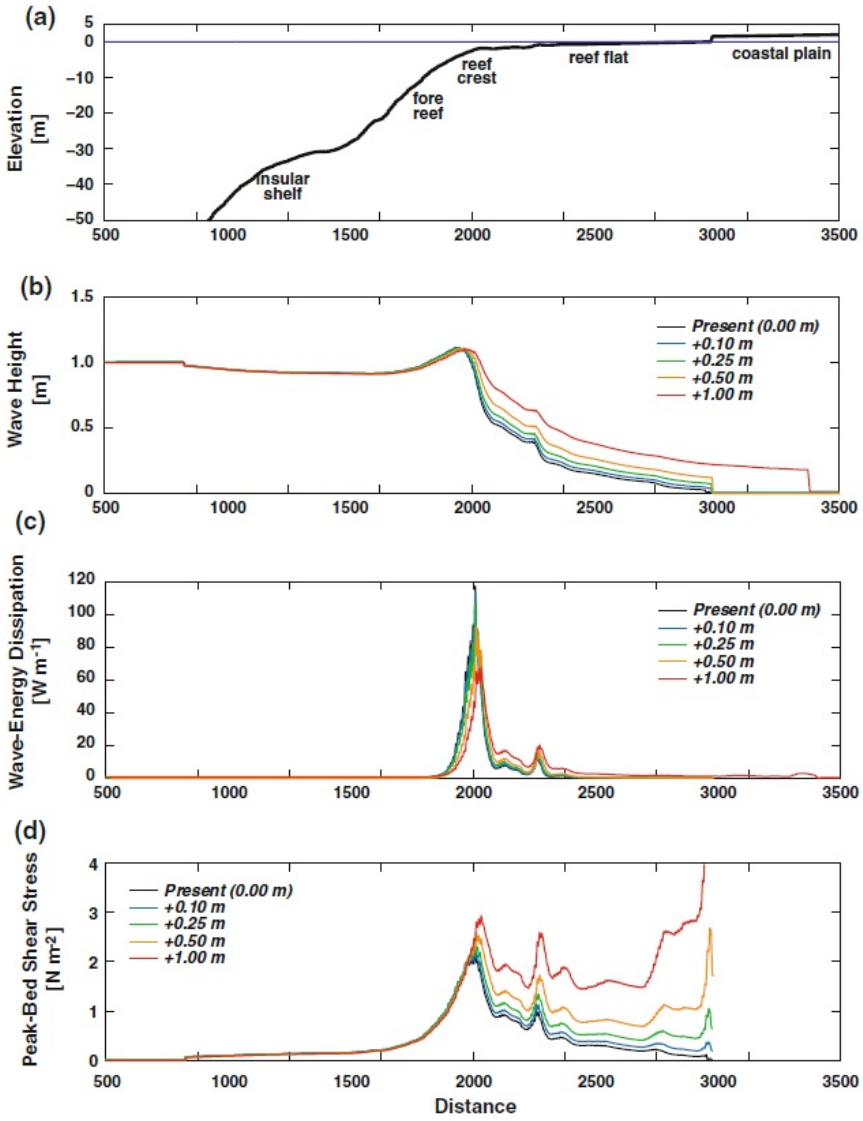

Figure 2.23: (a) The profile of the fringing reef. (b) Changing wave heights with the respective sea level change. (c) Decrease of wave energy dissipation with increase sea level. (d) Increased peak bed shear stress over the reef flat as larger waves propagate over the reef with increased sea level. Source: (Storlazzi et al., 2011)

The increased wave heights and currents over the reef flats expectantly increased wave-induced stresses. The critical threshold velocity for larger grain sizes was exceeded allowing a greater fraction of the sediment to be lifted into suspension. The larger orbital wave velocities and increased sediment concentration in the water column hindered settling, increasing suspension times and transport distances.The quasi equillbrium that the coast once had is now offset with the increased sea level and new greater wave climate resulting in erosion of the beach and additional sedimentary material onto the reef.

2.11 Coastal protection measures

There are various means of coastal protection and the choice of each follows the design conditions and criteria. Coral reef islands are however limited to softer structures and protection schemes.

2.11.1 Hard Structures

Rock structures are typically used to reflect incident wave energy creating a sheltered bay leeward of the structure. Their use on coral reefs though is not recommended. The loose rocks, if lifted into the water column, can result in further reef destruction and their large voids when placed limit their effectiveness in trapping sediments and preventing erosion.

Timber groynes placed perpendicular to the beach face are a popular method for the disruption of long-shore transport. The structures trap sediment increasing beach width up-drift of the structure. If readily available, timber is sometimes favoured over rocks structures as they are more aesthetically pleasing, have a smaller footprint and reduced cost. Casuarina trees, like those found on Mnemba Island, can provide adequate wood to create timber groynes that can be used to disrupt long-shore transport. The groynes effectivity like any structure is limited by its construction and design. The structures need to embedded deep enough to resist uplift forces from waves and large enough to actually trap sediment without it simply moving around or over the structure.

2.11.2 Soft Structures

Geotextiles

The need for soft structures that can be easily installed and removed has resulted in the development of geosynthetic containers or GSC's. GSC's are robust and versatile bags made from polymeric materials. The bags are filled with sand or similar grade material creating a soft structure that is both stable and aesthetically pleasing. Certain criteria define the success of Geotextiles:

- The physical container characteristics directly influences the strength and durability. Saathoff, Oumeraci, and Restall (2007) found that Ultraviolet (UV) degradation is a main factor for long term success of the container.
- The containers once placed will be subject to constant abrasion from sediments in the water column and is thus an important consideration.
- The seams must be able to withstand multiple loads during filling, placing and in-situ wave loads.
- The tensile strength requirement is critical during filling and placement of the geotextile.
- Damage due to vandalism is unavoidable in high pedestrian traffic and therefore must be considered. Puncture resistance from anthropogenic or natural causes must be considered.

  The use of GSC's have been an effective coastal protection method and their relative ease of filling and placement make them a viable option for the protection of embankments surrounding low-lying islands.

- The different production style of the geotextile effects its characteristics. Woven geotextiles exhibit high tensile strength, low elongation and reduced resistance to impact. Elongation allows the container to act as a self-healing device as it can move with the movement of the soil it rests on. Non-woven exhibit a lower tensile strength but are thicker, have high elongation and greater puncture resistance. Research by Krahn et al. (2007) showed that non-woven geotextiles had 50% higher relative friction when testing pull-out resistance of the GSCs.
- Insufficient sand-fill ratio can result in deformations of the bag increasing the risk of pull-out failure.
- Friction is essential for hydraulic stability. Friction is dependent on the type of geotextile, contact area, overlapping length and the sand-fill ratio. Insufficient friction can result in sliding and pull-out of geocontainers.

There are two main types of geotextiles, the Geotube and geocontainer. Geotubes are constructed from high strength woven or non-woven geotextile. They are a single unit and are thus typically more stable than individual bags. The mass of the tube is the main factor as it needs to be enough to resist the sliding and overturning forces from waves. Geotubes are filled with a sand slurry with the pores of the textile allowing the water to escape whilst the sand remains within the tube.

Figure 2.24: Geotube beach protection in DUBAI. Source: (PTSA, 2016)

Disadvantages include:

- Localized rupture can result in the entire tube failing.
- Insufficient filling ($< 80\%$) results in deformations and internal movement of sand within the tube.
- Poor filling techniques can result in differential filling and voids.

Geocontainers are much smaller than Geotubes. The bags generally have lengths of two metres and weigh anywhere between one hundred and five thousand kilograms. The main advantage over geotubes is that if an individual container fails, it can easily be replaced. Like the Geotubes they are designed to resist the sliding and overturning forces but make use of friction between each bag as well as the individual mass to keep the structure in place. They are filled by attaching the bags to a metal frame where they are filled using an excavator but can also be filled my hand.

Figure 2.25: Geocontainer example. Source: (PTSA, 2016)

The main disadvantage of containers is that they are succeptible to pull-out from wave run-up and down if mass and friction are insufficient.To prevent scour beneath the bags both the tube and container make use of either a scour membrane and/or a Dutch toe. The scour membrane prevents sediments being drawn out from behind bags during wave run-up and run down whilst the Dutch toe settles into the scour voids retaining structure stability.

The use of geocontainers can be a viable option towards the protection of low-lying reef Islands. The material to fill the containers in most cases is readily available and the filling of containers is achievable without machinery. Their effectiveness in disrupting longshore transport and dissipation of wave energy is evident in their local and global applications. In KwaZulu-Natal, South Africa, geocontainers have been successfully used in multiple locations along the coastline as embankment protection to limit damage on the landward structures. Figure 2.26 shows the use of geocontainers to create a defence wall to protect the car park from wave action and erosion on Isipingo beach,KwaZulu-Natal.

Figure 2.26: Geocontainers used for protection against wave action and erosion on Isipingo Beach, KwaZulu-Natal. Source: (Kaytech, 2016)

The low energy wave climate on protected coral reef islands can reduce the necessity for larger containers due to the decreased risk of pull-out or overturning. This can simplify the construction and placement of containers and perhaps even more importantly can result in cost reduction.

Sand nourishment

Beach nourishment is an effective beach management tool without the use of structures. It is the pumping of sand onto the beach to create a new beach or widen an existing beach. Nourishment does not stop the erosion, it creates a buffer zone which then erodes away and is thus a continuous process (Barber, 2000).

Sediment is typically dredged from a certified borrow pit and either pumped directly onto the beach by the dredger or put through various pumping stations from which it is pumped onto the desired location.

Disadvantages include:

- Nourished beaches typically erode faster as the beach is not at it's equilibrium profile.
- Expensive and needs to be repeated periodically.
- Risk of smothering Coral.

Two major disadvantages is availability and accessibility of dredgers. Dredgers in developing countries, like Zanzibar, are a rare commodity and can in some cases can not available at all. Secondly if the dredger is available, the coral reef structure can make access to eroded sites near impossible and then require the use of further equipment to reach sediment starved areas on the beach.

Chapter 3

Methodology

Chapter 3 explains the techniques used to address the research questions followed by the location and climate of the case study, the field work methodology and the model selection and setup.

3.1 Methodology explanation

To define the mechanisms responsible for the severe erosion of low-lying coral reef islands in a changing climate region, a detailed understanding of the current climate is required. Field work measurements of the existing bathymetry, wave and sediment transport climate thus had to be undertaken as no data was available for Mnemba Island or its surrounding reef. Numerical modelling makes use of this climate to simulate the hydrodynamics and morphological changes and help predict the future of low-lying reef islands based on reduced coral roughness and increased wave heights.

3.2 Case Study Location

Mnemba Island, shown in Figure 3.1, is located off the north-east coast of Zanzibar. Zanzibar experiences warm temperatures year round with mean annual temperature of 26°C. South-east trade winds blow from April to October followed by the north-east trade winds November through to March. The tropical climate experiences total annual precipitation averages of 1700 mm with April being the highest(Watkiss, Bonjean, and Shaghude, 2012). The Island is roughly triangular in shape and 11 hectares in size. The reef that borders the island on the eastern side can be considered a fringing reef spanning 180 degrees with a 3 km wide channel separating the island from Zanzibar on the western side. The Island is currently leased by *&Beyond*, a luxury travel company, who maintains the island as a premium and private resort. The island has twelve guest rooms that border the tree-line of the island along with various other utility structures constructed out of coral rock and local timber.

The fringing coral reef which stretches 3km east off the island and 7km from its bottom to top point. Although no formal study has been done, communication with long-term staff of the island suggest that the reef was once rich in biodiversity but over-fishing and increasing water temperatures has decimated coral populations. The ± 4 m tidal range drains the reef of water at low tide making it easy pickings for local fishermen whose boats then rest on the reef causing further destruction.

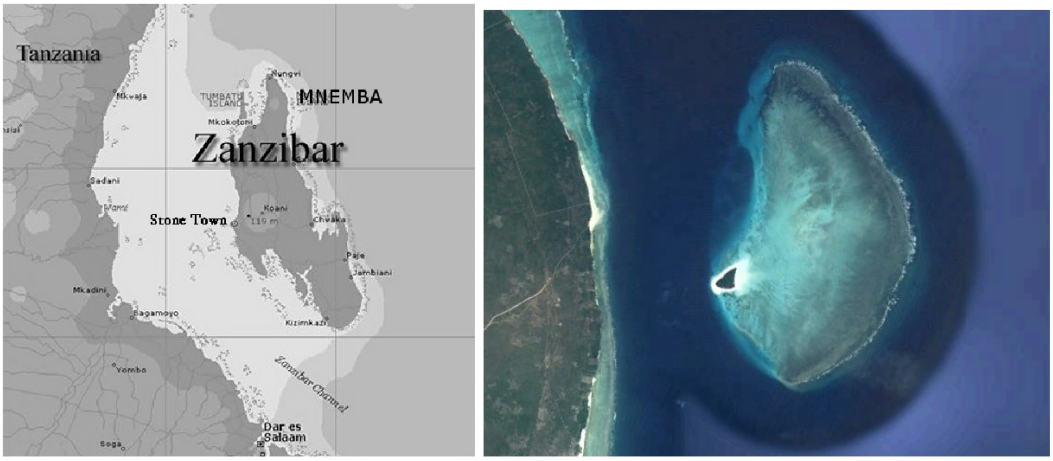

Figure 3.1: Mnemba Island Location. Source of imagery: Google Earth

3.3 Motivation

From 1973 to the mid-nineties the Island experienced constant growth after the introduction of the invasive *Casuarina* tree. The eastern Side of the Island rapidly became dominated by the *Casuarina* tree and the island grew eastward with particular growth in the north-eastern and south-eastern corners. Towards the mid-nineties growth slowed and the Island began to recede along the eastern corners with significant recession in the south-eastern corner. The recession continues to this day where points near the south-eastern corner are receding at approximately 5m per year. The increasing erosion rate has resulted in the destruction of several structures which make up the Mnemba resort placing increasing risks for guests and local staff along with increasing repair costs. The fallen *Casuarina* trees litter the eastern beaches which compounded erosion rates by increasing the turbalent zone as waves collided with them as well as making the area unsafe for guests to walk. The contrasting tree line where the *Casuarina* trees start on the eastern side of the island and their relative growth and recession is shown in Figure 3.2.

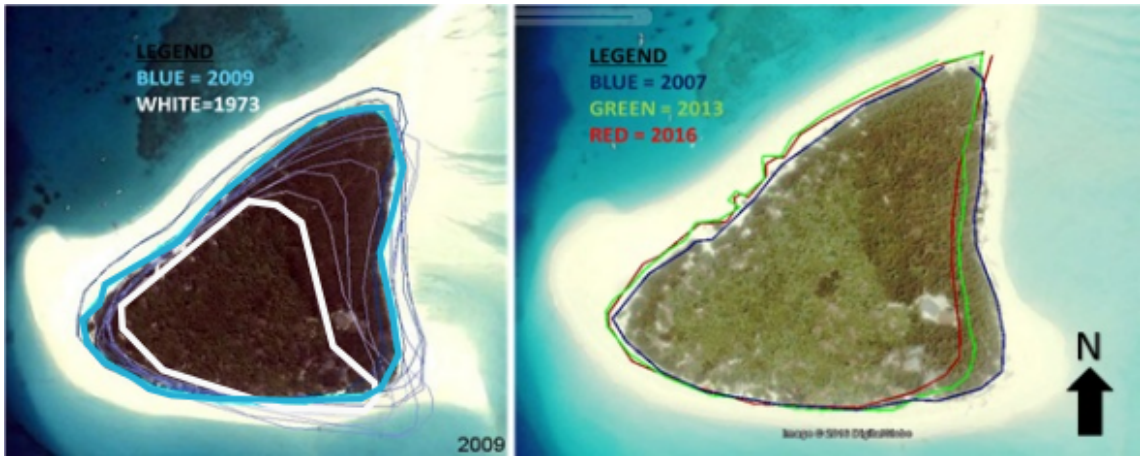

Figure 3.2: Island growth stages since 1973 (white line) and its shape as of 2009 (blue line). The recent island recession is shown on the right. Source of imagery:(Google Earth,2016)

The constant erosion and growing threat to the lucrative resort forced &*Beyond* to seek guidance on possible coastal protection schemes. This prompted the students trip to the Island to gather the necessary data to allow an informed decision on the actions that needed to be taken. Several unsuccessful attempts had already been implemented on the island in an attempt to slow the erosion and protect the staff quarters in the south-eastern corner of the island. Woven sugar/grain bags were stacked on the steep beach scarp but were quickly torn by the fallen trees.

Figure 3.3 illustrates the level of erosion as of 20 May 2016 along with the fallen Casuarina trees that were assisting further erosion. The damage to current structures and undermining of further structures is evident.

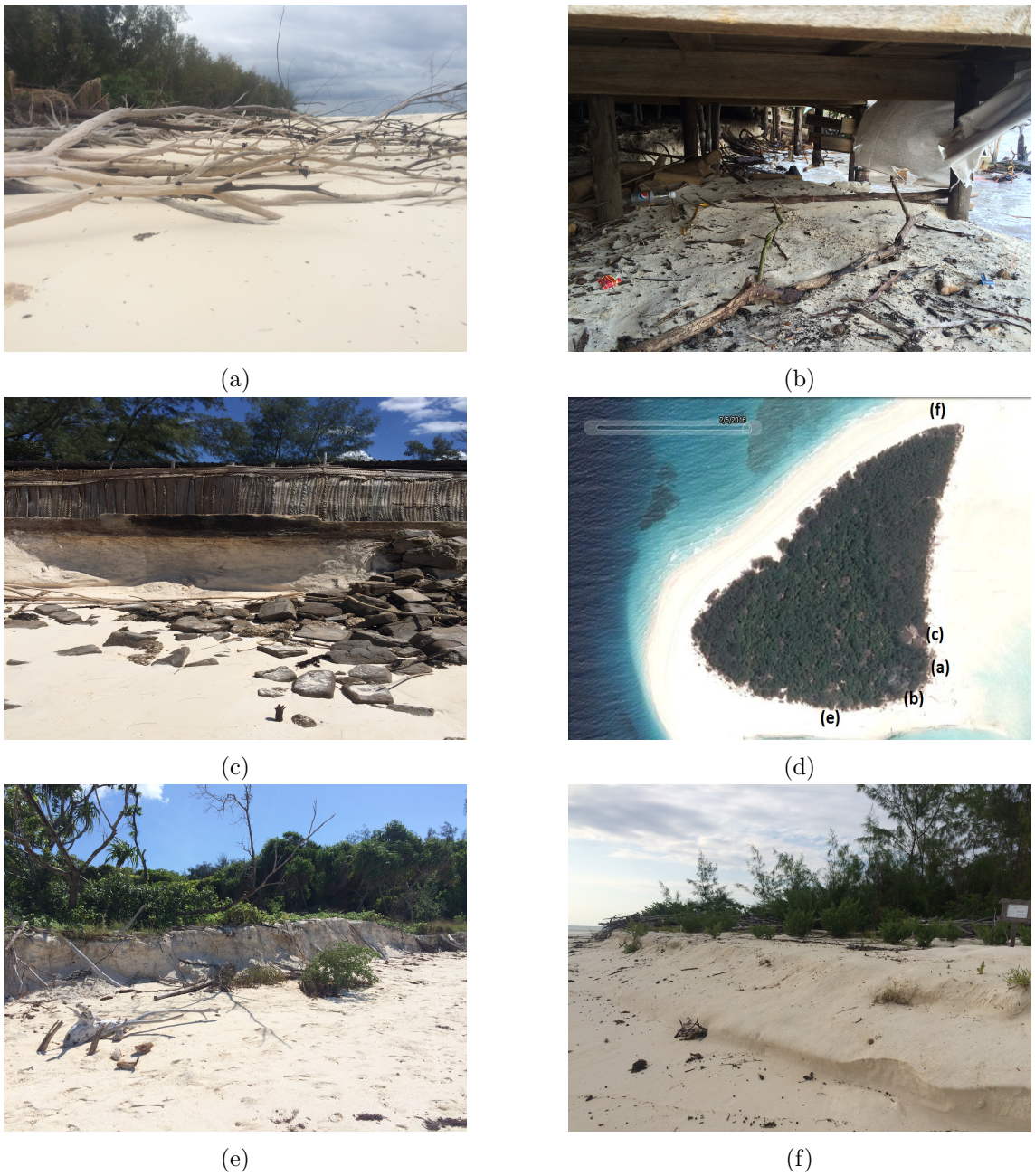

(a) (b) (c) (d) (e) (f)

Figure 3.3: Erosion state as of 20 May 2016.(a) Fallen Casuarina trees. (b) Erosion undermining structures.(c) Collapsed floor slabs.(d) Image locations (Not to scale).(e) Beach scarp southern Bank.(f) Beach scarp northern Bank.

3.4 Data

In order to investigate the hydrodynamics and sediment dynamics on Mnemba reef local high resolution data needed to be retrieved in addition to the low resolution bathymetry and ERA data that was already available. ERA, a global atmospheric reanalysis data was chosen because of the availability of data in the region (ECMWF, 2016). The insitu data measured included the following:

- Bathymetry surrounding Mnemba Island stretching to the reef edges and across the channel to Zanzibar.
- Current velocities
- Sediment transport rates
- Wind data
- Wave Height
- Water Depth
- Direction

3.4.1 Temperature

Findings of the current climate and climate variability Watkiss, Bonjean, and Shaghude (2012) show evidence of a constantly changing Zanzibar climate. Both Unguja(commonly known as Zanzibar) and Pemba show a rising temperature trend in air and water known locally as '*maji moto*', which alongside anthropogenic activities is a leading contributor to coral destruction (Knowlton, 2016).Wind data also exhibits an increasing trend as shown Figure 3.4 in where the frequency of winds over 10 kt has risen over the decades.

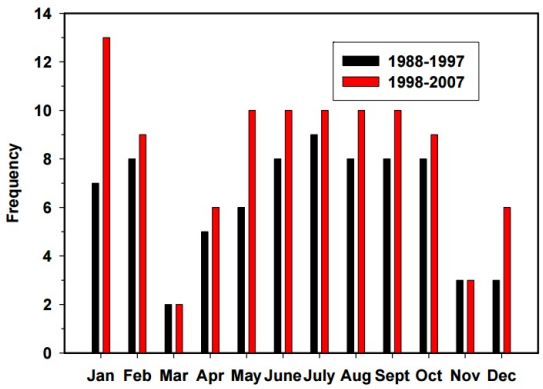

Figure 3.4: Frequencies of the monthly averages for the surface wind speeds exceeding 10 knots. Source:(Watkiss, Bonjean, and Shaghude, 2012)

3.4.2 Wind & Wave

ERA data was used to approximate the local wind and off-shore wave climate that would be used as the driving forces of the Delft3d model. A wind rose based on the ERA data for Mnemba Island for 2005-2015 is shown in Figure 3.5 alongside the wind rose retrieved from Kisauni Airport, Zanzibar. Visible is the Trade winds and the south to south-easterly annual bias. The data taken from ERA was compared against measured data from Kisauni Airport, Zanzibar, and showed similarities in direction and speed. Similarities were based on graph observations as input data for Kisauni airport graph was not available. Small discrepancies only occurred when north-easterly winds blew as a result of topographical effects from the central mountain ridge on Zanzibar Island.

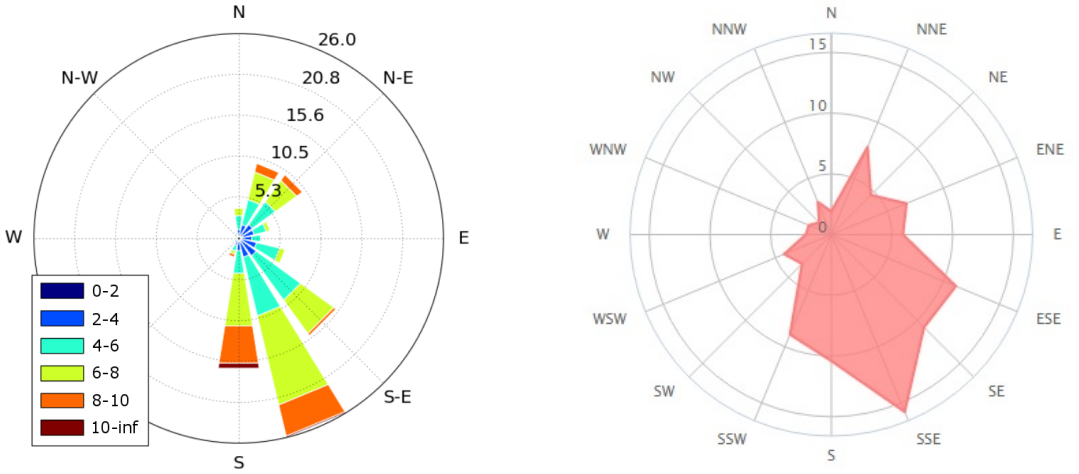

(a) (b)

Figure 3.5: Annual Wind Rose.(a) ERA dataset Mnmeba Island annual Wind Rose (2005-2015) Source:(ECMWF, 2016).(b)Kisauni Airport, Zanzibar, annual wind rose (2007-2016). Source:(Windfinder, 2016)

The monthly wave roses from ERA in Figure 3.6 show the Monsoon wind dependence of the wave direction. The highest wave height records typically occur between June and September when off-shore wave heights can reach up to 3 m. From the analysis an average significant wave height, average peak period and average direction of 1.34 m, 6.7 s and 110 degrees respectively were derived.

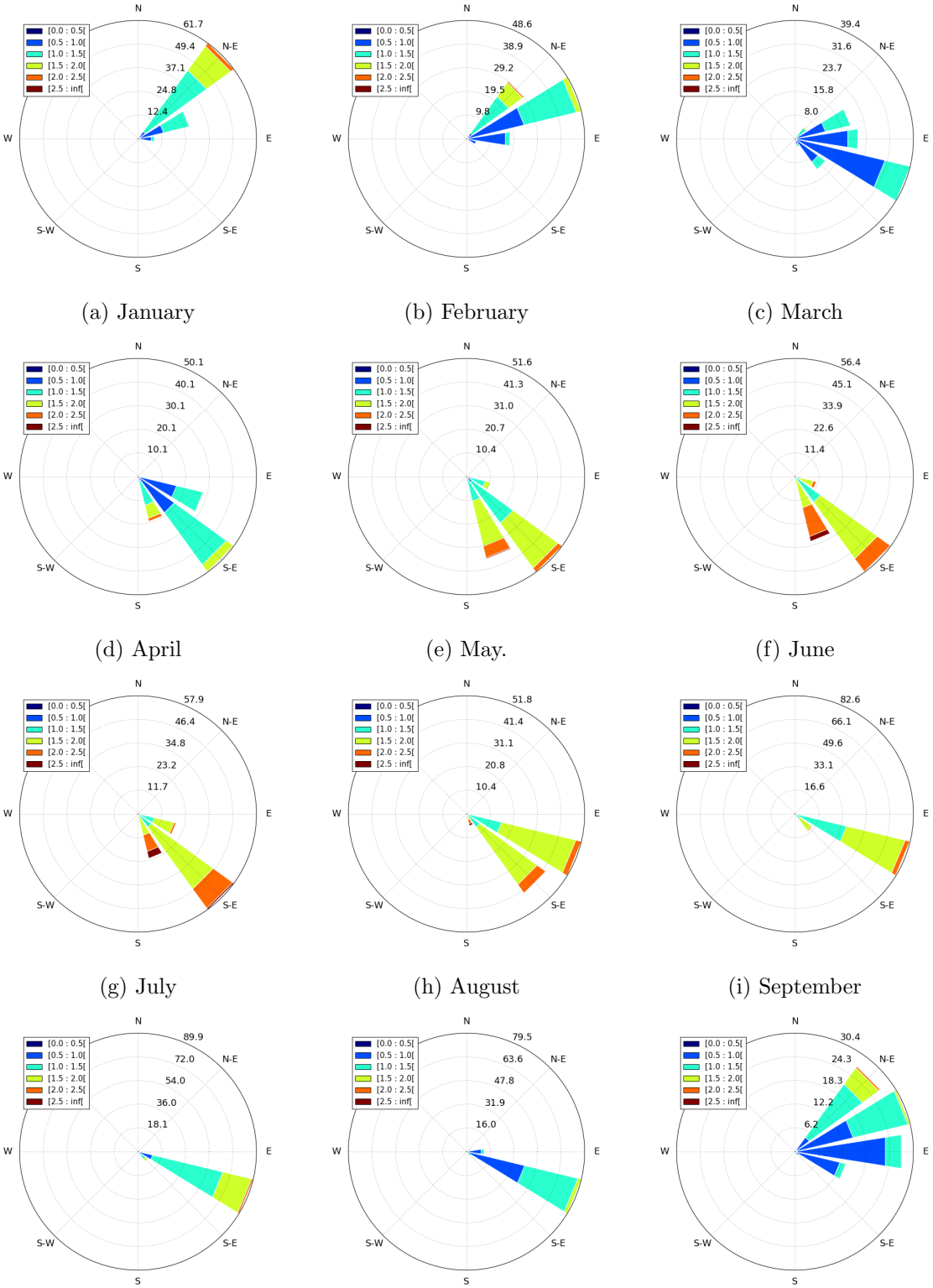

(a) January (b) February (c) March

(d) April (e) May. (f) June

(g) July (h) August (i) September

(j) October (k) November (l) December

Figure 3.6: Monthly wave Roses (2005-2015). Source:(ECMWF, 2016)

3.4.3 Currents

The northward flowing East African Coastal Current (EACC) shown in Figure 3.7 has a seasonal contribution to the currents around Zanzibar. Garcia-Reyes et al. (2009) found that during January, the weaker EACC mostly bypasses the southern entrance of the Zanzibar channel but gets diverted through the deeper Pemba channel entrance, some of which turns and flows southward into the Zanzibar channel. During February to March the Zanzibar channel is isolated from the EACC and the water temperatures rises. The EACC is strongest during April to August and is funneled through the Zanzibar channel reducing water temperatures. The seasonal surface current variations are shown in Figure 3.9.

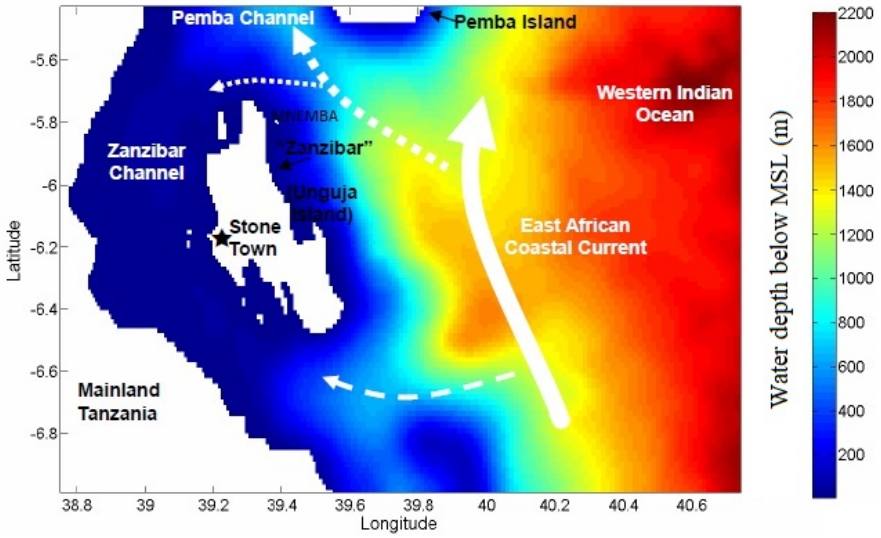

Figure 3.7: The East African Coastal Current and surrounding Zanzibar bathymetry (Colour bar in metres below MSL).The thick line represents the EACC with the dashed lines showing the inflow into the Zanzibar Channel. Source:(Garcia-Reyes et al., 2009)

The EACC that partly flows through the Zanzibar channel varies between 0.25 m/s and 2 m/s but local experts believe the tidal force to be the greater current generating force (Garcia-Reyes et al., 2009). There is a convergence of flows entering the Southern and northen entrances resulting in the water piling up in the centre of the channel and flowing out both entrances in the ebb, shown in Figure 3.8. This could be a possible explanation of the large tidal range experienced in the Zanzibar channel.

From the modelled output by Garcia-Reyes et al. (2009) and their insitu measurements, it is visible that the Mnmemba Island on the north-east coast of Zanzibar experiences continuous northward surface currents apart from January and early February. This is the only surface current data that was available for this area prior to the author's testing.

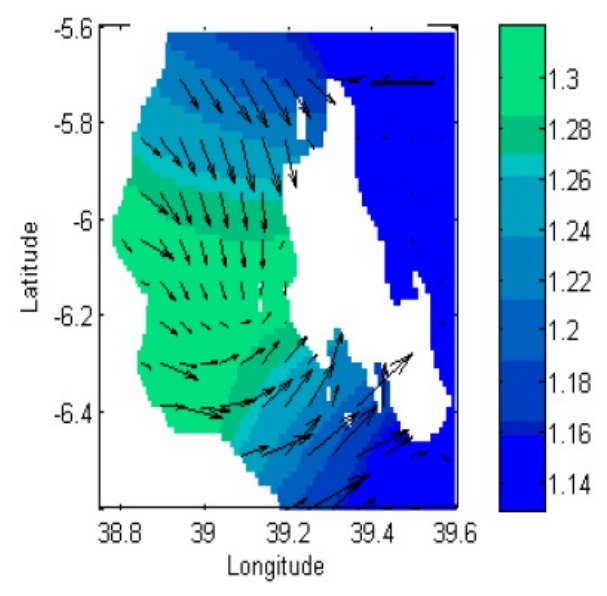

Figure 3.8: Convergence of flow during flood tide, Source: (Garcia-Reyes et al., 2009)

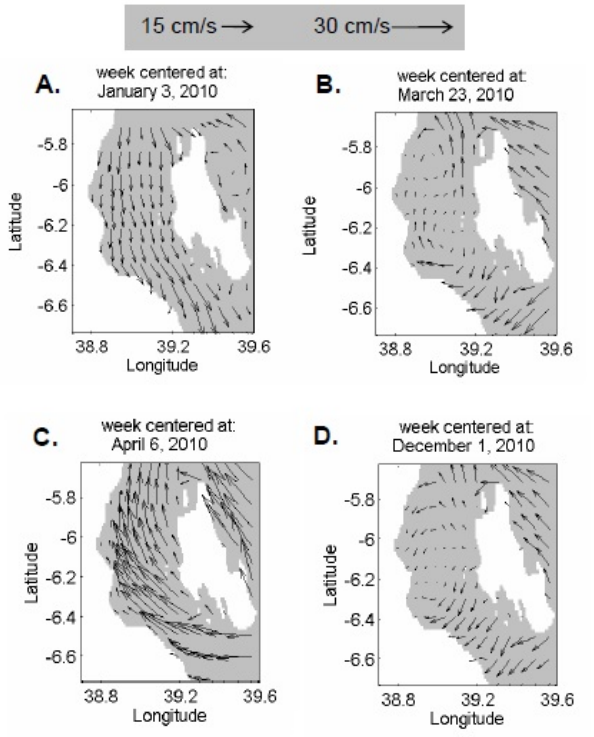

Figure 3.9: Simulated surface currents surrounding Zanzibar with seasons. (a) Driven by the north-easterly trade winds, flow within the channel is Southward.(b)Near the end of March surface currents weaken and change direction as the trade winds change.(c)Driven by the south-easterly trade wind, surface currents are strong and northward.(d)Currents weaken once more and change direction. Vectors represent the direction of current. Source:(Garcia-Reyes et al., 2009)

3.4.4 Seasonal variations of beach profiles

Neglecting the increased erosion experienced on the Island, variations in the beach profiles are visible corresponding to the seasonal winds.

During the April-October period a sand bank known locally as the October lip on the north-western corner of the Island is formed following prevailing southerly winds. Other observations include an accretion of sediment on the south-eastern corner along with a seemingly more northward pointing beach profile on the north-eastern corner (Figure 3.10).

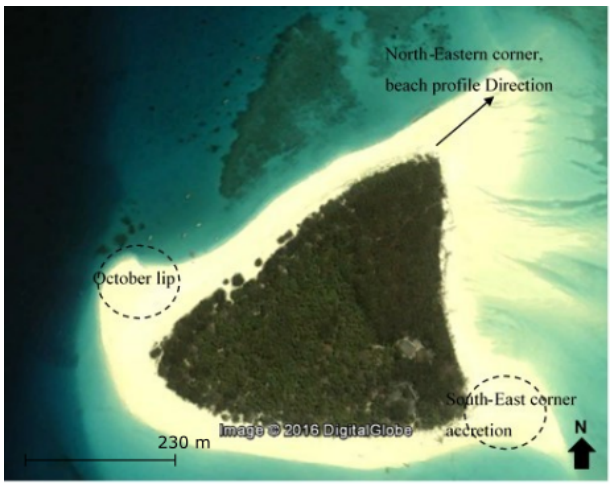

Figure 3.10: Seasonal beach profile variations following the southerly trade winds. Source of imagery: Google Earth 2016

Upon the arrival of the northerly Trade winds in November/December and the October lip shifts to south-western corner of the Island. Also observed is a southerly rotation of the north-east corner bank and a thinning of sediments located at the south-east corner shown in Figure 3.11 . These observations were based on historical satellite imagery along with personal communication with long-term Mnemba Island manager Mike Kelly.

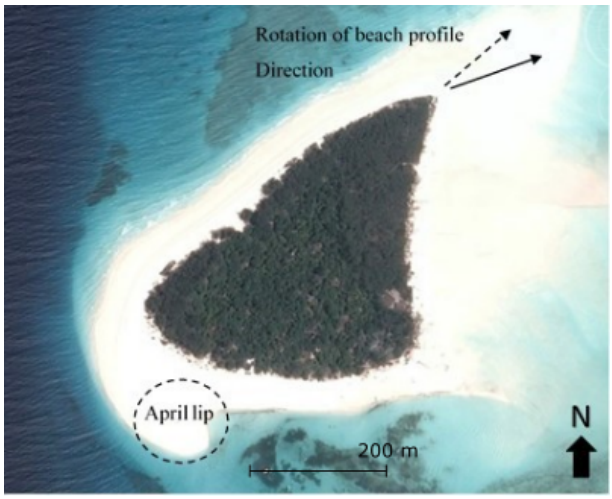

Figure 3.11: Seasonal beach profile variations following the northerly trade winds. Source of imagery: Google Earth

3.5 Field work methodology

This section outlines the various techniques used to gather the data and the calibrations done to ensure accuracy of the readings.

3.5.1 Beach Profiles

Beach profiles were necessary to illustrate the physical changes of the beach. The profiles were done using a typical dumpy level and staff at the locations marked on Figure 3.12. The locations were chosen to get a basic profile representation at both the corners and centre of the eastern bank. Extra points were then added where visible changes in the sand levels were occurring. The black markers represent the original profiles done with the additional yellow and green markers added later. Red markers are original profile markers that have been washed out.

Along with the dumpy level readings, bed level readings were measured directly off the markers (Figure 3.13). These readings were done following higher tidal ranges to investigate the changes of the bed level after spring tides. The measured values were then to be compared to the surveyed dumpy readings to ensure accuracy.

Figure 3.12: Marker locations for beach profiles. Source of imagery: Google Earth

Figure 3.13: Marker with bed level measurement points.

3.5.2 Sediment Transport

Two methods were used in an attempt to find the major sediment transport direction. These include the construction of Timber groynes and individual point traps (streamers).

Timber groyne impoundment method

To measure longshore and cross-shore transport three temporary 10 m long timber groynes were constructed from the fallen Casuarina trees littering the eastern banks. The locations and orientations of the groynes are shown in Figure 3.14. The groynes are an impoundment method used to obstruct the flow and either result in an accretion or erosion of sediment on a particular side of the structure, this would provide an indication of the direction of sediment movement.

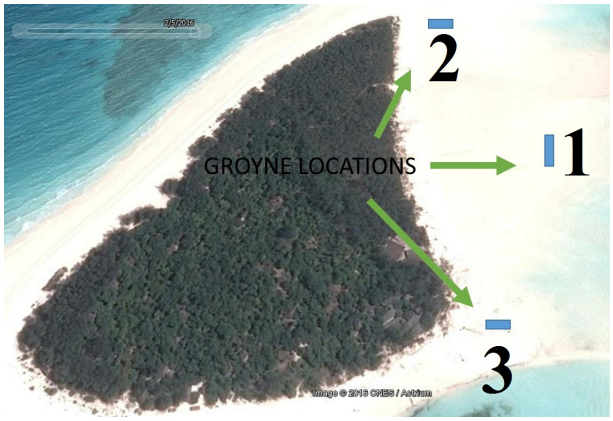

Figure 3.14: Temporary timber groyne locations. Source of imagery: Google Earth

Groyne 1 shown in Figure 3.15 was constructed using 10-15 cm diameter poles with no horizontal planks. Placed perpendicular to the shore line at mean sea level, this structure would aid in identifying the cross-shore sediment movement. groyne 2 shown in Figure 3.16 was constructed in the north-eastern corner at the beach profile slope change as this would be the point where maximum profile change would occur. Placed perpendicular to the shore, it was constructed using verticals placed behind and infront every 1 m and 2 m respectively with staggered horizontals placed in between. groyne 3 follows the same design as groyne 2 just placed at the south east corner. Both groyne 1 & 2 would aid in identifying long-shore sediment movement. The groyne's were fastened using 4 in nails along with hemp rope.

This method was chosen in order to satisfy the requirement of the authors stay that majority of the fallen Casuarina trees will be cut up and used, clearing the beach of debris. The fallen trees as stated earlier were placing staff and guests at risk and compounding erosion rates. This method if successful could also be used as the start of a permanent coastal protection scheme for the island.

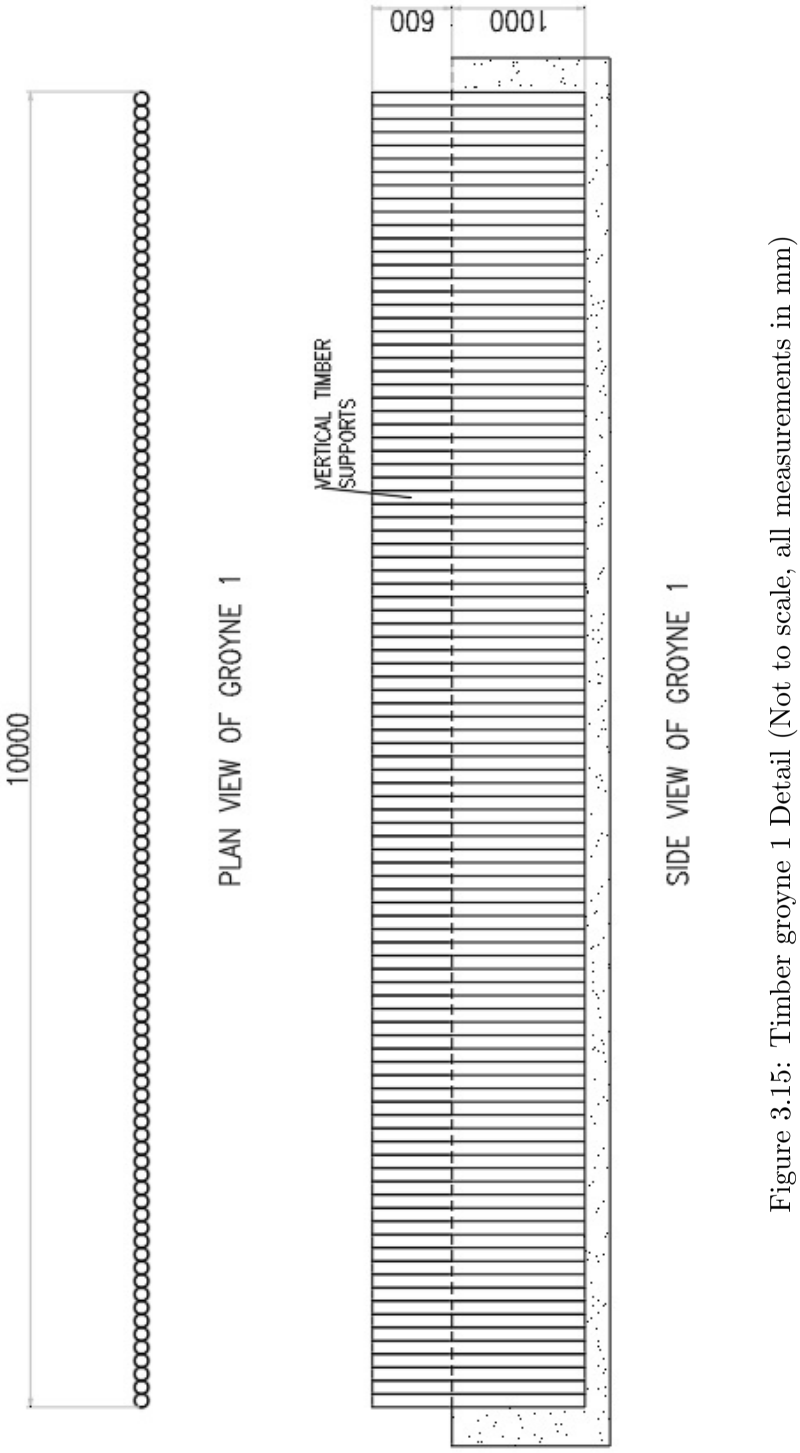

Figure 3.15: Timber groyne 1 Detail (Not to scale, all measurements in mm)

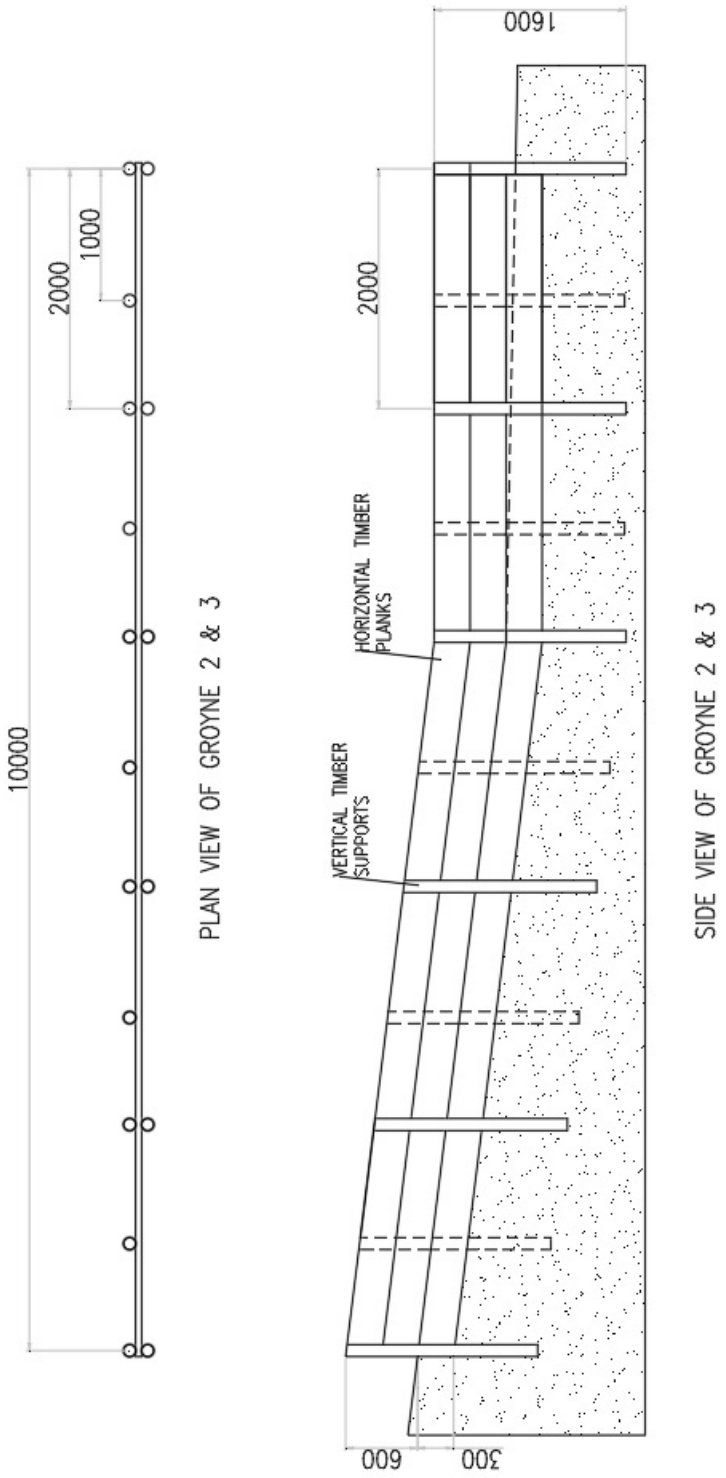

Figure 3.16: Timber groyne 2 & 3 Detail (Not to scale, all measurements in mm)

Streamer Sediment trap

The traps used in this case study had to be adapted from the Krauss (1987) streamers for several reasons. In order to deploy various traps at once the traps had to be self-supporting as the author was the only one to be operating the traps. The steel rack was also unusable due to weight limitations on the plane and thus 30 mm polyvinyl chloride (PVC) tubing was used instead. To avoid bed scour, and the streamer bag wrapping around the supports, the end of the streamer bag had to be held in place. The new design used is shown in Figure 3.17.

Figure 3.17: Mnemba Island Streamer trap Design. (1)Front supports for streamer mouth. (2)Streamer mouth opening 150x100 mm. (3)Mouth slightly raised to minimize streamer interaction with bed. (4) Duct tape used prevent sliding of streamer mouth cable ties. (5) Streamer bag rear tie down to prevent the bag wrapping around the structure.

The sieve cloth used was a 2 m long 50 micron mono-filament with a 150x100 mm mouth. The traps were placed at low tide in groups of four at the positions shown in Figure 3.18. Each trap in the group faced a different direction in order it identify the transport direction. The traps were closed by wrapping the sieve around the front supports until the mouth was completely submerged and then all traps in the group were opened and left for 45 minutes. In this time wave height and direction measurements were taken. The traps were placed at the bottom of the beach slope and near the MSL line to determine differences in transport quantity and direction in relation to distance from the island. The traps were then collected and the collected sediments weighed.

Figure 3.18: Trap position variations. Source of imagery: Google Earth

3.5.3 Bathymetry

The local bathymetry surrounding the island is an important factor governing wave characteristics and thus sediment transport. Depths of the Mnemba Island reef and the surrounding area had never been measured and thus had to be recorded. The bathymetry was recorded using a Sonarmite Echo Sounder mounted to one of the resorts dive boats. The transducer was mounted to a pole 15 cm beneath the water surface when stationery to reduce errors from the boat hopping along the surface when in motion. The transects shown in Figure 3.19 were completed as close to the same high tide level on each day to minimize depth discrepancies. The transects were then plotted using delft3D making use of triangular interpolation to determine the missing depth values between transects.

Figure 3.19: Transect lines surrounding Mnemba Island. Source of imagery: Google Earth

3.5.4 Wave Characteristics & Currents

Wave Characteristics

Pressure sensors were used to measure the wave characteristics. The sensors record hydrostatic pressure below the water surface at a set frequency of 4 Hz. From a single sensor, wave characteristics including wave height, water depth, period and wave length can be derived using linear wave theory.

The conversion from the raw sensor data into wave characteristics was computed by means of a wave-by-wave and spectral analysis. The wave-by-analysis outputs the parameters directly from the level-crossing analysis of the time series data. Linear wave corrections are applied to each detected wave based on its period and deduced wavelength. The sequence of waves is then analysed statistically to estimate the significant wave height and average period..

Both methods use the user defined sensor calibration Avolt and Bvolt parameters to transform the raw voltage data to pressure values.

The regression coefficients are calculated to compensate for change in water level. In the spectral method, the pressure data is Fourier -transformed and low pass filtered to remove high frequency noise. Then a linear wave correction is applied to each remaining mode before calculating the wave parameters from the corrected spectral using moments of the spectrum.

For further reading on the derivation of wave parameters from pressure sensors refer to Bishop and Donelan (1987).

The pressure sensors were used to determine the effect of the reef as waves propagate over. The sensors were placed at the locations shown in Figure 3.20 . Sensors A1 and A2 were in-situ for three days as a test period due to concerns of the sensors leaking. Their success then allowed sensors B1 and B2 to be placed for ten days in-situ.

The sensors had to be calibrated to ensure the results recorded were accurate and this was done by placing the sensor at known depths and using the output to derive the depths. The sensors were found to have a 90% accuracy. This also allowed the Avolt and Bvolt values to be determined.

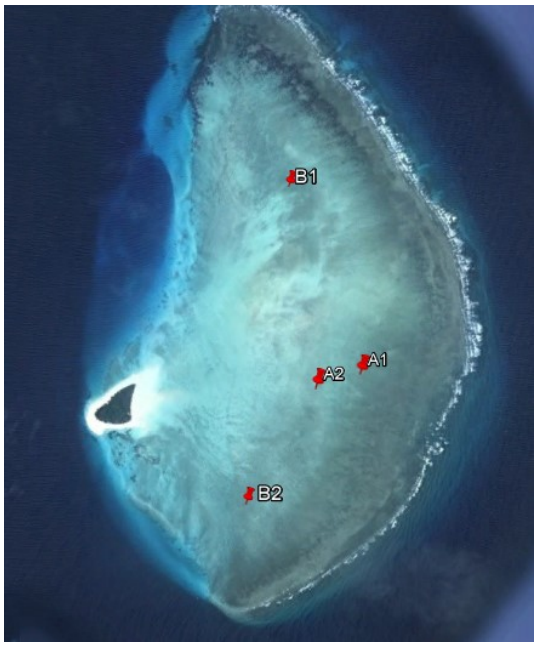

Figure 3.20: Pressure sensor locations. Source of imagery: Google Earth

Currents

The currents surrounding the island were measured using a make-shift beacon, stopwatch and GPS location. The beacon shown in Figure 3.21 was placed at varying points surrounding the island and its progress tracked and recorded. The beacon had a flag for easy identification in the water as well as to identify wind direction if any. From the recordings surface current velocities were calculated.

Figure 3.21: Current beacon

3.6 Modelling methodology

3.6.1 Delft3D

Delft3d is a modelling package used to investigate hydrodynamics, sediment transport and morphology on coastal and inland waters. The main components are the DELFT3D SWAN and FLOW modules coupled together to model the waves and currents respectively.

When coupled online the model can be used to dynamically resolve sediment transport and account for the effects waves have on the flow. The flow model acts as the core of the system by simulating water motion due to tidal and meteorological forcing conditions. This is done by solving the unsteady, shallow-water equations (continuity, horizontal momentum and transport). Radiation stresses and bed shear are then included into the flow model through the third-generation SWAN model. The SWAN model computes short-crested, wind generated waves in coastal regions.

3.6.2 Wave Model

The third generation SWAN model was used to compute wave characteristics as waves propagated from deep water over the fringing reef to the island. The radiation stresses that drive the hydrodynamics in the flow model are derived from the SWAN output.

Wave breaking in SWAN was determined using the default Battjies and Janssen (1978) depth-induced wave breaking model. The breaker index was set to 0.69 based on the recommendations for coral reefs by Filipot and Cheung (2012) with white-capping determined according to Komen, Hasselmann, and Hasselmann (1984). The bottom friction computation used the Madsen, Poon, and Graber (1988) friction formula. This formula was chosen to obtain spatially varying roughness by determining hydraulic roughness lengths based on the Manning's coefficient.

3.6.3 Flow Model

To achieve model stability the computational time step was 1.6 seconds relating to a courant number of approximately 0.3 over the reef flat to mantain numerical stability.

The stress forumlation due to waves used the default Fredsoe formulation.

3.6.4 Morphological model

The van Rijn transport model, default in Delft3D, was used to determine the sediment transport for both long-shore and off-shore movement. The model distinguishes between the bed load and suspended load based on a reference height at which a reference concentration is applied.

Transport is divided into suspended and near-bed load transport. The suspended load is calculated using GLM velocities. In contrary, the bed load is computed using the bed shear stress, which originates from Eulerian velocities (Walstra et al., 2000). The near-bed load consists of three components, namely:

- Bed-load due to currents (Sbc), acting in the direction of the (Eulerian) near-bed current.
- Bed-load due to waves (Sbw), acting in the direction of wave propagation.
- Suspended load due to wave asymmetry effects (Ssw), acting in the direction of wave propagation.

Previous studies have outlined the limitations of the van Rijn cross-shore transport which include the inability to produce both accretion and erosion. On-shore sediment transport was found to be sensitive to the manipulation of the wave related transport coefficient f_{sus} with results showing either accretion or erosion but never both. After a sensitivity analysis, the wave related transport factor f_{sus} was set to zero based on the morphological changes it produced closely mimicking observed changes.

The coupled online flow and wave model allows for changes in the morphology to effect the succeeding wave conditions in real time. Contrary to the short time-scales that flow changes take place on, morphological time-scales are in the order of weeks and months and hence the necessity of a morphological scale factor. The morphological scale factor was set to 26 effectively scaling the model up to a 1 year simulation..

3.7 Model Setup

3.7.1 Wave Climate Reduction

To decrease computational time a set of representative wave conditions was found by utilizing the Kamphuis bulk sediment transport formula shown in Equation 2.14.

This was done by using the frequency of conditions combined with their relative transport rates. The top 15 contributors to cumulative sediment transport were then chosen as the reduced wave climate shown in Figure 3.22. Fifteen conditions were chosen in order to encapsulate all major wave conditions and transport conditions from the north and south. The events were sequenced based on the seasonal characteristics of the Zanzibar wave climate and monsoon winds and are shown in Table 3.1.

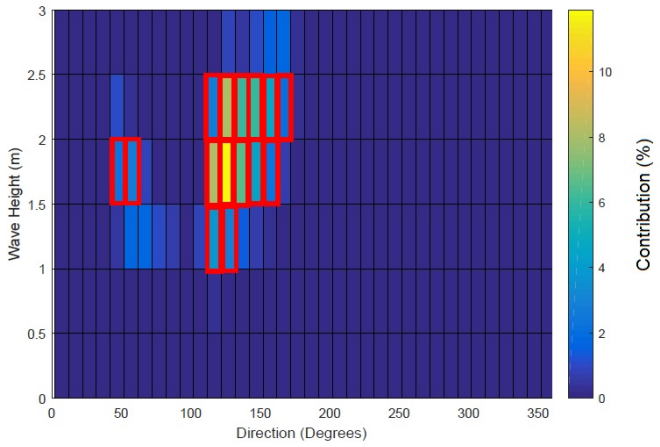

Figure 3.22: Sediment transport contribution based on 2.14

Table 3.1: Mnemba Island Wave climate reduction

Wave Condition	Hmo (m)	T (s)	Direction (Deg)	Time (%)
1	1.35	6.1	50	4
2	1.26	6.5	60	4
3	1.35	7.6	120	12
4	1.71	8.2	120	2
5	0.9	6.7	130	9
6	1.35	7.2	130	16
7	1.71	7.8	130	6
8	1.71	7.4	140	4
9	1.71	7.0	150	5
10	1.35	6.2	160	4
11	1.8	6.6	170	2
12	1.8	6.7	160	4
13	1.35	6.5	150	6
14	1.35	6.8	140	9
15	0.9	7.0	120	14

3.7.2 Case Study Model Domain

The case study domain consists of a fine curvillinear flow grid nested within a coarser wave grid which in turn is nested within a larger and coarser wave grid. This is shown in Figure 3.23 along with low resolution bathymetry data from General bathymetric chart of the oceans (GEBCO).

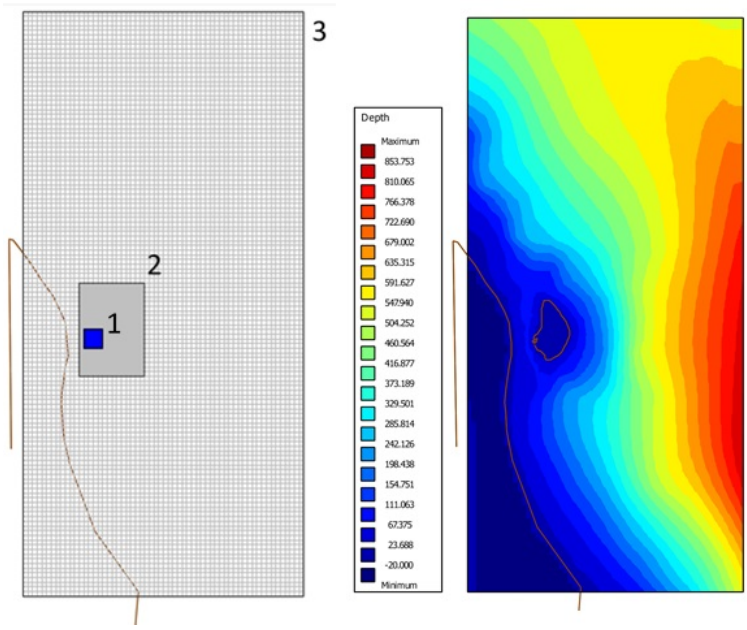

Figure 3.23: Model Domain and bathymetry in metres (MSL is at zero value). (1)Flow grid centered over Mnemba Island. (2)Wave Grid 1 encompassing the reef and Mnemba Island. (3) Extremely coarse wave grid 1

The flow grid is 2km^2 with Mnemba Island at it's centre and consists of 12x12m cells. The model was stable at this grid resolution with a 1 second time step.

The second grid encompasses the entire reef and the island. It consists of 25x25 m grid cells with a length and width of 10 km and 7 km respectively. The importance of this grid resolution is to maintain accuracy with wave-breaking at the reef crest in the model. The high resolution bathymetry for the reef is shown in Figure 4.19.

The final grid is a coarse grid with 500x500 m cell sizes. The length and width are 60 km and 30 km respectively. The large grid is the input for the off-shore wave forcing conditions from ERA. The grid was increased in size to create spatially varying conditions as the waves reached the reef surrounding Mnemba Island. The 500x500 m cells were substitued with 100x100 m cells to check for possible discrepancies caused by the large cell size change between nested grids but none were evident. The model just took significantly longer to run and thus the 500x500 m cells were used.

3.7.3 Time Frame

The model was run for a two week period to include a full tidal cycle and then scaled up to a period of 1 year using a morphological factor of 26.

3.7.4 Bottom Roughness

The effect of the spatially varying roughness of the fringing reef was incorporated into the model by creating a bottom roughness file. The mannings coefficient was altered according to observed roughness of the reef from the reef crest to beach.

Bed roughness on reefs can vary considerably and such these changes are reflected in the boundary layer and subsequently in the wave dissipation. The spatially varying roughness shown in Figure 3.24 was derived based on aerial photos from google earth ranging in hydraulic roughness from 0.1 m at the crest to 0.02 m at the beach. Although bed shapes can often be greater than 0.5 m in depth, values greater than 0.1 are not recommended in SWAN due to the little to no validation of this roughness range (Nunes and Pawlak, 2000).

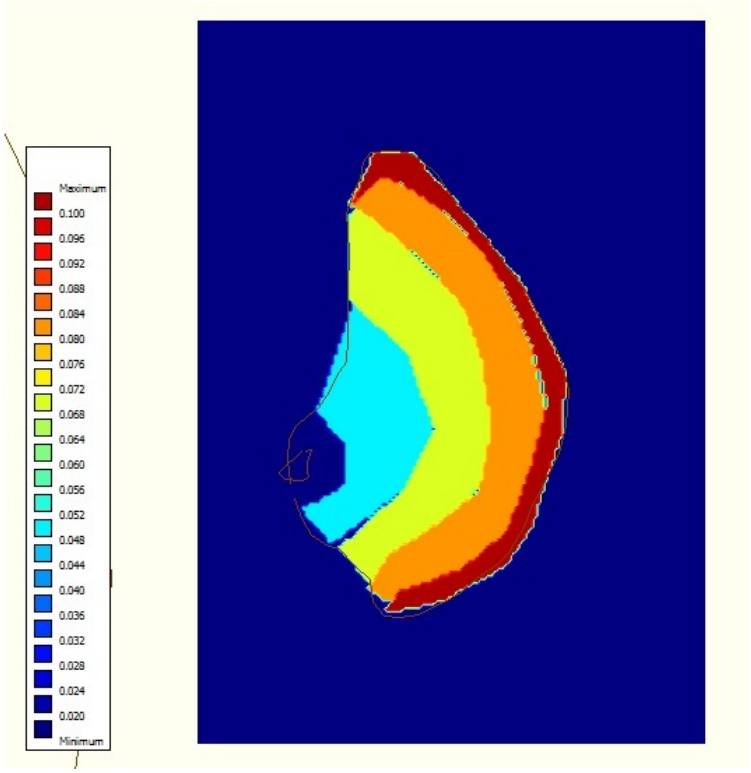

Figure 3.24: Varying bed roughness in metres from reef crest to Island beach

3.7.5 Boundaries

The reduced wave climate was uniformly imposed on the north, south and eastern boundaries of grid 3.

The flow grid was bounded by water level boundaries in the east and west with a Neumann boundary in the north and a current boundary in the south. The water level boundaries included the tidal level changes for two weeks, the Neumann boundary was set to have zero water level gradient for the simulation period and the current boundary was the input used to simulate currents in the channel. The tides were extracted from WXtide that makes use of data obtained from tidal gauges in Zanzibar. The water level variations were extended into the surrounding grids to allow for larger waves to propagate over the reef with the increased water depths.

The sediment boundary was changed to a Neumann boundary with the addition of the parameter *NeuBcSand* in the morphological input file. This specifies in the model that at all the open inflow boundaries, the flow enters carrying the same sediment concentration as computed at the interior of the model. This prevents the simulation from incorrectly modelling the accretion or erosion of sediment at the model boundaries.

Along with varying roughness a varying sediment depth was also incorporated into the flow domain in an attempt to restrict the amount of sediment available for transport. This was done because of the reduced sediment thickness on the actual coral structures as opposed to sediment rich areas surrounding the immediate island.

3.7.6 Sea level variations

To determine the effect of SLR the model was run with the existing water level and with an offset water level of +0.1 m. A rise of water of this magnitude is not just created by SLR but also through the effect of reduced bed roughness and flattening of the reef.

No vertical growth of coral was was accounted for in this thesis based on the current global and local trends of coral reach bleaching and degradation and not growth.

Chapter 4

Field work results

This chapter describes the results of the field work measurements taken between April and May 2016.

4.1 Beach Profiles

Based on the locations shown in Figure 4.1, the figures succeeding it show the profile changes between 19 April 2016 and the 29 May 2016.

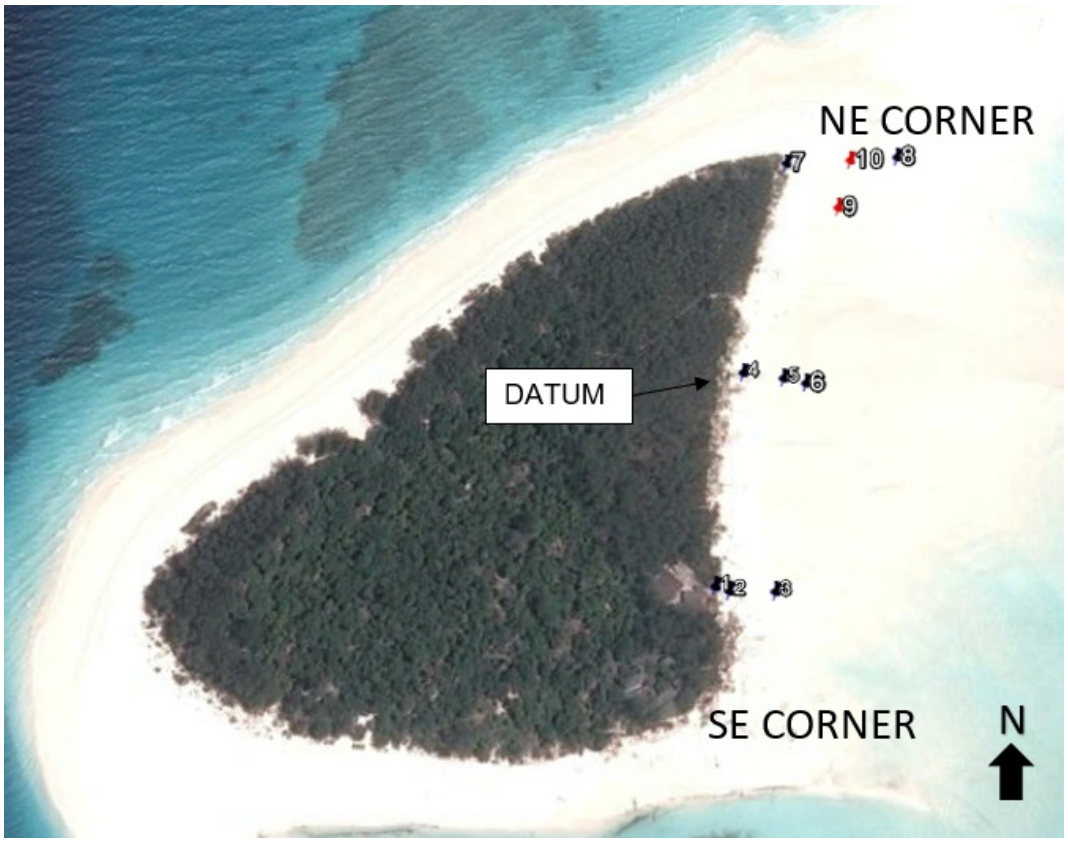

Figure 4.1: Beach profile location. SE corner profile (1-2-3). Middle Profile (4-5-6). NE profile 1 (7-9). NE profile 2 (7-10-8). Source of imagery: Google Earth

Figure 4.2 shows that the south-east (SE) corner profile experienced no level change at marker 1 due to its location on the concrete slab, significant erosion was however experienced beneath the slab and at the middle marker 2 shown in Figure 3.3. For clarity the measured data points are joined by the dotted lines in Figure 4.2 to illustrate the changing profile. The SE corner was a highly energetic and turbulent zone during high tides as waves interacted with the fallen trees. Full profiles at the south-east island edge where major erosion had occured were not measured because of the extremely dense collection of fallen trees blocking the area, individual points were thus measured.

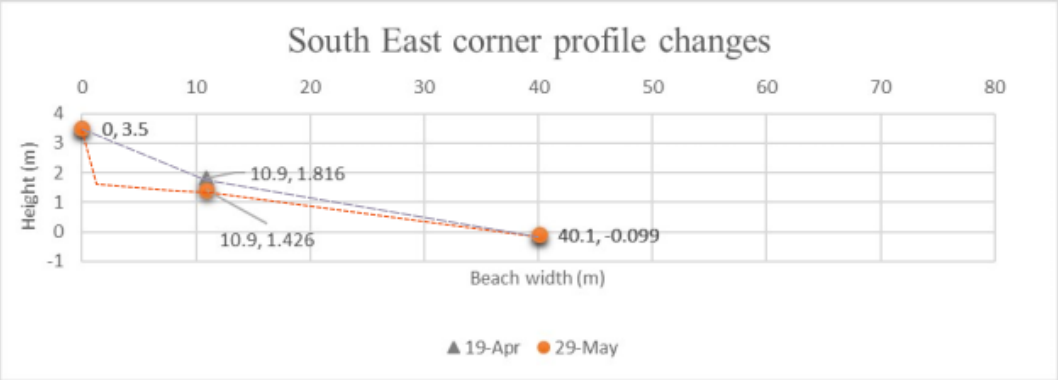

Figure 4.2: SE beach corner profile changes. Measured points represent the bed level above MSL and are joined by dotted lines for clarity.

The centre profile experienced little to no change maintaining an equilibrium as shown in Figure 4.3.

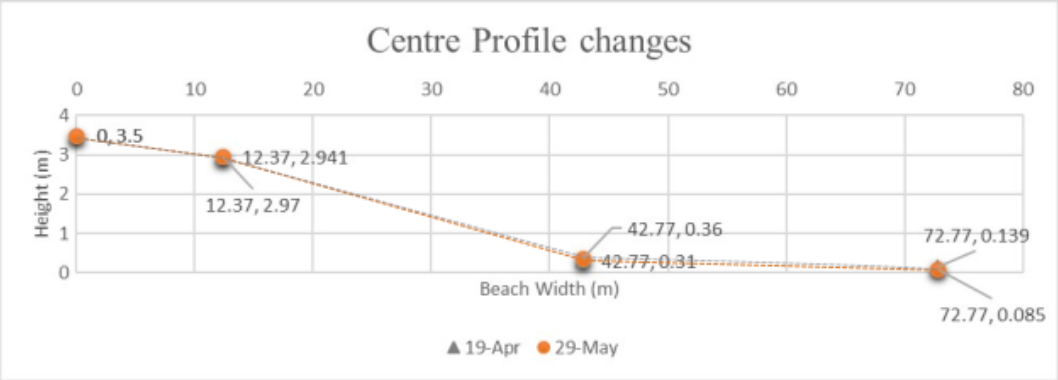

Figure 4.3: Centre Profile changes. Measured points represent the bed level above MSL and are joined by dotted lines for clarity.

Significant sediment loss of up to 70 cm at the seaward markers occurred at the NE corner. This followed the expected shift of sediments due to the southerly trade winds. Marker 7, which was the starting point for both NE corner profiles, remained unchanged at the top of the beach face as it was just above the wave run-up line for the duration of the profiles. Majority of the erosion occurred during the highest spring tides over a two-day period on the 6th and 7th of May with tidal ranges exceeding 3.5 m. Figure 4.4 and 4.5 show the beach profile changes between 19 April 2016 and 29 May 2016 measured at markers 7-9 and 7-10-8 respectively.

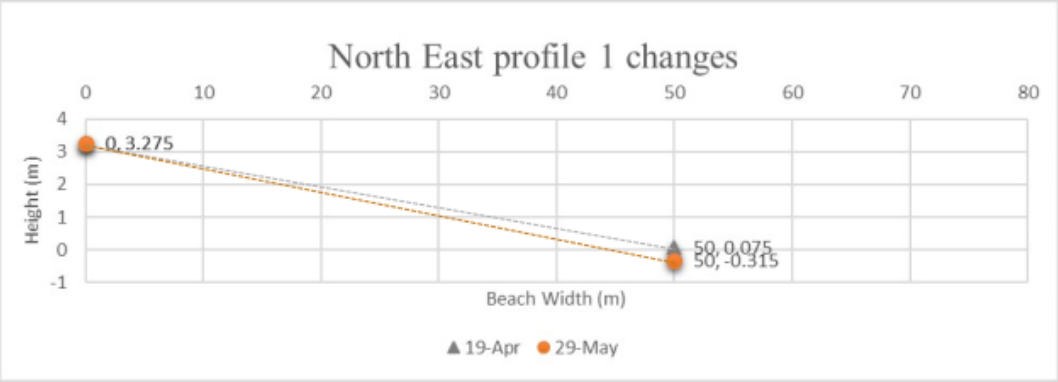

Figure 4.4: North-east profile 1 changes. Measured points represent the bed level above MSL and are joined by dotted lines for clarity.

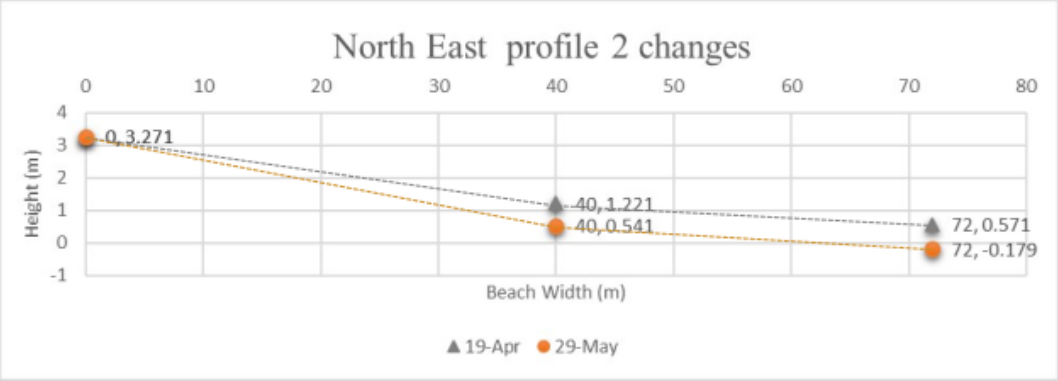

Figure 4.5: North-east profile 2 changes. Measured points represent the bed level above MSL and are joined by dotted lines for clarity.

Figure 4.6 illustrates the observed and measured movement of the north-eastern beach slope, a clear northward movement of the entire bank is visible. The same trend was visible on the south-eastern corner shown in Figure 4.7.

The remaining beach profiles surrounding the Island, although not surveyed, were carefully observed for noticeable changes. Over the two month period of April-May 2016 the effects of the trade winds were apparent as the April lip begin to erode as sediments moved Northward to begin formation of the October lip. Shallow scarp faces were created as the sediments moved northward along the western border of the island. Marker 14 shown in Figure 3.12 remained constant whilst at the top of the beach face marker 13 showed a bed level drop of 13 cm, a possible result of wave run-up.

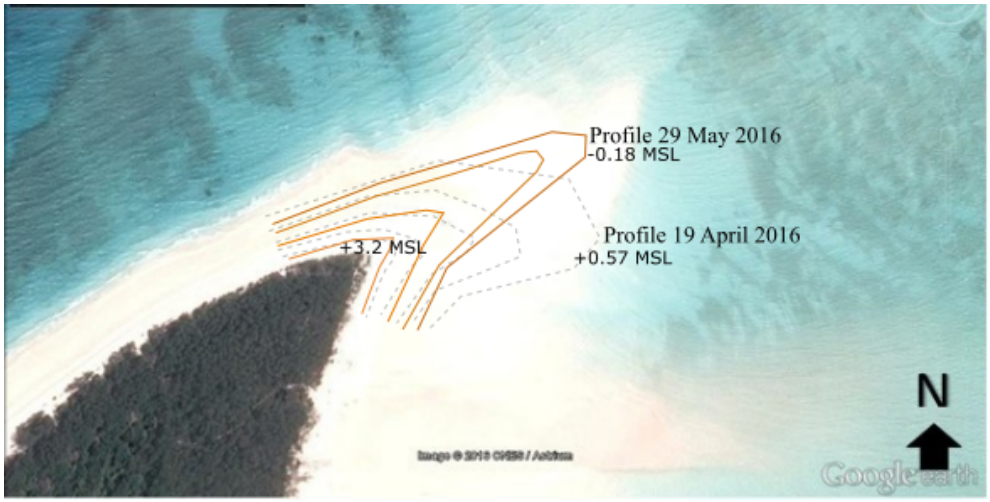

Figure 4.6: North-east profile changes illustrating northward movement of sediment. Dotted and solid lines represent changing contours derived from measured beach markers. Solid orange lines represents contours as of 29 May 2016 and dotted grey represents 19 April 2016. Source of imagery: Google Earth

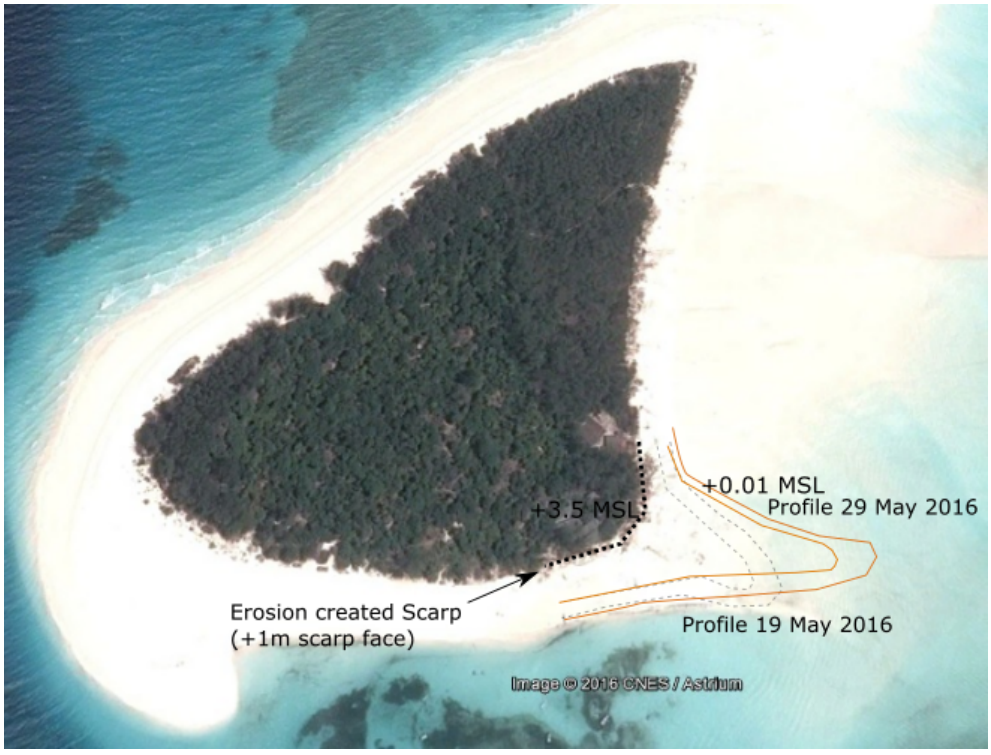

Figure 4.7: South-east profile changes illustrating northward movement of sediment, Dotted lines represent changing contours derived from measured beach markers. Solid orange lines represents contours as of 29 May 2016 and dotted grey represents 19 April 2016. Source of imagery: Google Earth

Table 4.1 shows the readings taken off the PVC markers placed at points 1-10 on Figure 3.12 on the specified days. Changes in profile shown in Figures 4.2-4.5 strongly correlate to the level readings taken during shorter intervals shown in Table 1. The greatest level changes coincide with the higher spring tidal ranges that occured on the $7th$ and $21st$ of May. The final values taken on 29 May indicating a relative drop or rise similar to the values recorded with the Dumpy level.

Table 4.1: Short- term Individual marker readings in cm rise or fall (-) from initial reading. LOST represents a marker that removed from its positioned and data is not available.

Marker	Location		Change in level on this date (cm)				
			19-Apr	3-May	7-May	21-May	29-May
1	0549'16.1"S	03923'05.4"E	0	-1	0	0	0
2	0549'16.2"S	03923'05.7"E	0	-3	-35	-39	-42
3	0549'16.2"S	03923'06.7"E	0	-3	-2	3	1
4	0549'11.3"S	03923'06.0"E	0	-1	0	4	2
5	0549'11.4"S	03923'06.9"E	0	3	3	-15	-5
6	0549'11.5"S	03923'07.4"E	0	-3	-4	-3	-7
7	0549'06.1"S	03923'07.0"E	0	-1	0	0	1
8	0549'05.9"S	03923'09.6"E	0	-20	-25	-57	-64
9	0549'07.2"S	03923'08.2"E	0	-3	LOST		
10	0549'06.0"S	03923'08.5"E	0	LOST			

4.2 Sediment properties

Suspended sediments trapped by the streamers revealed the particle size range that moves in the water column on an incoming tide. A particle size analysis, Figure 4.8, of several trapped streamer samples showed on average a d(0.1) of 123μm, d(0.5) of 215μm and a d(0.9) of 435μm. Wave conditions during collection period ranged from 10-30 cm wave heights with two to three second periods from the south-east.

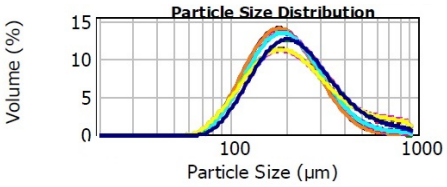

Figure 4.8: Particle size distribution of the suspended load caught by the 50 micron streamer traps.

In contrast to the finer suspended samples, in-situ bed samples varied by location along the eastern bank. Sediments collected at the south-east corner show on average a d(0.1) of 175 μm, d(0.5) of 324 μm and d(0.9) of 620 μm. The north-eastern corner sediments show on average a d(0.1) of 155 μm, d(0.5) of 455μm and d(0.9) of 807μm. The north-east corner samples show a larger content of coral remains and shell organisms responsible for the higher average grain diameter.

4.3 Timber Groynes

The constructed groynes fell short in both stability and effectiveness due to issues such as:

- The language barrier sometimes resulted in miss-communication.
- Untrained locals from Zanzibar were employed to cut the fallen Casuarina trees into planks and support poles with a chainsaw.
- The cut poles and planks were warped and skew.
- Locally sourced nails were extremely malleable.
- Construction was limited to low tide.
- The saturated beaches made digging pits for the vertical supports by hand slow and ineffective. The vertical poles had to be driven in by a 7 lb hammer whilst attempting not to split the poles.
- Vertical supports embedding was thus limited to a maximum of 1 m depth compared to the required 2 m.

Figure 4.9: The voids of Groyne 1 created from the skewness of the vertical supports. Source: Author

4.3.1 Groyne 1 - parallel to beach

The poor construction is evident in the lack of results however under the circumstances the untrained locals performed as best they could and deserved acknowledgement for their effort. Groyne 1 shown in Figure 4.9 contained excessive voids between the verticals preventing any major disruption in the flow. This method was both time consuming and used a large number of cut poles, equating to an insufficient design without perfectly straight poles or enough verticals to fill the voids. In an attempt to still gather usable results, horizontal planks were then added as shown in Figure 4.10.

Figure 4.10: The voids of Groyne 1 created from the skewness of the vertical supports. Source: Author

Similar erosion on both the sea-ward and landward side of the structure is visible as expected with the periodic flooding and drying caused by the tide. At the northern end of the structure although erosion on both sides were evident, a clear reduction in the erosion pit is visible along with accretion of sediment (Figure 4.11-4.12). One interpretation of this suggests a northward long-shore movement of sediment as would be expected with waves approaching from the south-east. The lacking of sufficient accretion around the structure removed the necessity for actual bed level change measurements therefore only photographic evidence was taken.

In terms of time scale, groyne 1 was in place with the horizontals from 8 May 2016 and still remained at the author's departure on the 30 May 2016. The pattern of Northward decreasing pit was consistent throughout this period, the depth and width of the erosion pit merely increased.

Figure 4.11: 30 May 2016, similar erosion pits on both landward(left) and seaward side of structure expected from periodic flooding and drying by tides. Source: Author

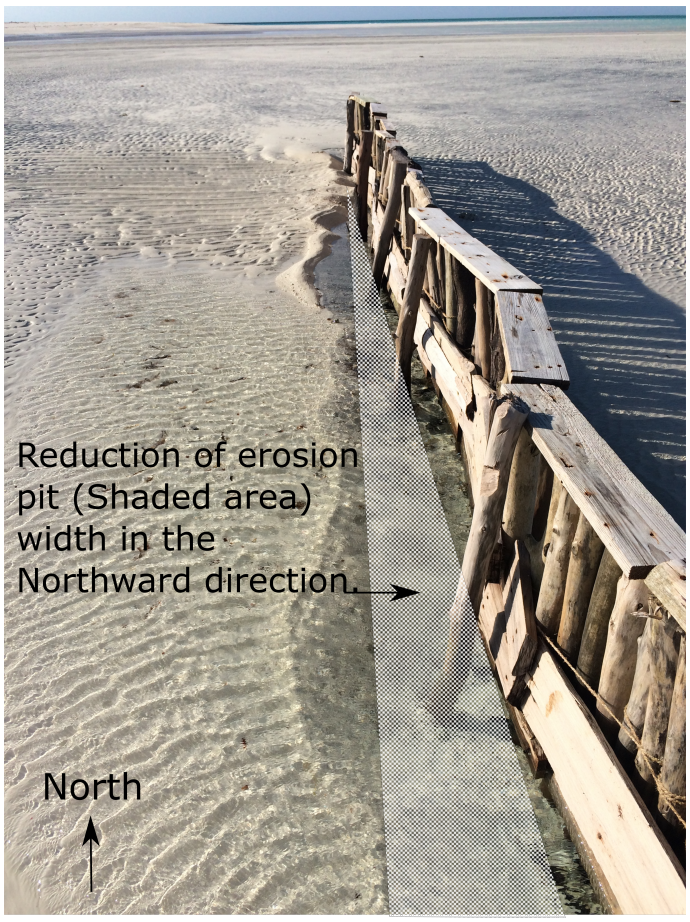

Figure 4.12: 30 May 2016, clear reduction of erosion pit width in the Northward(Top) direction. Source: Author

4.3.2 Groyne 2 and 3 - perpendicular to beach

The initial perpendicular groynes 2 and 3 are shown in Figure 4.13 and 4.14 respectively. Groyne 2 on the north-eastern corner was completely eroded the day after it's construction on 28 April 2016. The eroded structure remained partly intact with two metre long segments found in the shallow water north of the Island whilst the remaining planks and vertical were strewn along the north-eastern bank or not found at all. Two verticals remained in position but were pushed over as shown in Figure 4.15. The failure of the structure was speculated to be a result of insufficient skin friction to prevent pull-out or overturning. The inability to embed the vertical poles deeper resulted in the structure being rebuilt with an increased number of verticals on either side.

Figure 4.13: Groyne 2 at north-east corner

Figure 4.14: Groyne 3 at south-east corner.

Figure 4.15: Groyne 2 status one day after construction.

The rebuilt groyne 2 began to immediately show the shifting of the north-eastern bank in a northerly direction. Over the next six days the most landward point of the groyne became continously more exposed as the bank shifted whilst the seaward point of the structure remained relatively stationary (Figure 4.16). During this period the tide approached spring tides with tidal ranges in excess of four metres.

Figure 4.16: Bed level at the north-east groyne 2 on 9 May 2016 compared to the initial level on 3 May 2016 (red dotted line) and 6 May 2016 (green dotted line).

4.4 Streamer traps

The results from the streamer traps do not correspond to the prevailing wave and current direction.

Referring to Figure 4.17, the traps consistently showed the long-shore transport in zone two to be the highest area of sediment movement. Transport rates in the cross-shore direction were relatively similar for both zones. The contradiction was that the traps in both zone one and two show the major sediment transport to be southward, opposite to north-western wave direction and northerly current direction. During the periods the traps were deployed, wave height at the traps were typically consistent ranging from 10-15 cm at the beginning of deployment period and end with 20-35 cm wave heights. Although currents were not measured during trap deployment, the incoming tide and wave direction suggest a current direction similar to the wave direction.

One speculation for the sediment transport discrepancy is the trap location in the water column. The traps were placed 6 cm above the bed and testing began when the entire trap array was completely submerged above their opening. This equated to approximately 17 cm water depth. The test period ended 45 minutes later at which stage water depth at zone two depending on the tide phase (spring or neap) was between 90-150 cm. Initially northward sediment transport may have dominated while water depths were lower and the trap inlet covered majority of the water column. However as the depth increased the trap inlet covered a lower position in the water column where the effect of undertow ,bed ripples and oscillations at the bed transported sediment opposite to the direction in the upper section of the water column.

A second possible explanation is sediment losses out the traps. Although the trap net was closed at the end and restrained using a PVC pipe, the netting between the rear and front supports moved freely which could have resulted in sediments leaking out the front opening. The fine netting also trapped air if a passing wave lowered the water level enough for air to enter through the inlet, this air then travelled through the netting raising the netting in the middle to the water surface which could have also resulted in sediment leaking. The interaction between the free moving net and the bed was unavoidable and could too have resulted in excess sediment in the water column.

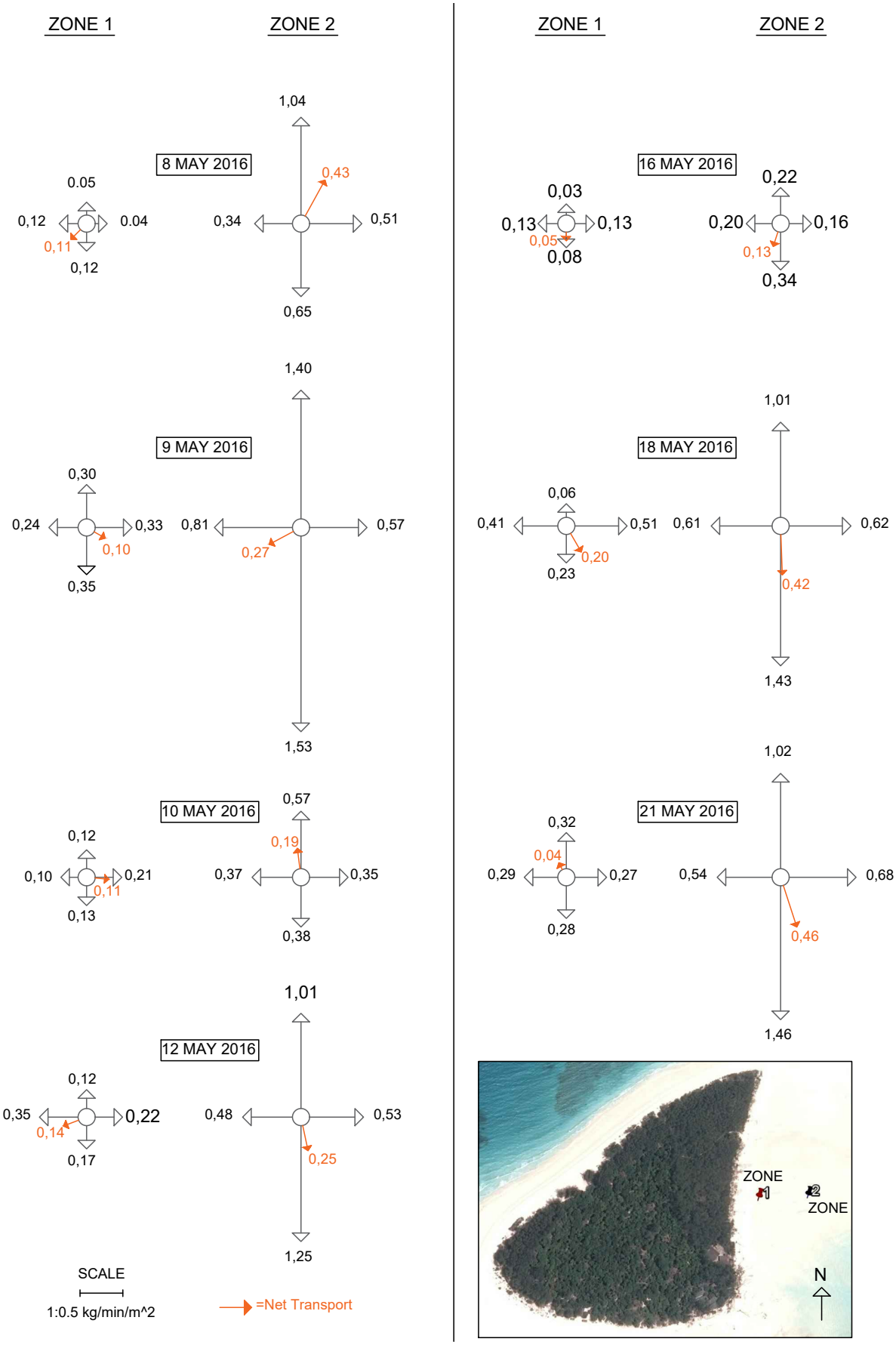

Figure 4.17: Sediment transport rate and direction in zone 1 and 2 (refer to map locations bottom right) from the streamer trap arrays on the specified days.

4.5 Reef Bathymetry

A channel deeper than 75 m separates Mnemba island from the coast of Zanzibar. The reef bathymetry, derived from the transects and triangular interpolation, shown in Figure 4.18, is relatively constant for the entire reef with varying degrees of coral population. The deeper northern and southern reef locations are shown in Figure 4.19 as the contours steepen into the channel, at no stage are these areas fully exposed and thus waves propagating from the south and north can effectively always reach the island with little attenuation.

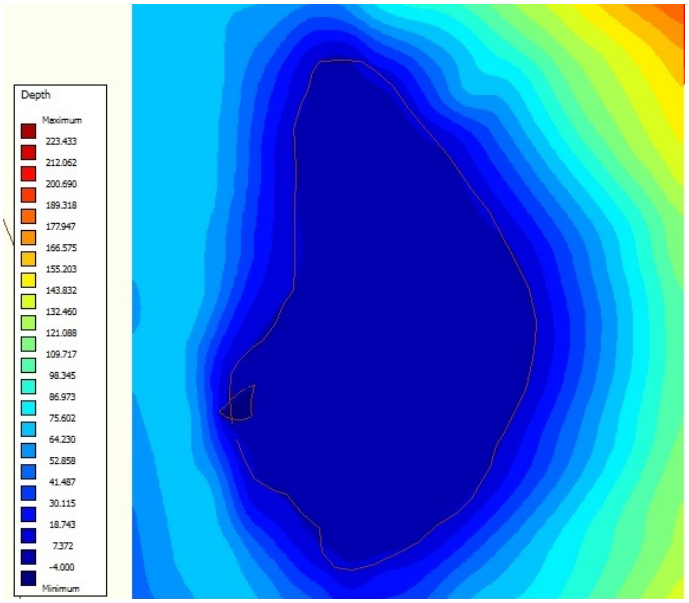

Figure 4.18: Full reef bathymetry in metres from the transect lines using triangular interpolation (MSL is at zero value).

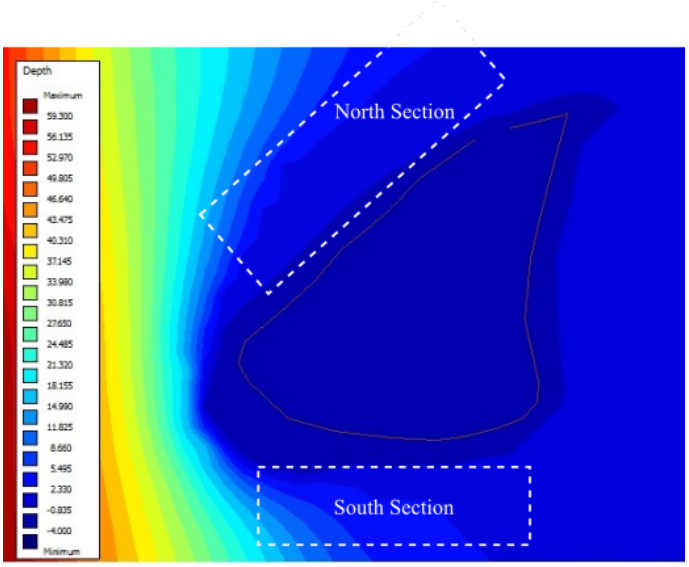

Figure 4.19: Outlining the northern and southern sections not exposed by the spring tide (MSL is at zero value).

The most populated coral region is the reef crest which has a higher elevation than the reef flats. From the crest the coral population diminishes as it approaches the island where fine carbonate sediments make up the sea-bed, this is visible in satellite imagery shown in Figure 4.20.

Figure 4.20: Coral population reduction from reef crest to beach face. Source of imagery: Google Earth

4.6 Waves

It is visible from Figures 4.22-4.25 that all three locations and time periods show a strong relationship between wave height and depth, which is an increase in water depth resulted in an increased wave height.

The reef is almost completely exposed at spring low and thus wave transmission from the outer edge to the eastern Banks of Mnemba is limited to high tide and therefore the time period of focus for this thesis. Waves that approach from the south and north can however still propagate towards the northern and southern side of the island.

At full high, white capping is visible at the outer edge of the reef as the waves interact with the reef crest. With a water depth of approximately 3.5 m at this tidal stage, most waves propagate over the reef crest unbroken. Wave parameters found at this tidal stage at the sensors include an average wavelength of 50 m, maximum wave heights of 0.48 cm with an average period of 10 seconds. As waves propagate from A1 to A2 over a distance of 500 m the water depth decreases by 40 cm. The average wave height decreases as much as 26 percent between these two points (Figure 4.24). Table 4.2 shows the maximum and minimum wave heights per sensor and date of occurrence relative to water depth at that point.

Although no directional wave data was obtained from the sensors, on the island two wave directions were experienced as shown in Figure 4.21. As waves approach the island beach face over the relatively flat shore-rise, depth limitation and wind effects are prevalent as the waves start to spill combining with a small collapsing breaker at the intermediate to steep beach face slope. The primary wave at the beach approaches from the south-east now characterized by short periods up to 4 s, short wavelengths up to 5 m and plunging wave heights up to 80 cm at spring tide after shoaling. A secondary wave with a slightly larger wave height and significantly longer period and larger wavelength approaching from the north-east was also consistently observed at high tides, conforming to the reduced wave attenuation effect of the reef at high tide and the effects of refraction.

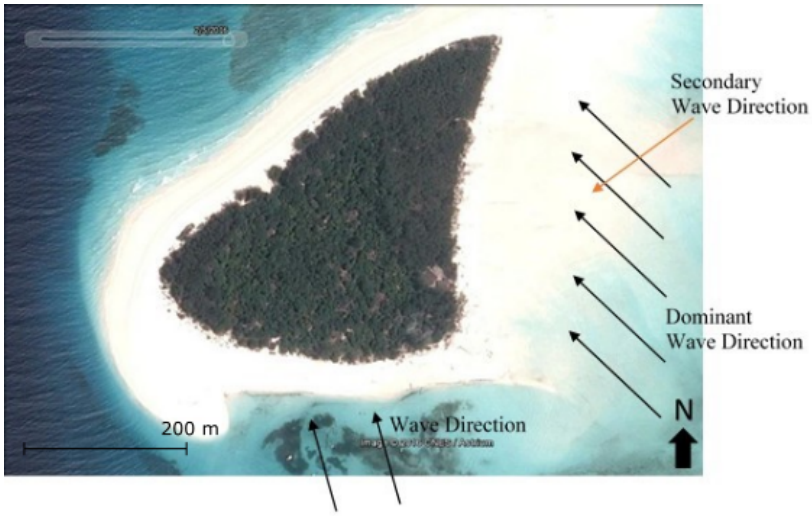

Figure 4.21: Observed wave directions at the Island. Arrow direction represent the wave travel direction. Source of imagery: Google Earth

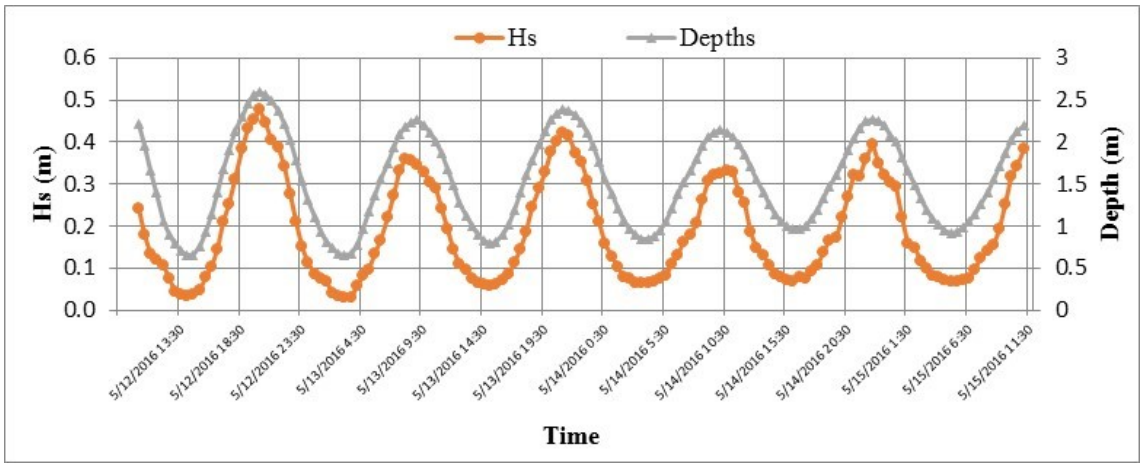

Figure 4.22: Wave and depth time series (in metres) at sensor A1. Refer to Figure 3.20 for locations of sensors.

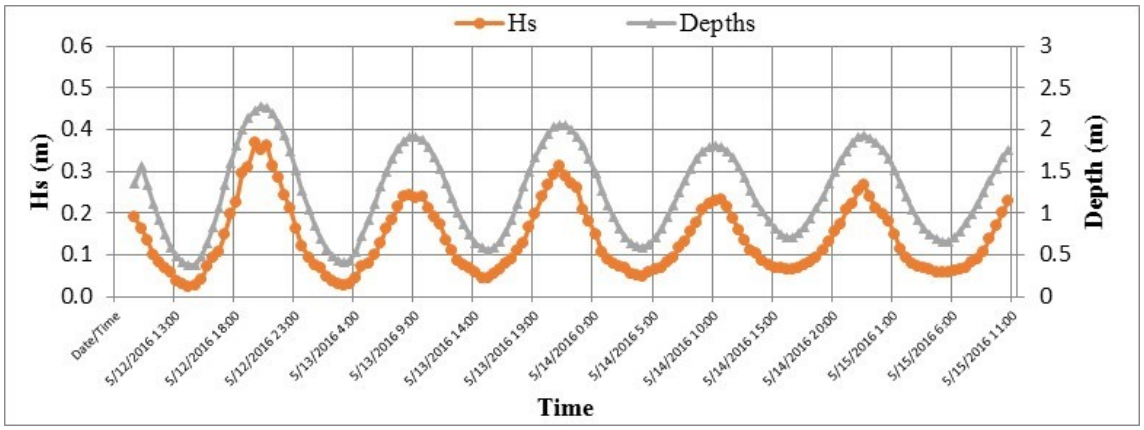

Figure 4.23: Wave and depth time series (in metres) at sensor A2. Refer to Figure 3.20 for locations of sensors.

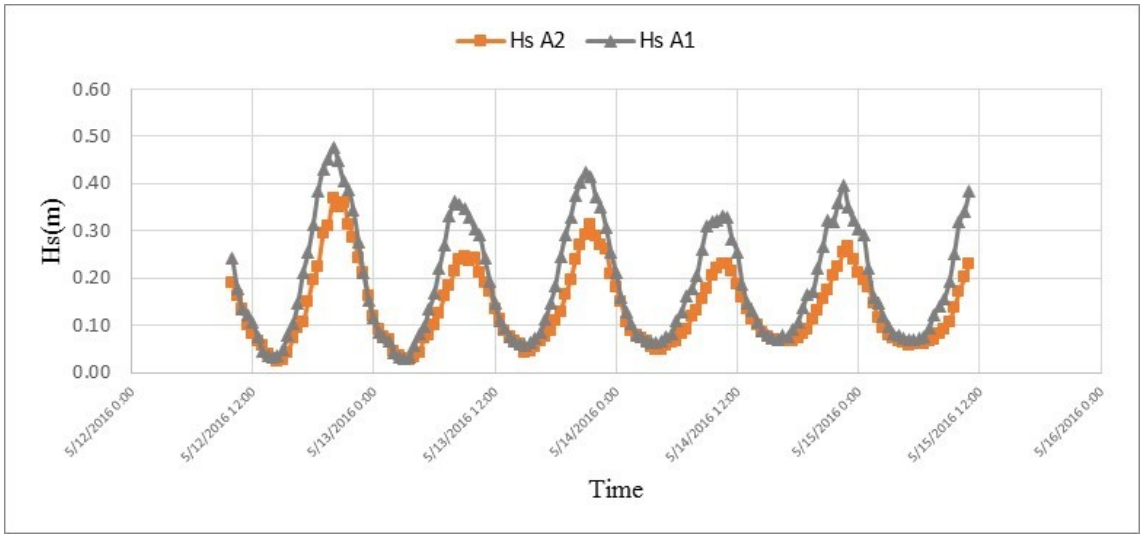

Figure 4.24: Time series of the wave heights at locations A1 and A2 for comparison.Refer to Figure 3.20 for locations of sensors.

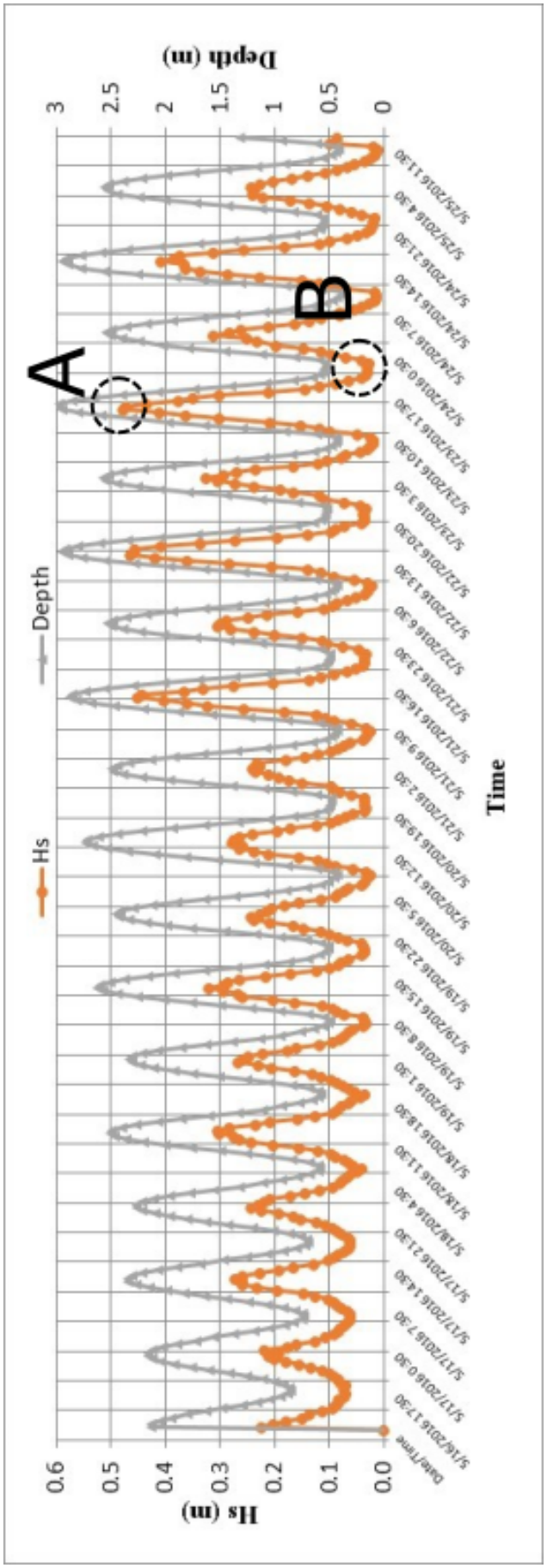

Figure 4.25: Wave and Depth time series at sensor B2. Refer to Figure 3.20 for locations of sensors. Point A refers to spectra at high tide shown in Figure 4.28. Point B refers to the spectra at low tide shown in Figure 4.29.

Table 4.2: Maximum and minimum wave heights (All measurements are in metres)

Day (May 2016)	Max Hs	Min Hs	Avg. Hs	Depth at max Hs	Date Max Hs	Max Depth	Min Depth	Date Max Depth
				SENSOR B1				
16-19	0.32	0.03	0.13	2.5m	5/19/16 15:00	2.62	0.49	5/19/16 15:10
20-25	0.48	0.01	0.15	2.94	5/23/16 16:30	3.01	0.39	5/23/16 17:00
				SENSOR A1				
12-15	0.48	0.03	0.19	2.6m	5/12/16 20:00	2.60	0.65	5/12/16 20:00
				SENSOR A2				
12-15	0.37	0.02	0.14	2.23	5/12/16 19:30	2.28	0.38	5/12/16 20:30

4.6.1 Spectra and wave-by-wave analysis

The two methods used for the derivation of the wave parameters are compared in Figure 4.26 and 4.27 . The depths were first computed to ensure the accuracy of the calibration factors across both methods. Figure 4.26 shows that both methods return the same water level profile.

The significant wave height plots show an discrepancies between the wave-by-wave and spectral analysis. The spectral method returns on average 40% larger wave heights, see Figure 4.27. The reason for the discrepancies between the two wave analysis methods is unclear. Both methods rely on assumptions that can influence their results. For example the wave-by-wave assumes that a sign change in slope is a reasonable detector of individual waves, while the spectral method method requires the highest resolved frequency to be estimated for low pass filtering. These factors can influence both results.

The SWAN wave model was calibrated to predict wave heights that were bounded by the estimates from the two methods.

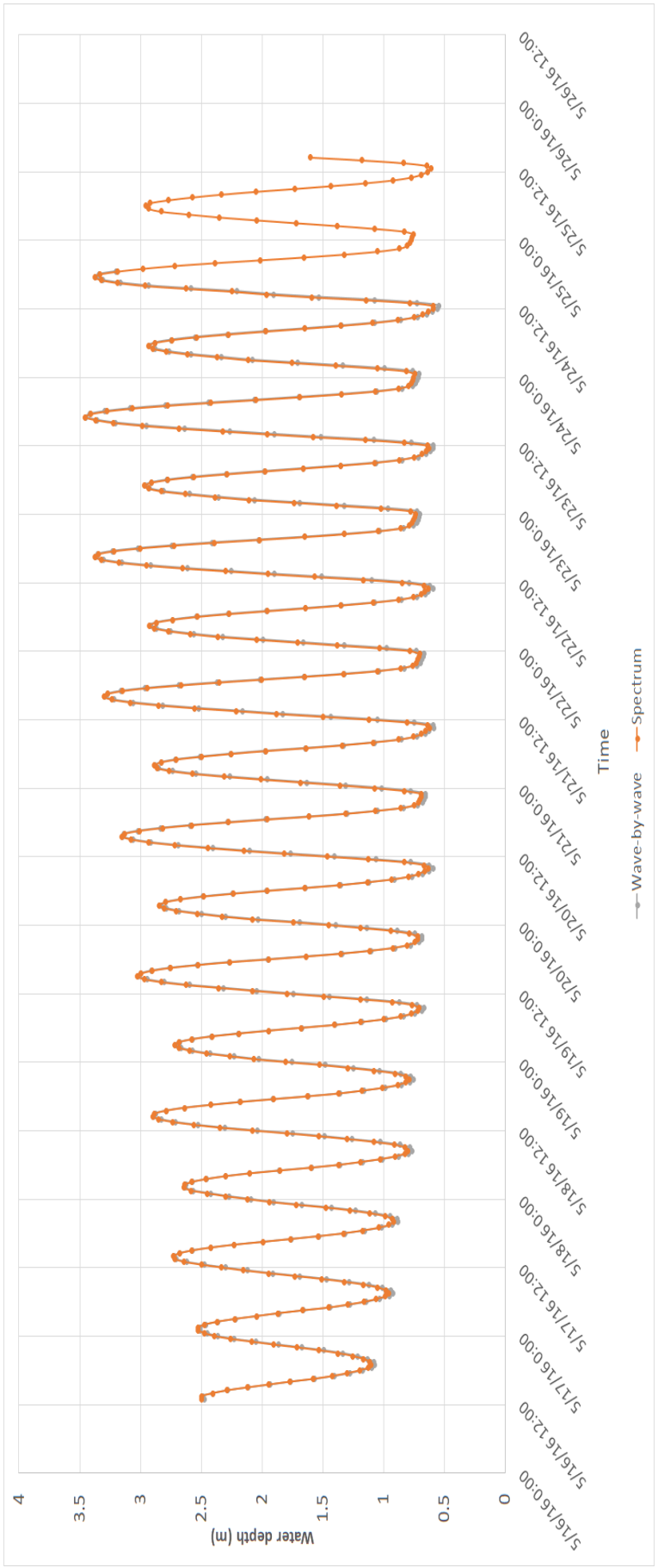

Figure 4.26: Depth time series at sensor B2. Orange markers represent the depth profile derived by the spectral approach. Grey markers represent the depth profile derived from the wave-by-wave analysis.

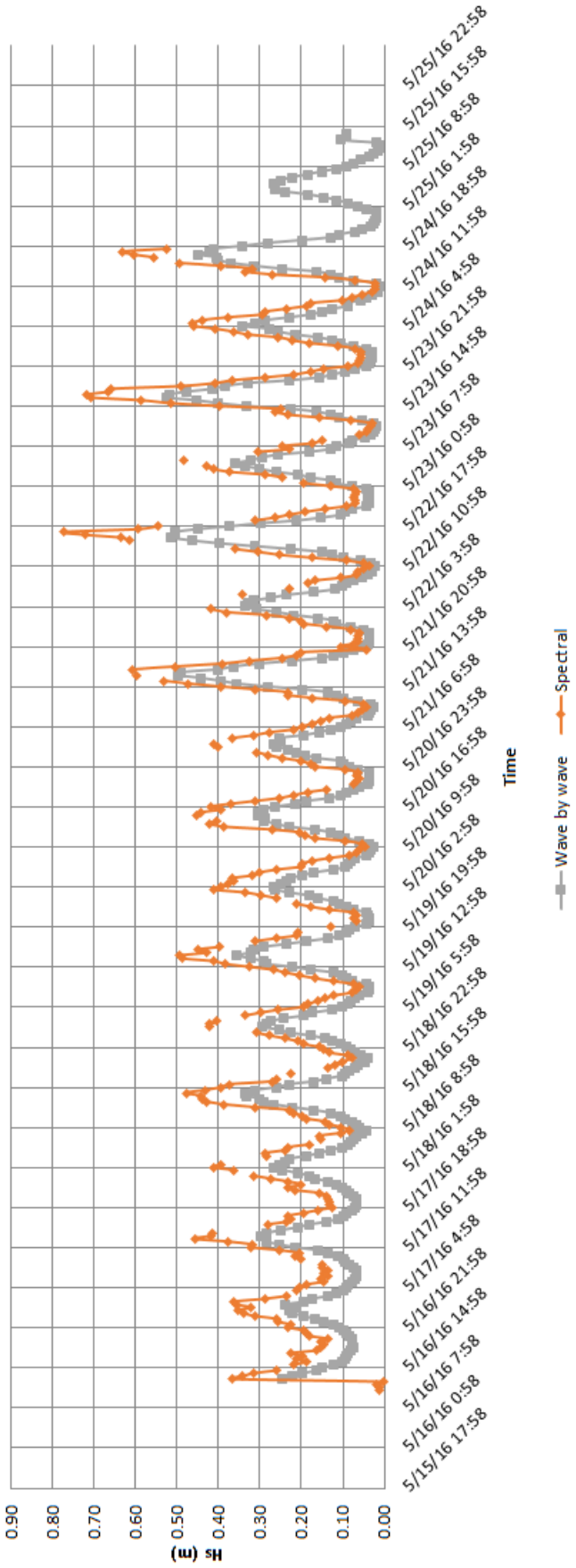

Figure 4.27: Wave time series at sensor B2. Orange markers represent the significant wave height profile derived by the spectral approach . Grey markers represent the significant wave height profile derived from the wave-by-wave analysis. Unexplained, consistently larger wave heights are derived from the spectral approach.

4.6.2 Spectra

The wave spectra were plotted at two hour intervals between spring high and spring low. This was done by utilising a MATLAB-script in which the pressure readings from the sensor are converted to a variance-density spectrum, showing the distribution of energy (Verhagen, 2013).

Figure 4.29 shows a depth limitation effect where long waves (lower frequency) are completely blocked off up to 2 hours before and after spring low tide. It is at this stage that the spectra can be described as low energy broadband noise since there are effectively no waves present that are resolvable by the pressure sensors. As the tide approaches spring high, the long waves propagate over the reef and enhance the wave erosion effects when they reach the island. The higher energy of long waves is shown in Figure 4.28 as the tidal phase approaches spring high tide. The spectra provide quantitative evidence of the on-site wave observations on Mnemba island.

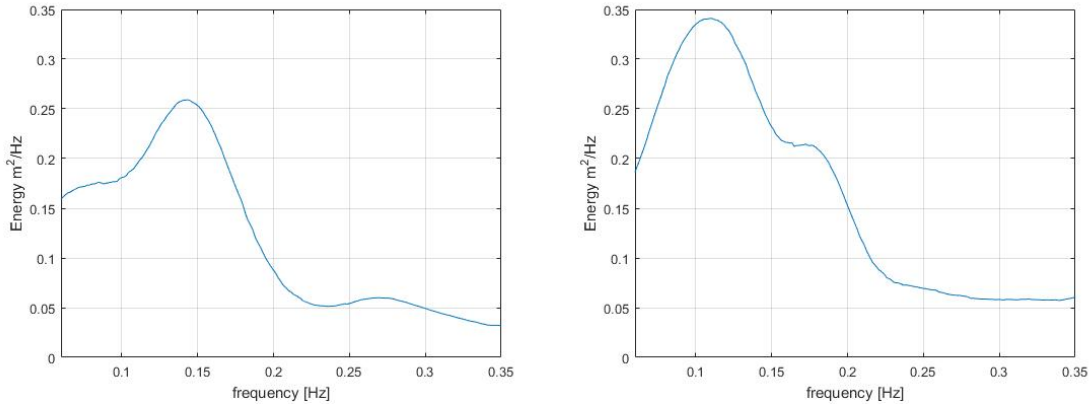

(a) (b)

Figure 4.28: Wave spectrum illustrating the high energy of the low frequency waves as the tidal phase approaches spring high. (a)Represents the wave spectrum 2 hours before spring high tide. (b) Represents the wave spectrum at spring high tide. Refer to figure 4.25 point A which shows the point at which the greatest wave energy is experienced.

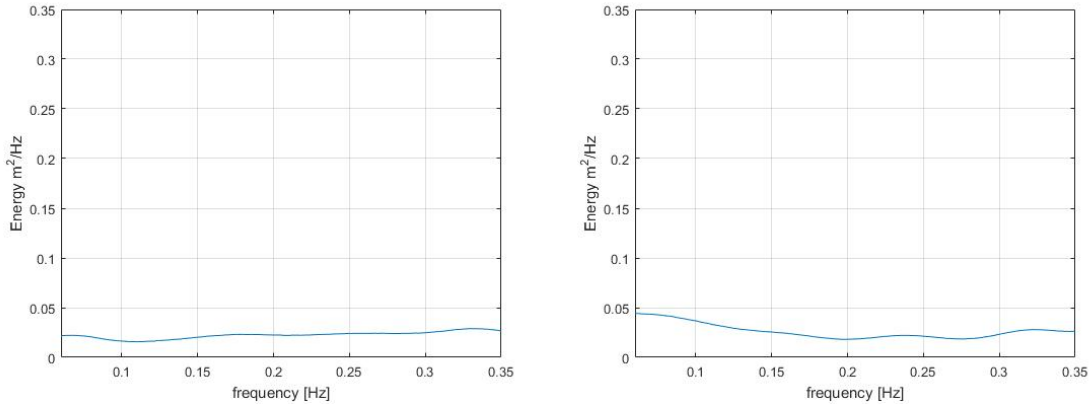

(a) (b)

Figure 4.29: Wave spectra illustrating the little to no wave energy as the tidal phase is near spring low. (a)The wave spectrum at spring low. (b) The wave spectrum 2 hours before spring low. Refer to figure 4.25 point B which shows the point at which little to no wave energy is experienced.

4.7 Currents

The measured surface current directions predictably followed the trade winds. The currents approaching from the south wrapped around the Island and converged at the north-eastern border of the Island. Although the currents follow trade winds, the effect of local winds on the currents were not measured as the currents were measured on mornings when there was effectively no wind.

The greatest surface currents were measured just off the Island in the western channel of 0.47 ms^{-1}. On the eastern side the surface currents are much weaker with maximum velocity measured at 0.22 ms^{-1}. Table 4.3 shows the measured readings according to the beacon paths in Figure 4.30.

Table 4.3: Surface current measurements 28/29 May 2016

Date	Point	Distance (m)	Time (s)	Velocity (ms^{-1})
28-May	1–2	224	1016	0.22
	2–3	120	666	0.18
	3–4	315	1861	0.17
	5–6	108	2181	0.05
	7–8	80	366	0.22
	9–10	134	507	0.26
	10–11	134	505	0.27
29-May	1–2	78	581	0.13
	3–4	515	2320	0.22
	5–6	307	649	0.47
	6–7	90	300	0.30

Figure 4.30: Surface current beacon paths 28/29 May 2016. Source of imagery: Google Earth

Figure 4.31 shows the surface current directions and the convergence point at the NE corner. At the higher tidal levels this point is a highly turbulent area as waves that approach from the SE collide with waves that approach from the north. Significant sediments are disturbed and suspended in the water column.

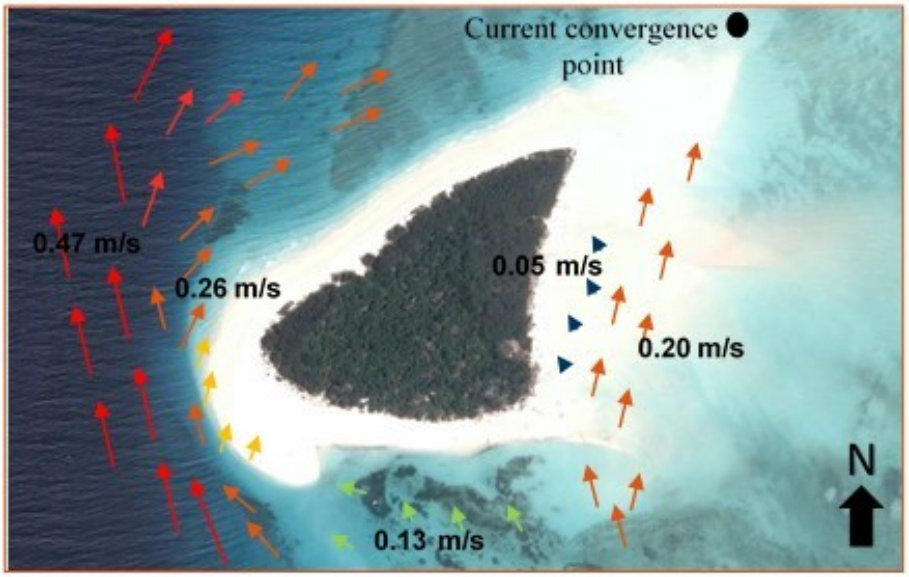

Figure 4.31: Representative Surface current directions and convergence point 28/29 May 2016. Source of imagery: Google Earth

Chapter 5

Modelling results

This Chapter presents the model results which are critically analysed and compared to the field work results and existing literature. The effect of the coral reef roughness on wave attenuation and sediment transport is identified along with the impact of SLR.

5.1 Model verification

No formal wave direction measurements were taken on the reef flat and thus model calibration relied on replicating measured wave heights at the sensor locations. The measured and simulated wave heights at SENSOR B2 location show strong similarities between them which serves as a basic verification of the SWAN wave output, see Figure 5.1. The in-situ observations also closely match the simulated flow directions. Figure 5.1 also shows the zero wave height at low tide.

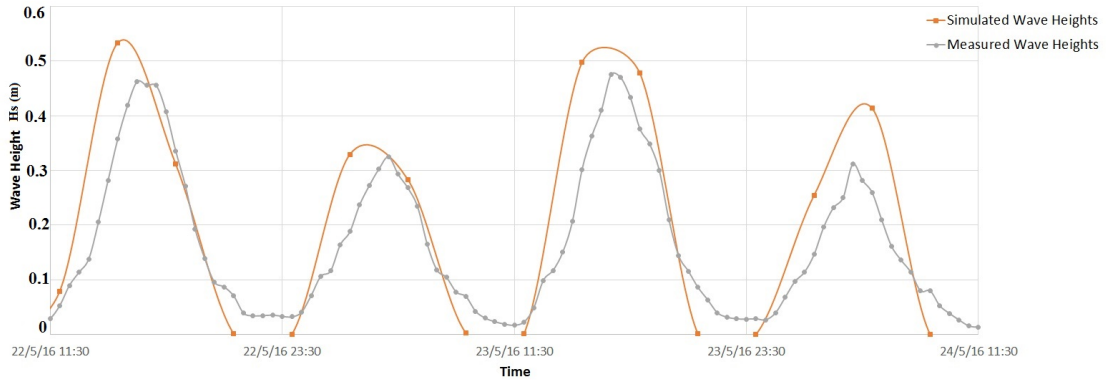

Figure 5.1: Validation of the SWAN output comparing simulated wave heights at SENSOR B2 with in-situ measurements. Sensors were positioned in holes to keep them submerged at all times.

5.2 Wave Transformation over reef

The transformation of the waves as they approach the reef crest are shown in Figure 5.2 for a spring high (blue line) and spring low (red line) respectively. As expected, the majority of wave dissipation occurs at the reef crest regardless of tidal phase. The approaching deep-water waves steepen and break as they interact with the steep slope onto the reef platform.

Figure 5.3 illustrates the dissipation zone near high spring tide at the reef crest along with the dissipation line at Mnemba Island. Evident is the major dissipation on the reef crest with the reef flat dissipating the remainder of the wave energy. The contrasting high dissipation zone on the southern side of Mnemba Island compared to the eastern side can be attributed to the reduced reef zone south of Mnemba Island that allows larger and more frequent waves to reach the island.

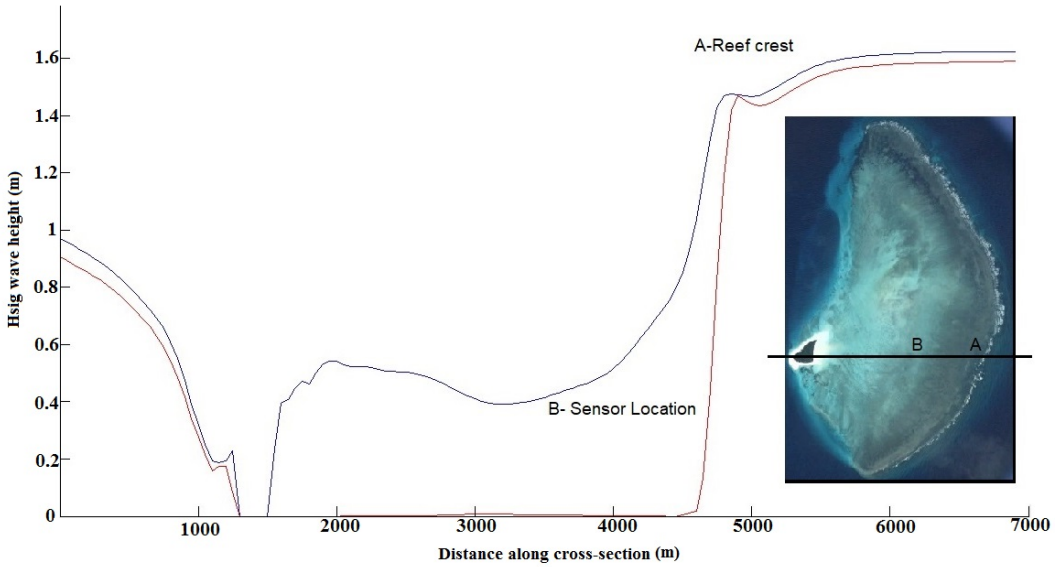

Figure 5.2: Cross-section of the wave dissipation (change is significant wave height) at Spring High (blue) and low (red).

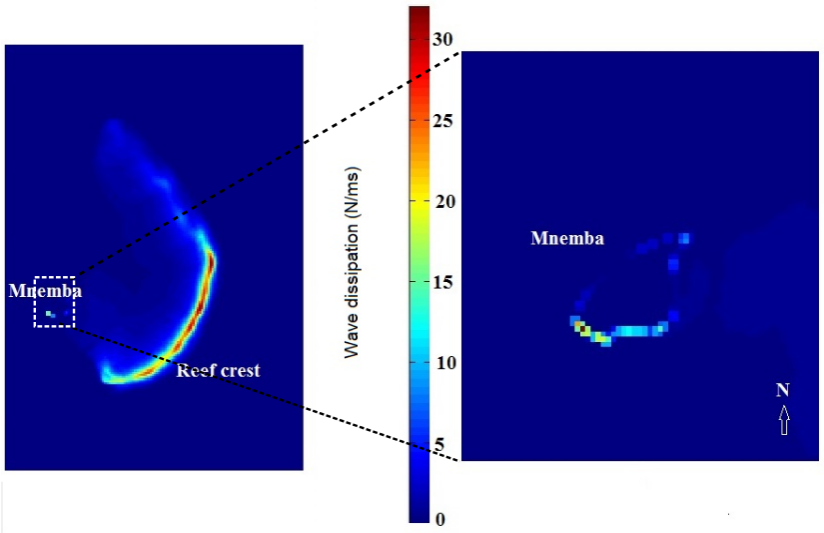

Figure 5.3: (left) Wave dissipation approaching spring high showing the entire reef. (Right) Focused view of wave dissipation around the southern and eastern border of Mnemba Island.

At spring high the significant wave height drops by up to 70% between point A (reef crest) and B (sensor A1 locaction). At this stage the wave heights begin to increase as shoaling occurs until breaking once again at Mnemba Island. Evidence of shoaling is drawn from this increase in wave height combined with the reduction of wave length as the waves propagate over the platform towards Mnemba Island.

At spring low when the reef is exposed complete dissipation of wave energy occurs at the crest. As the tide rises the dissipation line shifts forward as waves are allowed to propagate onto the reef. As the dissipation line shifts landward the reef flat begins to play its role in energy dissipation.

Simulated wave heights and directions are shown in Figure 5.4 and 5.5 for spring high and low respectively. The platform's elliptical geometry refracts the waves which partly converge on the eastern side of Mnemba Island. The Southern side of the island is exposed to larger wave heights as a result of the reef crest shape. Waves that approach from the South are able to propagate closer to Mnemba island in deeper water unaffected by bed roughness until less than 1 km from the southern beach face. At spring low no waves are able to propagate onto the reef and hence the increased shadow zone northward of the island.

Point (a) illustrates the shadow zone created by the predominately northerly directed waves and hence the relatively low energy zone at the beach face. Point (b), although not observed in-situ, is an effect of refraction calculations at the southern reef edge. The refraction calculations are based on a refraction approximation which in turn is based on the mild-slope approximation. The refraction is essentially expressed in terms of the directional turning rate of individual wave components in the 2D spectrum (Holthuisjen, Booij, and Rise, 1993).

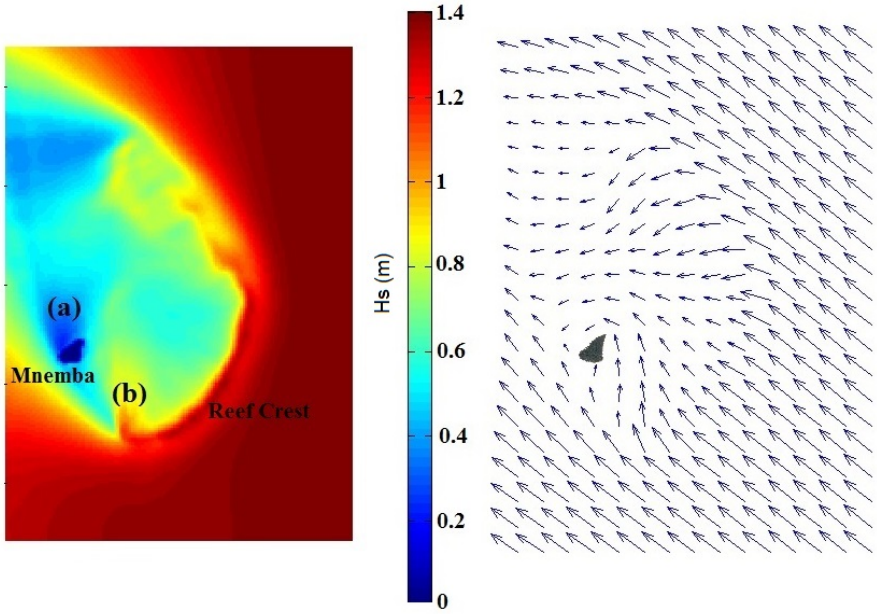

Figure 5.4: (left) Significant wave height approaching spring high showing majority of attenuation at the reef crest. (Right) Wave direction converging on Mnemba Island south-eastern corner.

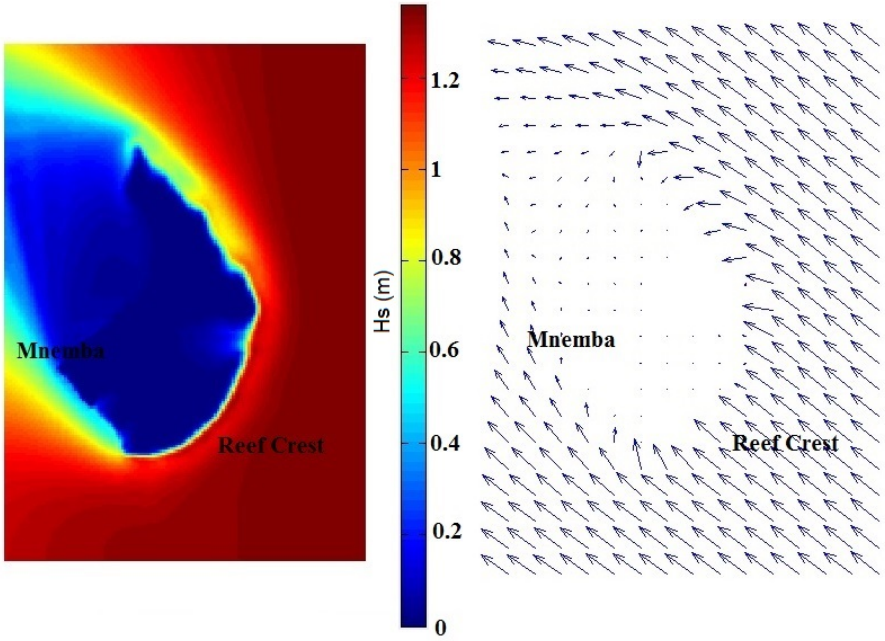

Figure 5.5: (left) Significant wave height at spring low over the reef showing complete dissipation at the crest. (Right) Wave direction at spring low

5.3 Near-shore wave analysis

Once the waves reach Mnemba Island they begin to interact with fallen Casuarina trees that litter the eastern and southern vegetation line. The dense concentration of sediments in the water column are visible in Figure 5.6 in contrast to the clear water sea-ward of the wave breaking zone.

Figure 5.6: High concentrations of sediments in the water column at the south-eastern corner of Mnemba Island.

Although relatively small in height (< 0.6 m) on the eastern side, the wave-tree interaction and wave breaking creates a turbulent zone, lifting the fine sediments into suspension. The less protected south-eastern bank is exposed to more consistent wave heights directed perpendicular to the southern Mnemba Island boundary. This consistency could is explained by the deeper water and reduced reef zone on the approach to the southern bank of Mnemba, allowing waves to reach the island more frequently. The average wave heights predicted by the model show an average wave height at point (40,25) of 0.3 m in contrast to 0.1 m at point (43,38).The locations are shown in Figure 5.7 with the simulated wave height for each point shown in Figure 5.8 and 5.9.

Figure 5.7: Locality view of near-shore measurement points. Source of imagery: Google Earth

The percentage increase in wave height between tidal phases also gives another indication of the effect of the reef geometry on wave measurements and the more consistent wave heights on the southern border. At cell (43,38) the increase in wave height is as much as 5.6 times as the tidal phases moves to spring tide. At cell (40,25) the increase in wave height is below 2.5 times the wave height experienced during neap cycles.

Waves in the channel on the western bank besides those refracted to the island are mostly directed away from the island or parallel to the channel and do not play a major role in erosion. However the current in this area as shown in Figure 5.11 plays a major role in the transport of sediment along this plane and are responsible for the October and April 'lip' referred to in Section 3.4.4.

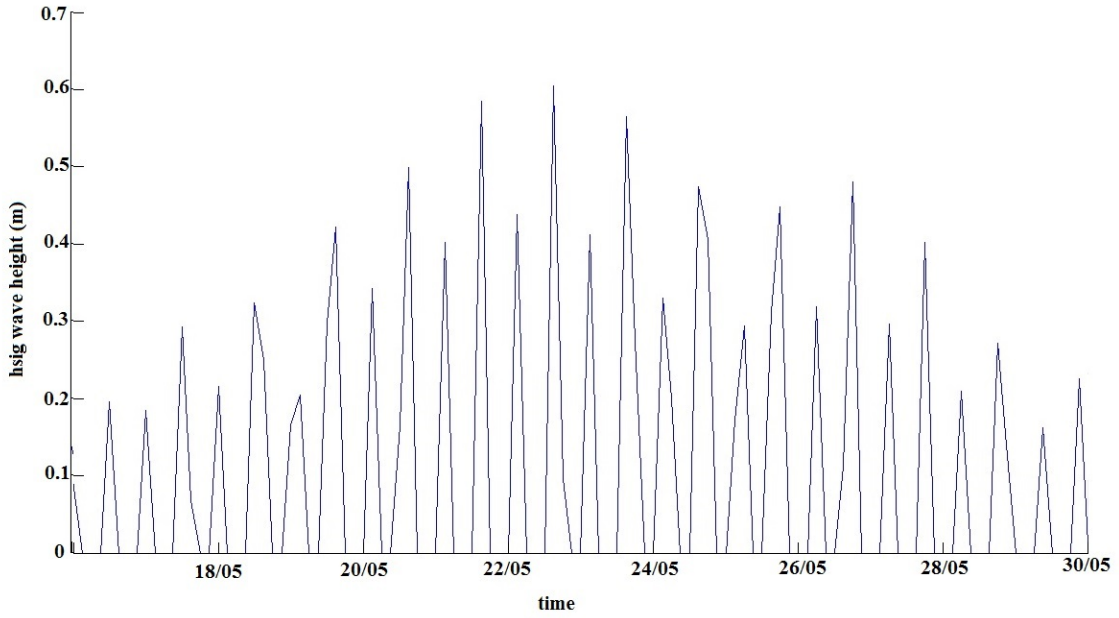

Figure 5.8: Significant wave height at grid cell (43,38) on the eastern island boundary. Periods of no wave height indicate a dry bed.

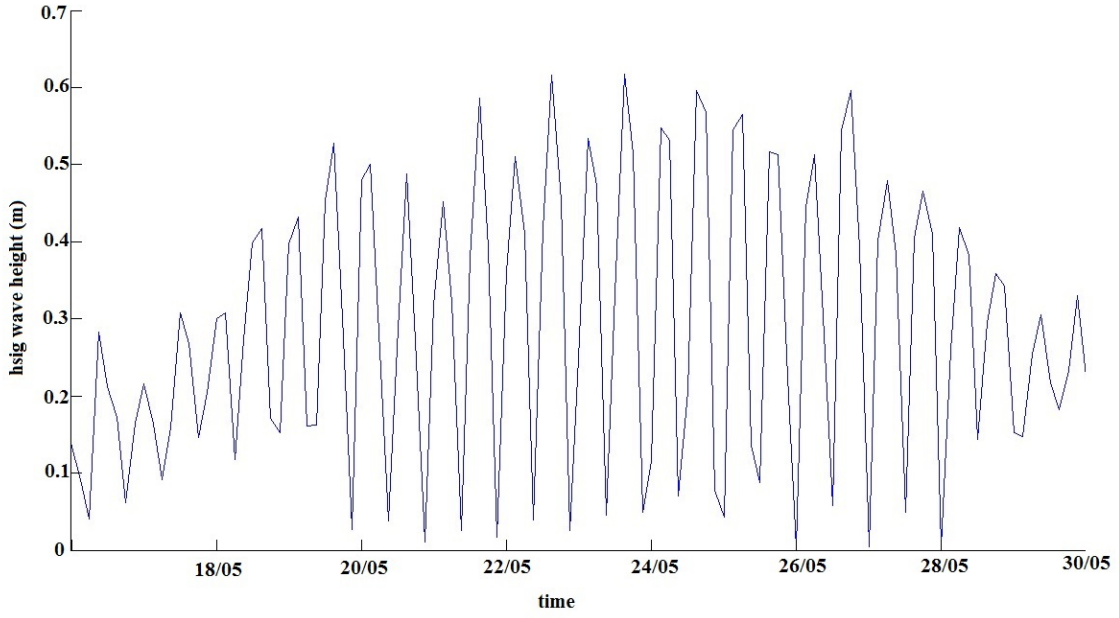

Figure 5.9: Significant wave height at grid cell (40,25) on the southern island boundary. Periods of no wave height indicate a dry bed.

The north to north westerly wave direction along the eastern boundary, see Figure 5.10 is the driving force of the long-shore current shown in Figure 5.11. The current is a result of the combination of the spring tide, larger waves during this period and their respective wave directions.

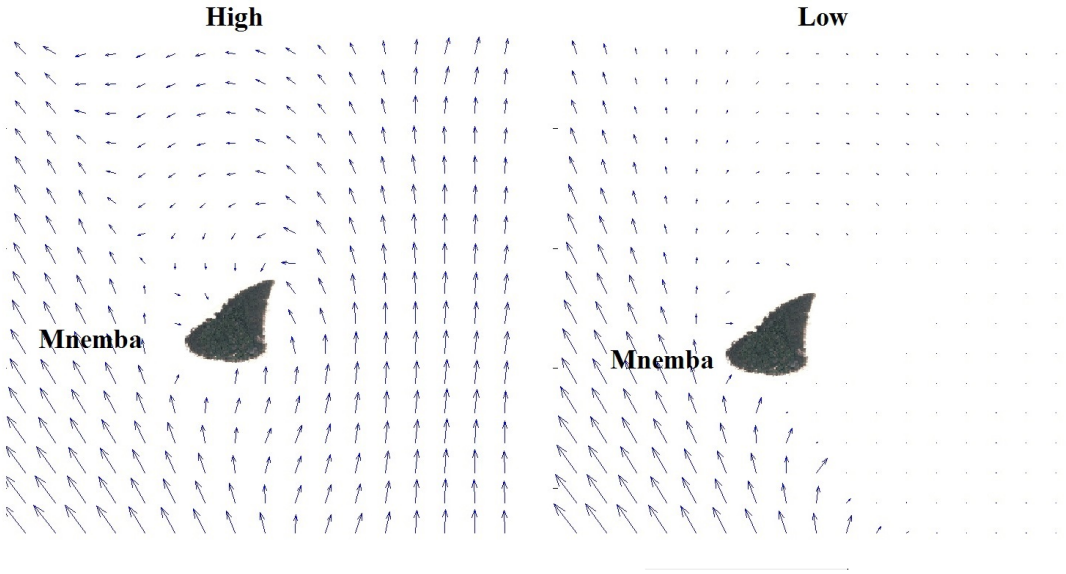

Figure 5.10: Wave direction surrounding Mnemba Island at high (left) and low (right) tide.

Simulated depth-averaged velocities correspond to those measured in-situ in both direction and ratio of velocities between different areas. Complete agreement of measured and simulated results is not expected as the in-situ measurements were taken on the surface whereas the model produces depth-averaged velocities. The ratio of velocities between different zones and directions is however a necessary requirement in order to simulate transport direction and magnitudes qualitatively.

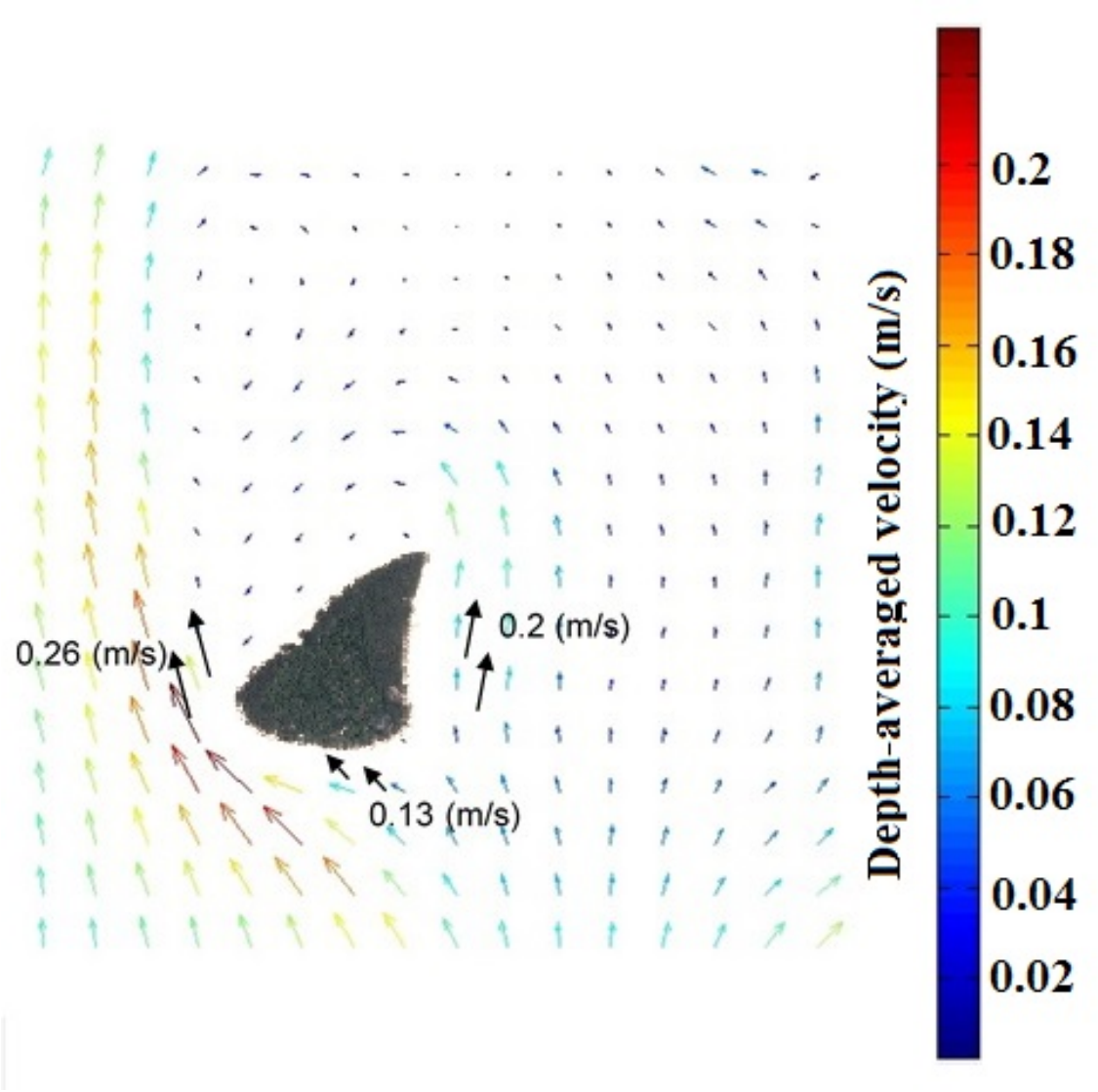

Figure 5.11: Simulated depth-averaged velocities and measured surfaced velocities (Black) surrounding Mnemba Island during spring high tide

5.4 Effect of bed roughness on wave dissipation

As waves propagate onto the reef and interact with the spatially varying roughness illustrated in Figure 3.24, they break and dissipate energy. The model showed its sensitivity to roughness in Figure 5.12 and 5.13. The spatially varying bed roughness (that represents the varying coral communities which cover the reef) was substituted with the reduced roughness height for sand ripples of 0.02 m throughout. The results show larger wave heights at both the outer edge and near-shore points on the reef during neap tides.

At sensor A1 location and point (43,38), little to no variation in wave height was experienced during periods of larger tidal ranges (spring tides). In contrast, during neap tidal phases when tidal ranges were of the order of 1-2 m, wave heights increased with the reduced bed roughness by up to 40%.

Where the reef crest once reduced wave heights by up to 70% once it had reached sensor A1, the reduced roughness simulation shows a wave height attenuation of just 54% illustrated in Figure 5.13.

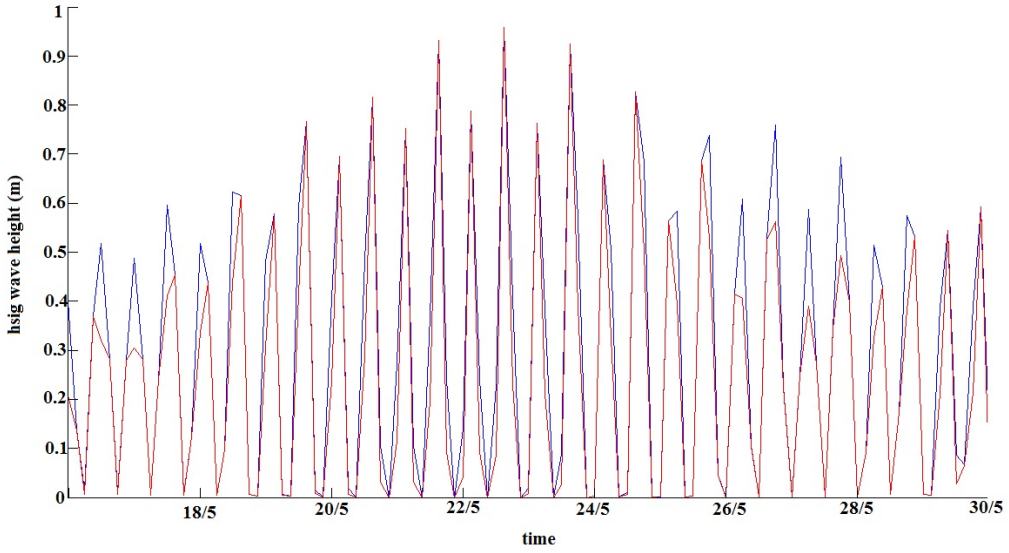

Figure 5.12: Effect of reduced bed roughness. Red line represents the wave height with the coral reef bed. The blue line represents the increased wave height for a sand ripple bed of 0.02 m throughout the reef.

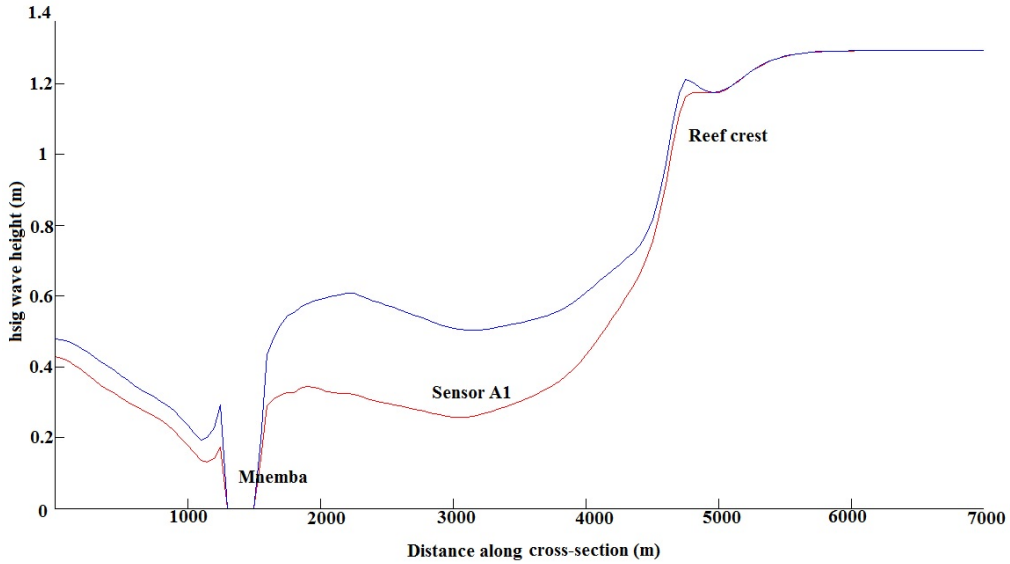

Figure 5.13: Effect of reduced bed roughness during neap tide. The red line represents wave height with current reef roughness. The blue line represents the reduced bed roughness.

Near-shore wave measurements at point (43,38) and (40,25) followed the same pattern with an increase in wave height limited to lower tidal ranges. Although limited to lower tidal ranges, larger waves more frequently reached Mnemba Island increasing the islands vulnerability to erosion.

5.5 Effect of SLR combined with reduced bed roughness

The concurrent impact of SLR and reduced bed roughness showed minor increases in wave height during smaller tidal ranges as seen in Figure 5.14. An average wave height during the simulation rose from 0.3 m to just 0.33 m. Again this translated to a similar increase in wave height at Mnemba Island with wave heights increasing less than 12% during lower tidal ranges.

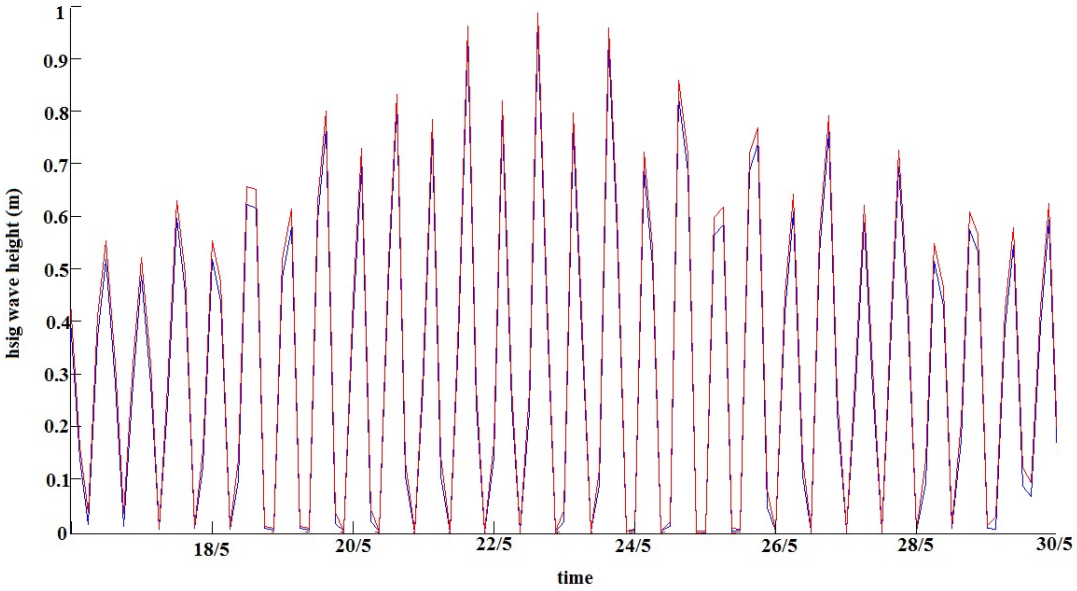

Figure 5.14: Combined effect of reduced bed roughness and 0.1 m SLR

5.6 Verification of model tide inputs

A sensitivity analysis was done to substantiate the use of the real-life tidal phase periods in the simulation(i.e. Two weeks of tide data is input as two weeks and not up-scaled to 1 year of tidal changes to reduce computation time). This was done to by inputing the largest experienced off-shore wave height of 1.8 m with a period of 6.6 seconds as a constant whilst the tide and wave direction continued to vary. This forcing method was important to investigate whether the highest total sediment transport rates around Mnemba Island were not biased by the coinciding largest waves heights and largest tidal range.

The results show that even with the same wave height and period the largest sediment transport rates and direction are still linked to the Spring tide conditions. Figure 5.15 as expected does not show the same transport rates but shows how the peak transport rates still occur at the same point.

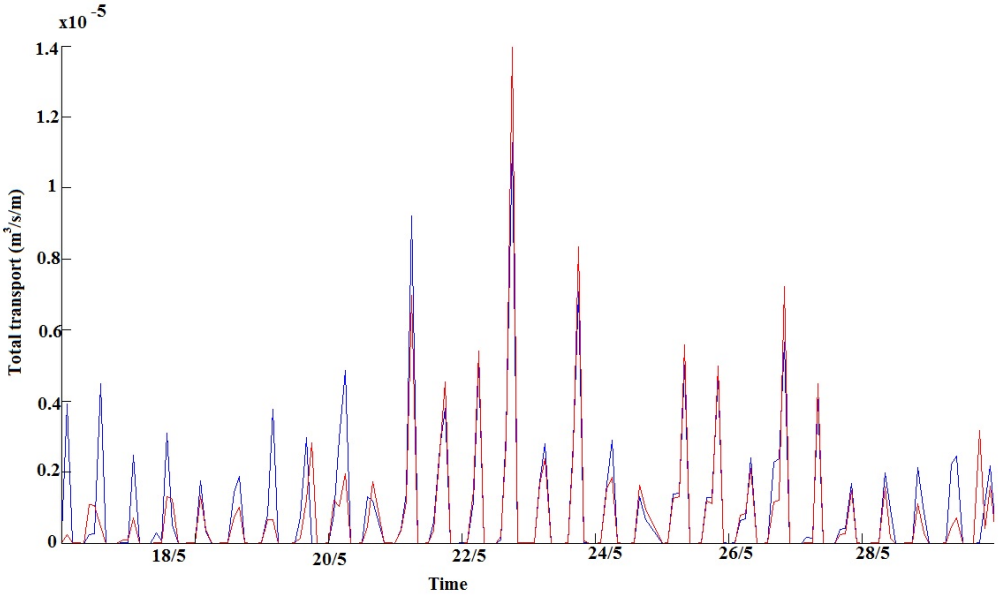

Figure 5.15: Comparison of peak transport periods between single wave input (blue line) and seasonal wave variation (red line).

5.7 Sediment Transport

The bedload transport rate and direction approaching full spring tide is illustrated in figure 5.16. No significant transport is visible on the eastern border at this stage because it is currently dry. The sediment on the remaining beach faces is directed away from the island pulling sediment from the beaches and lifting it into the water column. The fine characteristics of the carbonates sands allows the particles to be lifted high into the water column. Hindered by the high concentration the sediments remain in suspension allowing the current to transport them along the eastern and southern border of Mnemba Island shown in Figure 5.17.

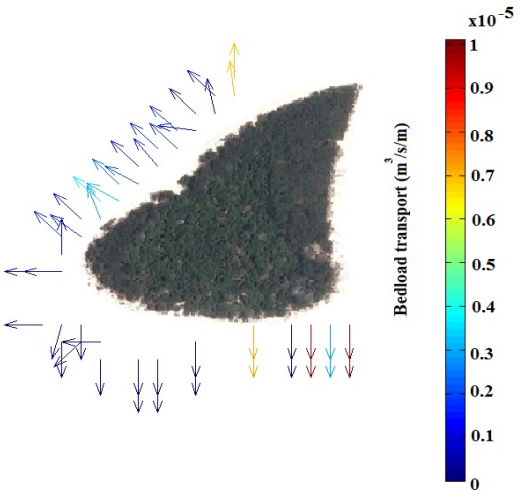

Figure 5.16: Bed load transport surrounding Mnemba Island. Arrows represent the transport direction.

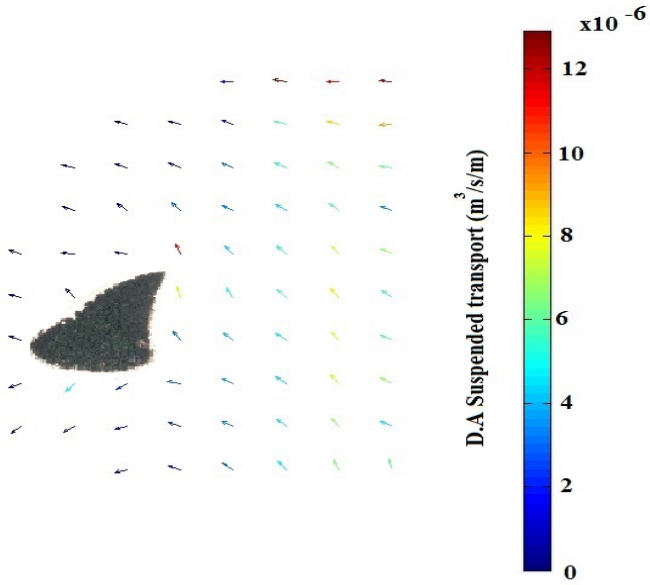

Figure 5.17: Suspended load transport surrounding Mnemba Island at Spring high. Arrows represent the transport direction.

At full spring tide, at which tidal ranges are the order of 3-3.5 m, the bed load transport shifts towards the immediate northern and southern reef edge illustrated by points (a) and (b) respectively. It is at this stage the sediments are lost to the deeper water surrounding the reef. This loss of sediments is shown in Figure 5.19.

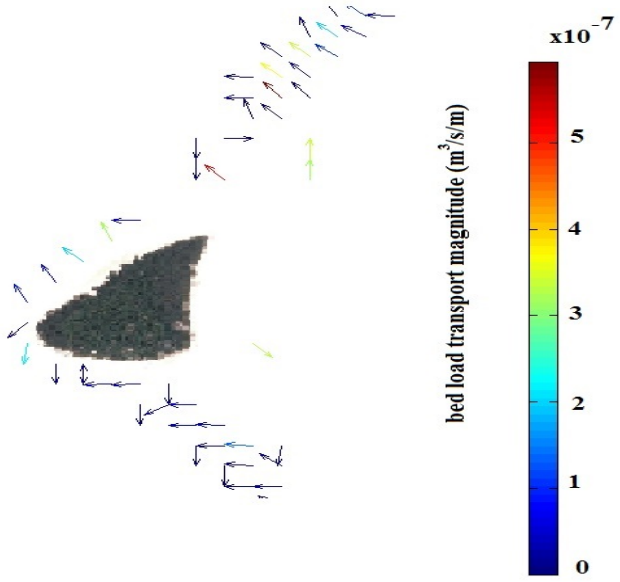

Figure 5.18: Bed load transport surrounding Mnemba Island at spring high. Arrows represent the transport direction.

In total the sediment transport follows the dominant northerly wave direction pushing sediment along the southern and eastern boundary. Severe erosion is evident on the south eastern border correlating to observations on Mnemba Island.

Figure 5.19 shows the change in sediment thickness surrounding Mnemba, the initial sediment thickness was chosen as 2 m based on excavations on site during groyne construction and 0.2 m for reef outcrops. Point (1) represents the erosion of "April Lip" described in chapter 3. Point (2) represents the collection of sediments off the reef from which it is vulnerable to the strong currents in the channel. Point (3) illustrates the northward movement of the bank described in chapter 3 further verifying the model output. Point (4) shows the formation of the "October lip". The reef outcrops (R.O) reduce the amount of sediment available for transport to represent true sediment volumes as closely as possible.

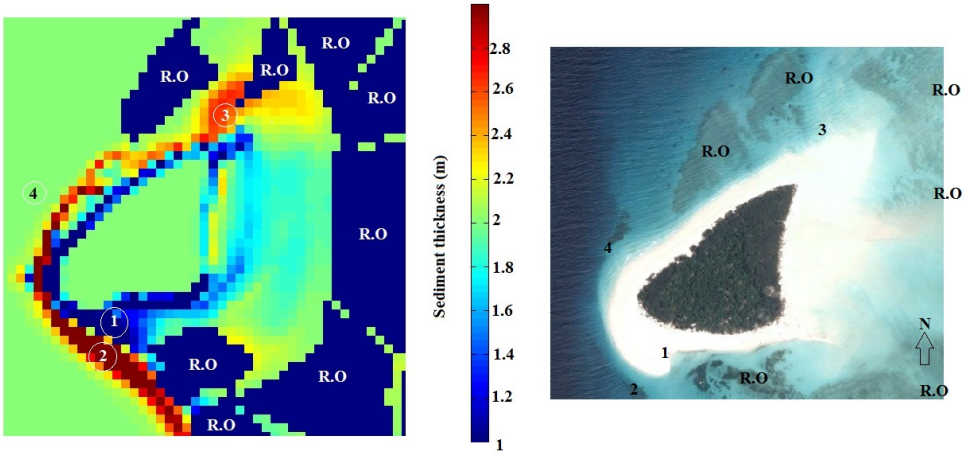

Figure 5.19: Sediment thickness surrounding Mnemba Island showing areas of accretion and erosion. Reef outcrop areas were given an initial sediment thickness of 0.2 m with the remaining areas given 2 m.

The bed level at point (40,25), identified as the major erosion zone, is shown in Figure 5.20. The comparison is drawn between the current reef geometry to the default sand scenario. The erosion of the bank was achieved by setting the erosion of dry-cells parameter to 1 to translate all erosion in the immediate wet cell to the dry cell.

The red line illustrates the erosion with the current reef outcrops on Mnemba and the blue without. The clear increase in erosion is evident with the reduced roughness and increased wave height reaching the island.

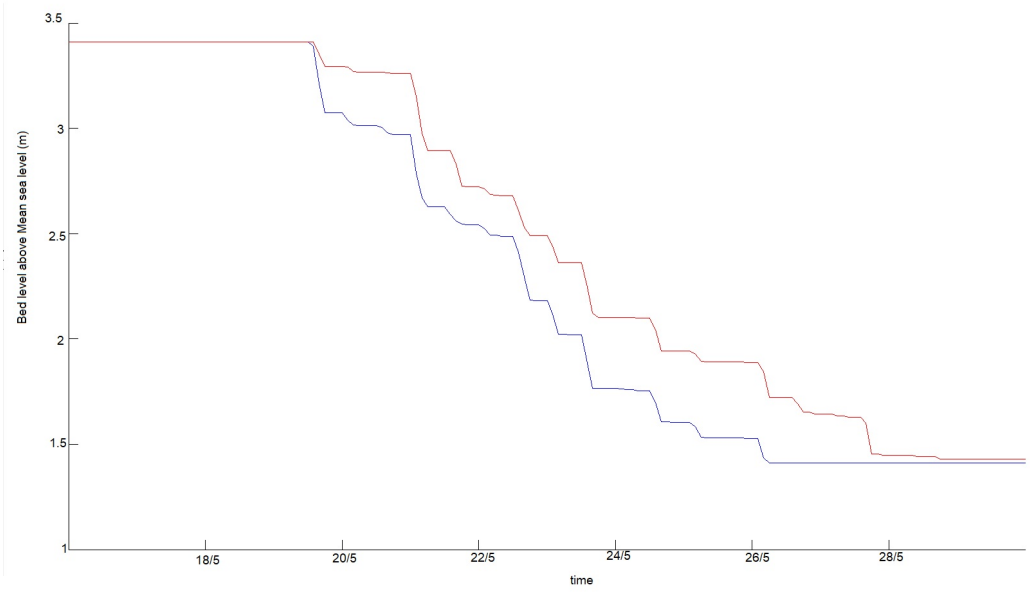

Figure 5.20: Comparison of erosion at point (40,25). Red line represents bed level changes with current reef population and outcrops. Blue line is with the default sand hydraulic roughness.

Chapter 6

Discussion & Conclusions

The overall aim was to identify the main erosion mechanisms for low-lying coral reef islands and the implications of reduced coral reef roughness and sea level rise on these mechanisms. This was achieved by in-situ measurements of sediment transport, wave properties and bathymetry. These were then implemented in Delft3D replicating the processes over the reef in terms of wave transformation and sediment dynamics.

6.1 Waves

The effect of coral reef platforms on wave propagation is evident in both this thesis and those mentioned in the literature review. The wave decay mechanisms are broken into three stages. The initial steepening and breaking of the wave as it propagates to the reef crest at which stage most of the incident wave energy is lost. The remaining wave energy propagates onto the reef flat where the wave continues to lose energy as it interacts with the rough coral bed and the final energy loss during wave breaking at the Island. The fallen trees enhance the erosion effects of the breaking waves and also create large moving debris field capable of further reef destruction.
The synergy of the wave height and water depth illustrates the depth limitation of the waves propagating over the reef which is directly supported by observations, wave spectra and modelling. At high tide waves interact less with the reef crest and coral bed allowing the low frequency waves to propagate further onto the flats before losing energy. It is at the highest tides where significant erosion on Mnemba was experienced as more wave energy reached the reef. The geometry of the reef, convergence of the waves at the eastern Island boundary and reduced dissipation of waves that approached from the south and onto the reef platform promoted severe erosion of sediments on the south-eastern perimeter of Mnemba Island.

The effect of coral reduction acts as an increase in water depth which allows waves to theoretically travel further with reduced interaction with the bed. Although no official study has been done on the status of reef flat, the constant over-fishing and destruction caused by anchors can produce a flattening of the bed profile and reduction in bottom friction.

6.2 Currents

Increased water depths and larger waves from the reduced bed roughness result in stronger currents all across the reef. The reduced hydrodynamic roughness height relative to the water depth allows for faster currents to develop. A greater water exchange and lower residence time on the reef can potentially disturb both the physical and chemical properties of the water column. This in turn can decimate the sensitive reef communities.

The flow pattern and dependence on the trade winds is consistent with the formation of seasonal beach profiles. The strong currents formed in the channel, partly contributed to by the East African Current, and the wave-induced currents along the eastern side of the island transport sediments along the island border where the formations of 'lips' occur.

6.3 Sediment Transport

The variation of reef geometries produce characteristic wave patterns which control the sediment transport. The refraction and centripetal wave motion is expected with the elliptical shape of the reef. The described wave motion can create a convergence point where the sediment would accumulate. If the convergence point lies off the reef platform there is a higher potential for off-reef transport and thus promoting sediment loss.

The collection of sediment surrounding Mnemba island itself owes to this convergence. The 600 metre fine, carbonate sand perimeter is a result of the convergence. The exposed reef within close proximity (<100m) of the island on the northern and southern sides further strengthens the idea that this convergence lies on the eastern side not allowing sediment to cover this area of the reef.

With the convergence point established, unrefracted waves from the south-east create an alongshore current traveling northward along the eastern banks. This current is evident in readings taken on site. The combination of the wave induced current and turbulent zone from wave-fallen tree interaction promotes a northern and western transport of sediment during the dominant south easterly trade winds. The shifting banks described in the case study can be explained by this flow regime of seasonal dependence. Based on the flow regimes dependence on the trade winds, the periods not tested can be expected to show the same dependence on wind direction.

Although the streamer traps showed multi-directional net transport inconsistent with the current and wave direction at the time, overall the defining pattern was evident. The simulated transport directions and in-situ streamer trap results illustrated the dominance of the long-shore transport relative to the cross-shore movement of sediment during the simulated period. The success of the timber groynes was limited by difficult construction conditions, lack of necessary equipment and possibly insufficient length to successfully trap sediments. Despite this limitation, the results of groyne 2 situated on the north-eastern bank of Mnemba island clearly illustrated the northward shifting bank. For this reason the timber groyne can be regarded as a basic means of identifying sediment transport direction.

The described flow is also the basis of why the sediment that is being lost is not returning. The increased wave sizes interacting with the banks lead to increased concentration of sediment in the water column. The high concentration and persistent turbidity of larger waves hinders the settling velocity allowing sediments to be transported further. Larger

orbital velocities from larger waves can also alter abrasion patterns of the coral possibly increasing coral loss in areas exposed to more sediment transport. The transported sediments move northward and westward where they are lost off the reef. The reduced wave heights and shortened seasonal winds from the north lack the energy to pick up the sediments form the deeper drop offs to return them back onto the reef.

As identified by Ogston and Field (2010a) the increased sea level and reduced roughness increases delivery of energy to the island. Critical shear stresses can then be exceeded and hence the promotion of erosion. The effect of increased concentrations of sediment in the water column can suffocate the coral bed killing the reef.

6.4 Future of Mnemba Island

The outlook of the island without intervention is bleak. The reduced roughness and hence increased water depth of the reef will continually allow larger waves to propagate closer to the island. The south-eastern section of the island is particularly vulnerable because of the dominant swell from the south-east. The island's northern vegetation line is expected to be maintained but the sediments on the south-eastern corner will continually be eroded and transported off the reef platform. Some of the sediment is trapped at the north-eastern section before being lost as the reef descends into the deeper sections and ultimately into the channel separating Mnemba from Zanzibar.

Although conflicting reports of sea level rise were identified, global trends of climate change and rising sea levels provide the same impact as reduced bed roughness. Increased water levels allow waves to propagate further across the reef before losing energy and rising water temperatures are responsible for large-scale coral bleaching. The impact from both of which is unavoidable.

The introduction of the Casuarina trees, although they increased the island area, had disturbed the natural conditions of the island's climate and this erosion is possibly just returning the Island to its natural state. This suggests the island's climate would return to similar conditions once this state is met, however with expected coral reef destruction from anthropogenic causes coupled with sea level rise can result in continued erosion beyond this natural state.

6.5 Environmental and Economic considerations

Mnemba Island, although differing in function to the likes of the disappearing Solomon Islands, plays a pivotal role to the success of &Beyond and the tourism of Zanzibar but more importantly to the livelihood of the local employees and even to local fishermen who hunt the reef. The collapse of the reef system and continued severe erosion of the Island could eventually prompt &Beyond to leave the Island removing one of the major components of Zanzibar's tax revenue.

The continued destruction of the reef from over-fishing is diminishing the product the very same fishermen wish to exploit to support their families as they have done so for decades before.

6.6 Coastal protection scheme

The exclusivity and premium experience expected by high-paying guests translates into difficult design choices. Any implemented scheme would ultimately create trade-offs whether it be on ease of construction, aesthetics or cost and accessibility. The use of hard, obtrusive structures would tarnish the aesthetics of the Island and also create a structure that impedes passage. Timber groynes constructed out of fallen Casuarina trees are feasibly viable because the material is freely available but again aesthetically displeasing and difficult to cross.

Soft structures like geosynthetic containers provide a solution that is more aesthetically pleasing and achievable in terms of availability of filling material and ease of construction. Containers do still however impede the passage of guests and limit movement around the island.

Annual beach nourishment is the only scheme that does not require an artificial structure but is limited by accessibility and availability. The dredger would only be able to pump material at spring high with the use of floating pipes and a material source would still need to be located. The use of a dredger would also be extremely costly.

Defining the entire reef as a Marine Protected Area (MPA) would allow coral communities to regenerate and increase the bed roughness but on a time scale of decades. The protected area would be strongly opposed by locals from Zanzibar who so heavily depend on it along with no guarantee that the coral communities would actually regrow.

6.7 Recommendations for future work

An in-depth analysis of coral reef populations is essential to further substantiate this research. Data on the reduction of the coral communities and the resultant impact on fish species would allow for a closer comparison between reduced bed roughness and propagating wave height over reefs.

The research can be enhanced by obtaining accurate sediment transport,wave characteristics and current measurements over varying seasons and not just limited to a single period. This would allow for higher accuracy in predicting future trends of erosion.

By incorporating the varying protection schemes into the model a more accurate recommendation of a protection scheme can be made.

Bibliography

Albert, S, Leon, J.L, Grinham, A.R, Church, J.A, Gibbes, B.R, and Woodroffe, C.D (2016). Interactions between sea-level rise and wave exposure on reef island dynamics in the Solomon Islands. *Environmental Research Letters* Vol.11.No.3.

Barber, D (2000). *Beach Nourishment*. visited on 14 February 2017. URL: `http://www.brynmawr.edu/geology/geomorph/beachnourishmentinfo.html`.

Battjies, J. and Janssen, J. (1978). Energy loss and set-up due to breaking of random waves. *Proceedings 16th International Conference Coastal Engineering*. No.16.. Hamburg, Germany, 569587.

Battjies, J.A (2011). Surf Similarity. *Proceedings 14th International Conference on Coastal Engineering*. Vol. Vol.1. No.14, pp. 466–480.

Bishop, C.T and Donelan, M.A (1987). Measuring Waves with Pressure Transducers. *Coastal Engineering* Vol.11, pp. 309–328.

Bosboom, J. and Stive, M. (2012). Sediment Dynamics. *Coastal Dynamics 1*. 3rd ed. Netherlands: DELFT University of Technology. Chap. 5, p. 190.

Brown, E., Colling, A., Park, D., Phillips, J., Rothery, D., and Wright, J. (2008). Waves. *Waves, tides and shallow water processes*. 2nd ed. Butterworth-Heinemann. Chap. 1, pp. 14–20.

Buddemeier, R.W. and Smith, S.V. (1988). Coral reef growth in an era of rapidly rising sea levels: predictions and suggestions for longterm research. *Coral Reefs* Vol.7, pp. 51–56.

Chee, C.L., Singh, A., Persad, R., and Darsan, J. (2014). The Influence of Tidal Currents on Coastal Erosion in a Tropical Micro-Tidal Environment the Case of Columbus Bay, Trinidad. *Global Journal of Science Frontier Research* Vol.14 (5).

Davidson-Arnott, R. (2010). Sediment Transport. *Introduction to Coastal Processes and Geomorphology*. Cambridge University press. Chap. 7, pp. 139–181.

Dean, R.G and Dalrymple, R.A (2004). Wave Transformation. *Coastal processes with engineering applications*. Cambridge University press. Chap. 5, pp. 94–96.

DeConto, R.B, and David, P. (2016). Contribution of Antarctica to past and future sea-level rise. *Nature* Vol.531, pp. 591–597.

ECMWF (2016). *ERA Interim*. Visited on 10 June 2017. URL: `http://apps.ecmwf.int/datasets/data/interim-full-daily/levtype=sfc/`.

Ferrario, F., Beck, M.W, Storlazzi, C.D., Micheli, F., SHephard, C.C., and Arioldi, L. (2014). The effectiveness of coral reefs for coastal hazard risk reduction and adaptation. *Nature communications* Vol.5.

Filipot, J.F. and Cheung, K.F. (2012). Spectral wave modeling in fringing reef environments. *Coastal Engineering* (67), pp. 67–79.

Garcia-Reyes, M., Mayorga-Adame, G., Moulton, M.R., and Nadeau, P.C (2009). Modeling of the Zanzibar Channel. *The Zanzibar Project*.

Grauss, R.R. and Macintyre, I.G. (1998). Global warming and the future of Caribbean reefs. *Carbonates Evaporites* Vol.13, pp. 43–47.

Grinsted, A., Moore, J.C., and Jevrejeva, S. (2009). Reconstructing sea level from paleo and projected temperatures 200 to 2100 AD. *Clim Dyn* Vol.34.No.4, pp. 461–472.

Holthuisjen, L., Booij, N., and Rise, R. (1993). A spectral wave model for the coastal zone. *Proceedings of 2nd International Symposium on Ocean Wave Measurement and Analysis*. New Orleans, Louisiana, United States.

Jonsson, I.G (1963). Measurements in the turbulent wave boundary layer. IAHR conference. Vol. Vol.10. London, pp. 85–92.

Jonsson, I.G. (2011). Wave boundary layers and friction factors. *Coastal Engineering Proceedings*. Vol. Vol.1. No.10, pp. 127–148.

Kench, P.S., Owen, S.D, and Ford, M.R (2014). Evidence for coral island formation during rising sea level in the central pacific ocean. *Geophysical research letters* Vol.41.No.3, pp. 820–827.

Kench, P.S, Thompson, D., Ford, M.R., Ogawa, H., and Mclean, R.F (2015). Coral islands defy sea-level rise over the past century: records from a central Pacific atoll. *Geology* Vol.43.No.5, pp. 515–518.

Knowlton, N. (2016). *Corals and coral reefs*. Visited on 21 July 2017. Smithsonian National Museum of Natural History. URL: `http://ocean.si.edu/corals-and-coral-reefs`.

Komen, G., Hasselmann, S., and Hasselmann, K. (1984). On the existence of a fully developed wind-sea spectrum. *Journal of Physical Oceanography* No.14, 12711285.

Krahn, T., Blats, J., Alfar, M., and Blathurst, R.J. (2007). Large scale interface shear testing of sand bag dyke materials. *Geosynthetics International* Vol.14, pp. 119–126.

Krauss, N.C (1987). Applications of portable traps for obtaining point measurements of sediment transport rates in the surf zone. *Journal of Coastal Research* Vol.3.No.2, pp. 139–152.

Madsen, O., Poon, Y.K, and Graber, H. (1988). Spectral wave attenuation by bottom friction. *In Proceedings 21st International Conference Coastal Engineering*. Torremolinos, Spain, pp. 492–504.

Mahongo, S.B and Francis, J. (2012). Monthly variations in sea level at the Island of Zanzibar. *Western Indian Ocean Journal of Marine Science* Vol.9.No.1, pp. 1–16.

Mandlier, P.E (2013). Field observations of wave refraction andpropagatio n pathways on coral reef platforms. *Earth surface processes and landforms* Vol.38, pp. 913–925.

Mather, A.A (2012). "The risks, the management and adaptation to sea level rise and coastal level rise and erosion along the southern and eastern african coastline." PhD thesis. University of Kwa-Zulu Natal.

Nelson, R.C (1996). Hydraulic roughness of coral reef platforms. *Applied Ocean Research* Vol.18, pp. 265–274.

– (1997). Hydraulic roughnesss of coral reef platforms. *Applied ocean research* 18.

Nielsen, P (1992). Bottom boundary layer flow. *Coastal bottom boundary layers and sediment transport.* World Scientific Publishing Company. Chap. 1, pp. 127–140.

Nunes, V. and Pawlak, G. (2000). *Observations of Bed Roughness of a Coral Reef.* Manoa, U.S.A: University of Hawaii.

Ogston, A.S. and Field (2010a). Predictions of turbidity due to enhanced sediment resuspension resulting from sea level rise on a fringing coral reef:evidence from Molokai. *Journal of coastal Res* 26.6, pp. 1027–1037.

Ogston, A.S. and Field, M.E. (2010b). redictions of turbidity due to enhanced sediment resuspension resulting from sea-level rise on a fringing coral reef: evidence from Molokai, HI. *Coast Res* Vol.26.No.6, pp. 1027–1037.

Partnership, Global Climate Adaptation (2012). The economics of cliamte change in Zanzibar.

Presto, M.K., Ogston, A.O., Storlazzi, C.D., and Field, M.E. (2006). Temporal and spatial variability in the flow and dispersal of suspendedsediment on a fringing reef flat, Molokai, Hawaii. *Estuary Coast Shelf Sci* Vol.67, pp. 67–81.

PTSA (2016). *Elcorock.* Visted on 16 December 2016. URL: `http://www.sahabatagritama.com/index.php/products/94/GEOFABRICS`.

Rijn, L.C van (2002). *Longshore sand transport.* Netherlands: DELFT University of Technology.

Saathoff, F., Oumeraci, H., and Restall, S. (2007). Australian and German experiences on the use of geotextile containers. *Geotextiles and Geomembranes* 25, pp. 251–263.

Smith, E.R, Wang, P., Ebersole, B.A, and Zhang, J. (2009). Dependence of Total Longshore Sediment Transport Rates on Incident Wave Parameters and Breaker Type. *Journal of Coastal Research* Vol.25 (3), pp. 675–683.

Smith E, R, Wang, P., and Zhang, J (2003). Evaluation of the CERC formula using large-scale laboratory data. *Geology Faculty Publications.*

Storlazzi, C.D, Elias, E., Field, M.E., and Presto, M.K. (2011). *Numerical modeling of the impact of sea-level rise on fringing coral reef hydrodynamics and sediment transport.* No.30, pp. 83–96.

Swart, D.H (1974). *Offshore sediment transport and equilibrium beach profiles.* Report. Deltares, p. 131.

Verhagen (2013). EMS wave logger data processing. *Communications on Hydraulic and Geotechnical Engineering* No.1, pp. 3–34.

Watkiss, P., Bonjean, M., and Shaghude, Y.W (2012). Current weather data for Zanzibar and the effects of climate variability and extremes. *The economics of climate change in Zanzibar.*

Windfinder (2016). *Wind Statistics.* Visted on 15 November 2016. URL: `https://www.windfinder.com/windstatistics/ras_nungwi_zanzibar`.

Appendix A

A.1 Modified SWAN input file

The swan.bat file personally created to input the spatially varying roughness file manually.

```
@echo off

set swanexec=%D3D_HOME%\%ARCH%\swan\bin\swan_4072ABCDE_del_w32_i11_omp.exe

rem
rem swan40.72AB and newer runs parallel, using the total number of cores on the machine
rem to force the number of parallel processes, remove the "rem" in front of the following line and adjust the number
rem set OMP_NUM_THREADS=1

@echo SWAN batchfile executed for Delft3D
@echo Using swan.bat in directory %~dp0
@echo Using %swanexec%
@echo Performing wave computation for: %1.swn

if exist PRINT del PRINT
if exist INPUT del INPUT
if exist swaninit del swaninit
if exist Errfile del Errfile
if exist errpts del errpts
if exist %1.erf del %1.erf
if exist %1.erp del %1.erp
if not exist %1.swn goto error1
if not exist "%swanexec%" goto error2

rem SPATIALLY VARYING BOT ROUGHNESS
copy %1.swn test.swn
if not exist INPUT1 goto overallgrid
if exist INPUT1 goto nestedgrid

:overallgrid
copy test.swn INPUT1
goto commonexit

:nestedgrid
mod.exe -l "26" "INPGRID _" test.swn
```

```
mod.exe -l "27" "FRICTION  CURV  0. 0. 141 201" test.swn
mod.exe -l "28" "READINP FRICTION  1.0 'roughnessgrid.dep' 4 0 FREE" test.swn
mod.exe -s "FRIC JON      0.0670" "FRICTION MADSEN kn=0.05"  test.swn
del INPUT1
goto commonexit

:commonexit
copy test.swn INPUT
"%swanexec%"

copy PRINT %1.prt
if exist errfile copy errfile %1.erf
if exist errpts copy errpts %1.erp
if exist swaninit del swaninit
goto finish
:error1
@echo
@echo    ************************************************************
@echo            SWAN input file %1.swn does not exist
@echo    ************************************************************
pause
goto finish
:error2
@echo
@echo    ************************************************************
@echo            SWAN executable does not exist
@echo            (%swanexec%)
@echo    ************************************************************
pause
goto finish
:finish
@echo on
rem exit
```

A.2 Mnemba Island Erosion update

Figure A.1: 20 October 2016 South Eastern corner of Mnemba Island. Further collapse of concrete floor slab

Figure A.2: May 2017 South Eastern corner of Mnemba Island. Complete loss of concrete floor slab